이학박사학위논문

오토파지의 후성 유전 및 전사 조절 기작에 대한 연구

Studies on the Epigenetic and Transcriptional Regulation of Autophagy

2016년 8월

서울대학교 대학원

생명과학부

신 희 재

Studies on the Epigenetic and Transcriptional Regulation of Autophagy

by

Hi-Jai R. Shin

Advisor

Professor Sung Hee Baek, Ph.D.

A Thesis for the Degree of Doctor of Philosophy

August, 2016

School of Biological Sciences
Seoul National University

오토파지의 후성 유전 및 전사 조절 기작에 대한 연구

Studies on the Epigenetic and Transcriptional Regulation of Autophagy

지도교수 백 성 희

이 논문을 이학 박사 학위논문으로 제출함

2016년 05월

서울대학교 대학원

생명과학부

신 희 재

신희재의 이학박사 학위논문을 인준함

2016년 05월

위 원 장 정 종 정 (인)

부위원장 백 성 희 (인)

위 원 김 빛 내 리 (인)

위 원 이 원 재 (인)

위 원 김 은 일 (인)

Studies on the Epigenetic and Transcriptional Regulation of Autophagy

A dissertation submitted in partial fulfillment of the requirement for the degree of

DOCTOR OF PHILOSOPHY

TO THE FACULTY of
THE SCHOOL of BIOLOGICAL SCIENCES
at
SEOUL NATIONAL UNIVERSITY
by

Hi-Jai R. Shin

Date approved

May 25, 2016

ABSTRACT

Hi-Jai R. SHIN
School of Biological Sciences
The Graduate School
Seoul National University

Autophagy is a highly conserved self-digestion process, essential to maintain homeostasis and viability in response to nutrient starvation. Although the components of autophagy in the cytoplasm have been well-studied, molecular basis for the epigenetic and transcriptional regulation of autophagy occurring in the nucleus is poorly understood. Here, I identify coactivator-associated arginine methyltransferase 1 (CARM1) as a novel component and followed histone H3R17 dimethylation as a critical epigenetic mark of autophagy. Intriguingly, CARM1 stability is regulated by SKP2-SCF (Skp1-Cullin1-F box protein) E3 ubiquitin ligase complex in the nucleus, but not in the cytoplasm, under nutrient-rich condition. Further, I found that nutrient starvation induced-AMP-activated protein kinase (AMPK) phosphorylates FOXO3a in the nucleus, which in turn transcriptionally represses SKP2 leading to increased CARM1 protein levels and subsequent increase in histone H3R17 dimethylation. CARM1 dynamically

regulates the outcome of autophagy from the nucleus as genome-wide analyses reveal that CARM1 exerts transcriptional coactivator function on autophagy-related genes and lysosomal genes through Transcription Factor EB (TFEB). Taken together, my work unravels a new signaling axis of AMPK-SKP2-CARM1 in autophagy induction under nutrient starvation. My findings provide a conceptual advance that activation of specific epigenetic programs is indispensable for a sustained response to autophagy and demonstrate a previously unrecognized role of CARM1-dependent histone arginine methylation in the process of autophagy.

Key words

Coactivator-associated arginine methyltransferase 1 (CARM1), Autophagy, Histone arginine methylation, Epigenetic regulation, Transcription, Transcription Factor EB (TFEB), AMP-activated protein kinase (AMPK), S-phase kinase-associated protein 2 (SKP2),

Student Number: 2009-20340

CONTENTS

LIST OF FIGURES AND TABLES

CHAPTER I

Introduction

I-1. Coactivator-associated arginine methyltransferase 1 (CARM1)

1.1 CARM1 is an arginine methyltransferase

Arginine methylation is a post-translational modification found in a variety of cellular proteins that has been implicated in signal transduction, RNA processing, and transcriptional regulation (Bedford and Clarke, 2009; Lee and Stallcup, 2009; Paik et al., 2007; Stallcup, 2001). It is carried out by a family of protein arginine methyltransferases (PRMTs). PRMTs transfer the methyl group from S-adenosylmethionine (AdoMet) to the terminal guanidino nitrogens of arginine residues generating monomethyl-arginine, symmetric dimethyl-arginine (SDMA), and asymmetric dimethyl-arginine (ADMA). At least nine PRMTs have been identified and classified into class I and class II enzymes: class I PRMTs catalyze the formation of asymmetric dimethylarginine (ADMA), whereas class II enzymes are responsible for generating symmetric dimethylarginine (SDMA) (Gary and Clarke, 1998).

The class I enzyme CARM1 was the first PRMT to be functionally linked to transcriptional regulation (Lee et al., 2005a; Wysocka et al., 2005). As it was the fourth arginine methyltransferase described, CARM1 is also referred to as PRMT4. CARM1 is responsible for dimethylation of histone H3 on arginine 17 and 26 as well as many other non-histone proteins including p300/CBP, SRC3, BAF155, RNA Pol II, and various RNA-binding proteins (Chevillard-Briet et al., 2002; Feng et al., 2006; Fujiwara et al., 2006; Lee et al., 2005b; Li et al., 2002; Naeem et al., 2007; Schurter et al., 2001; Sims

et al., 2011; Wang et al., 2014)

1.2 The structure of CARM1

CARM1 contains 608 amino acids in both mouse and human and its architecture has been schematically divided into three domains. CARM1 is built around a catalytic core domain, also called methyltransferase domain (residues 150–470 in mouse CARM1), that is well conserved in sequence and therefore in structure among all PRMTs members (Troffer-Charlier et al., 2007; Yue et al., 2007). CARM1 possesses two unique additional domains attached, respectively, at the N-terminal and at the C-terminal end of the PRMT active site (Fig. I-1). Both N-terminal domain (residues 1–130 in mCARM1) and C-terminal domain (residues 480–608 in mCARM1) have been shown to be required for the coactivator function of CARM1 (Teyssier et al, 2002).

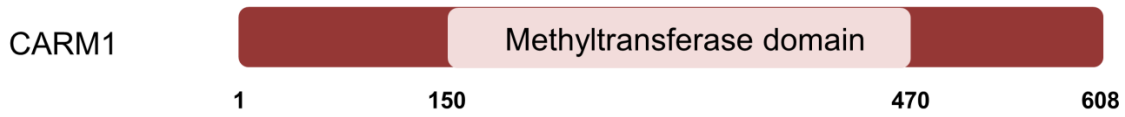

Figure I-1. Illustration of CARM1 functional domains
CARM1, also known as PRMT4, consists of 608 amino acids. As a member of the PRMT family, it contains a highly conserved methyltransferase domain (150-470 amino acids). The N-terminal and C-terminal regions are unique to CARM1.

1.3 Physiological functions of CARM1

Carm1 knockout (KO) mice survive the entire development but die shortly after birth, suggesting that the enzyme is required for postnatal survival (Yadav et al., 2003). The enzymatic activity of CARM1 is critical, at least for its *in vivo* functions, since the enzymatic dead mutant of *Carm1* knockin (KI) mice show similar defects as to *Carm1* KO mice (Kim et al., 2010a). Through arginine methylation of its substrates, CARM1 regulates a great number of cellular processes, including cell cycle progression, DNA damage response and RNA processing (Cheng et al., 2007; El Messaoudi et al., 2006; Kuhn et al., 2011; Lee et al., 2011; Ohkura et al., 2005). Indeed, various roles of CARM1 have been reported in muscle (Chen et al., 2002; Wang et al., 2012), T cell (Kim et al., 2004) and lung development (O'Brien et al., 2010), stem cell maintenance (Torres-Padilla et al., 2007; Wu et al., 2009), and tumorigenesis (Yang and Bedford, 2013). Increasing evidence support the oncogenic properties of CARM1 in various cancers including breast, prostate and colon. CARM1 is overexpressed in human cancers and elevated levels correlate with poor prognosis (Davis et al., 2013; Hong et al., 2004; Kim et al., 2010b; Mann et al., 2013). CARM1 transactivates many cancer-associated transcription factors such as NF-κB, p53, E2F1, FOS, WNT-βcatenin, steroid hormones estrogen receptor alpha (ERα) and androgen receptor (AR) and promotes cancer cell proliferation (Copeland et al., 2009). CARM1 overexpression has been shown to not only activate multiple oncogenic pathways, but also promote a favorable microenvironment for tumor growth and metastasis.

As a transcriptional coactivator CARM1 is a key player in the formation of large

complexes at gene promoters leading to chromatin remodeling and gene activation. CARM1 is best known to form a complex with ATP-remodeling SWI/SNF factors (Xu et al., 2004). The recruitment of CARM1 results in arginine methylation of histone H3R17 (H3R17me2), which has been linked to transcriptional activation (An et al., 2004; Bauer et al., 2002; Daujat et al., 2002; Yue et al., 2007).

I-2. AMP-activated protein kinase (AMPK)

2.1 AMPK structure and activation

AMPK is a critical energy sensor highly conserved in all eukaryotic organisms. Mammalian AMPK is a heterotrimer composed of catalytic α- and regulatory β- and γ -subunits. There are two α- (α1 and α2), two β- (β1 and β2) and three γ –subunits (γ1, γ2 and γ3), making a total of 12 possible heterotrimeric combinations (Hardie et al., 2012). However, the physiological significance of these different subunit combinations needs to be further determined. AMPK is activated when intracellular ATP level decreases whereas AMP or ADP level increase. Under lowered intracellular ATP levels, AMP or ADP directly binds to the γ regulatory subunits of AMPK, leading to a conformational change that promotes AMPK phosphorylation and activation. The α-subunit contains the AMPK serine threonine kinase domain and the phosphorylation site threonine (Thr) 172. The phosphorylation of this amino acid by upstream kinases is essential for AMPK activation (Hawley et al., 1996; Suter et al., 2006). Liver kinase B1 (LKB1), also known

as STK11, is a tumor-suppressor gene responsible for AMPK phosphorylation (Shackelford and Shaw, 2009). LKB1 is the main serine/threonine kinase responsible for AMPK phosphorylation but AMPK can also be activated in response to calcium flux by calcium/calmodulin-dependent protein kinase kinase 2 (CAMKK2), also known as CAMKKβ (Hawley et al., 2005; Hurley et al., 2005; Shaw et al., 2004; Woods et al., 2003). Interestingly, sequence homology showed that CAMKK2 is the closest mammalian kinase of LKB1. Mitogen-activated protein kinase kinase kinase (MAPKKK) family member transforming growth factor beta-activated kinase 1 (TAK1) has also been reported to phosphorylate Thr 172 of AMPK (Herrero-Martín et al., 2009; Momcilovic et al., 2006; Xie et al., 2006). Many types of cellular stress can lead to AMPK activation: low nutrients, prolonged exercise, pathological conditions such as ischemia, naturally occurring compounds such as resveratrol, a polyphenol found in grapes, and pharmacological agents such as metformin, the most widely prescribed type 2 diabetes drug (Hardie et al., 2006; Kudo et al., 1996; McGee and Hargreaves, 2010; Zhou et al., 2001).

2.2 AMPK expression and its function in autophagy

AMPK has been considered to be a cytoplasmic enzyme but evidence is emerging that it can also target to the nucleus and specific membrane domains. AMPKα1 is mainly localized in the cytoplasm and AMPKα2 is mainly nuclear (Jakub et al., 1998). Both AMPKα1 and α2 contain a nuclear export sequence (NES) but only the α2 subunit of AMPK has a nuclear localization signal (NLS) (Suzuki et al., 2007). AMPKα1 is

ubiquitously expressed whereas the expression of AMPKα2 is clearly abundant in metabolic tissues such as liver and skeletal muscle.

The energy sensor AMPK was previously thought to activate autophagy entirely through its ability to inactivate mTOR complex1 (TORC1). AMPK phosphorylates both TSC2 (Inoki et al., 2003) and Raptor (Gwinn et al., 2008) resulting in TORC1 inhibition. Since TORC1 suppresses autophagy, it has been assumed that AMPK could indirectly trigger autophagy. However, recent papers provided evidence that energy stress triggers autophagy in mammalian cells by activating AMPK, which in turn directly phosphorylates ULK1, the mammalian orthologues of ATG1 and key upstream serine/threonine kinase that initiates the autophagy cascade (Egan et al., 2011; Kim et al., 2011). As for many core autophagy proteins, ULK1 is required for cell survival upon nutrient starvation and this also requires the phosphorylation of ULK1 by AMPK. Similar results were obtained in budding yeast and in *C. elegans*, suggesting that AMPK-ULK1 pathway is well-conserved (Egan et al., 2011; Wang et al., 2001). Together, AMPK activates autophagy through inactivation of TORC1 but also through direct phosphorylation of ULK1.

I-3. S-phase kinase 2 (SKP2)

3.1 SKP2 structure and regulation

S-phase kinase associated protein 2 (SKP2) is an F-box protein component of the Skp1/Cullin1/F-box (SCF)-type E3 ubiquitin ligase complex (Fig. I-2). It has been first identified to play an important role in cell cycle progression (Jin et al., 2004; Zhang et al., 1995). SKP2 contains the N-terminal domain, F-box domain and C-terminal leucine-rich repeats (LRR) (Frescas and Pagano, 2008; Nakayama and Nakayama, 2005). The crystal structure revealed that SKP2 interacts with Skp1 through its F-box domain, whereas it does not directly bind with Cullin1 (Schulman et al., 2000; Zheng et al., 2002). As a result, deletion of SKP2 F-box domain compromises its E3 ligase activity by preventing SKP2 from forming a SCF E3 ubiquitin ligase complex. SKP2 LRR domain is responsible for the interaction of SKP2 with its substrates.

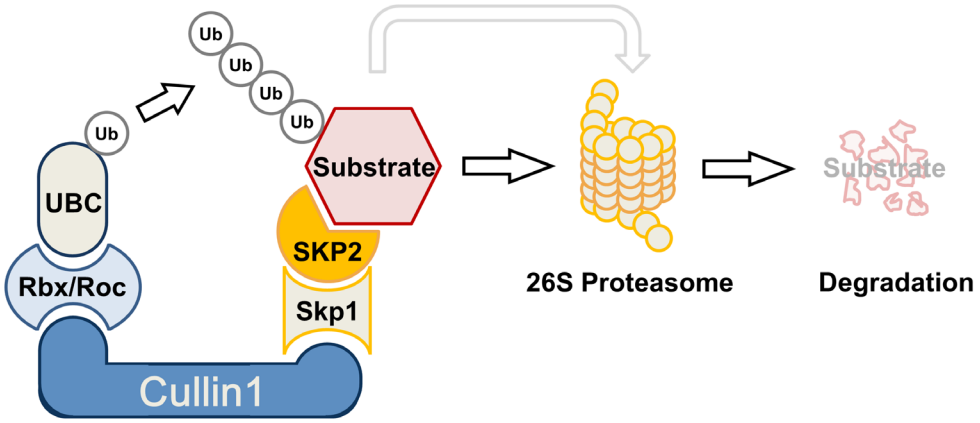

Figure I-2. Illustration of the SKP2-SCF E3 ligase complex

The SCF (Skp1–Cullin1–F-box) E3 ubiquitin ligase complex consists of four components: Skp1, Rbx1, Cullin1, and the variable F-box protein. SKP2 is an F-box protein component. It recognizes the targeted proteins and promotes the ubiquitin transfer to the substrate protein by UBC (the E2 enzyme). The addition of polyubiquitin targets substrates for degradation by the 26S proteasome.

SKP2 is ubiquitinated by the E3 ubiquitin ligase anaphase promoting complex (APC)/Cdh1 complex in early G1 phase, further supporting the role of SKP2 in cell cycle (Bashir et al., 2004; Wei et al., 2004). SKP2 also undergoes phosphorylation during cell cycle progression and growth factor stimulation (Bilodeau et al., 1999). However, the kinases involved in the phosphorylation of SKP2 are still under debate. Recent studies revealed that SKP2 is phosphorylated by Cdk2 and Akt kinases, which play an important role in SKP2 stability and localization (Gao et al., 2009; Lin et al., 2009; Rodier et al., 2008). SKP2 is primarily localized in the nucleus but Akt signaling has been reported to influence SKP2 cytosolic localization, especially during cancer progression (Inuzuka et al., 2012; Lin et al., 2009).

SKP2 expression is also regulated at a transcriptional level. Indeed, CBF1 (Sarmento et al., 2005), GABP (Imaki et al., 2003), E2F (Zhang and Wang, 2006) and FOXM1 (Wang et al., 2005) are shown to bind to SKP2 promoter and induce its expression. The transcriptional repressors of SKP2, on the other hand, are less clear.

3.2 Physiological functions of SKP2

The SKP2-SCF complex interacts with p27 to promote its degradation through the ubiquitin-proteasome pathway and SKP2-dependent degradation of p27 is essential for cell cycle entry (Ganoth et al., 2001; Sutterlüty et al., 1999). Interestingly, SKP2 targets many cell cycle regulators including p21, p27, Cyclin D and Cyclin E (Bornstein et al., 2003; Ganoth et al., 2001; Nakayama and Nakayama, 2005; Spruck et al., 2001; Yeh et

al., 2001; Yu et al., 1998).

SKP2 deficiency results in profound impairment in proliferation accompanied by nuclear enlargement, polyploidy, and centrosome over-duplication (Nakayama et al., 2000). Lines of evidence suggest that SKP2 has oncogenic properties as it promotes the degradation of numerous tumor suppressor proteins, including p21, p27 and FOXO (Cardozo and Pagano, 2004; Frescas and Pagano, 2008; Gstaiger et al., 2001). Indeed, recent reports using genetic approaches have provided compelling evidence that SKP2 is required for tumorigenesis upon BCR-ABL overexpression, PTEN loss or pRB inactivation (Agarwal et al., 2008; Frescas and Pagano, 2008; Lin et al., 2010; Wang et al., 2010). Further, overexpression of SKP2 is frequently observed in human prostate cancers and is significantly associated with cancer metastasis (Gstaiger et al., 2001; Hershko, 2008; Yang et al., 2002).

I-4. Transcription Factor EB (TFEB)

4.1 TFEB, a member of the MiTF family

TFEB is a basic helix-loop-helix leucine zipper (bHLH-Zip) transcription factor of the microphthalmia-associated transcription factor (MiTF) subfamily (Steingrímsson et al., 2004). There are four related genes in the MiTF family: TFE3, TFEB, TFEC and MiTF. The *Mitf* gene was isolated through transgene insertion events at the mouse *microphthalmia* locus (Hodgkinson et al., 1993) while the human *TFEB* and *TFE3*

genes were both isolated on the basis of their ability to bind the E-box sequence (CANNTG), the DNA sequence recognized by bHLH-Zip transcription factors. *TFEC* was isolated from rat osteosarcoma cDNA library based on sequence similarity to *TFE3* (Zhao et al., 1993). All four proteins have identical DNA binding domain and very similar HLH and Zip dimerization domains.

TFEB was first known as an oncogene as it was found to be translocated in a subset of renal tumors (Medendorp et al., 2007; Rehli et al., 1999). Indeed, TFEB and more commonly TFE3 are found fused to other genes in sporadic renal cell carcinoma (RCC) tumors. These gene-fusion associated kidney cancers are common in children, representing 20-50% of all pediatric RCC cases (Bruder et al., 2004; Ramphal et al., 2006). Although TFE3 fusion is associated with aggressive and metastatic cancer, the TFEB fusion carries good prognosis (Kauffman et al., 2014).

4.2 TFEB in autophagy

Recent studies have identified TFEB as a master transcriptional regulator of lysosomal biogenesis and autophagy (Sardiello et al., 2009; Settembre et al., 2011). TFEB rapidly moves into the nucleus to function as a transcription factor and activate critical target genes involved in lysosomal biogenesis and autophagy under starvation or lysosomal dysfunction, whereas under basal conditions, it is mainly located in the cytoplasm (David, 2011; Settembre and Ballabio, 2011). This process is controlled by TFEB phosphorylation status: phosphorylated TFEB is located predominantly in the cytoplasm, whereas the

dephosphorylated form is found in the nucleus. Phosphoproteomic approach revealed at least ten different phosphorylation sites and at least three different kinases involved in TFEB phosphorylation, suggesting a complex regulatory mechanism (Dephoure et al., 2008). TFEB specifically recognizes and binds to the coordinated lysosomal expression and regulation (CLEAR)-box sequence (GTCACGTGAC) present in the regulatory region of many lysosomal and autophagy genes (Palmieri et al., 2011) (Fig. I-3).

Interestingly, other members of the MITF family show similar sequences to TFEB. Their functions in lysosomal signaling and autophagy need to be defined but recent study has shown that TFE3 exhibit lysosomal localization and nuclear accumulation in response to lysosomal stress (Martina et al., 2014). It is proposed that TFE3 could also function as an important regulator of the lysosomal response and autophagy as for TFEB, depending on its relative abundance.

Accumulating evidence indicates that lysosomal and autophagy dysfunction is one of the main mechanisms underlying neurodegenerative diseases such as Parkinsosn's disease, Alzheimer's disease and Huntington's disease as well as lysosomal storage diseases (LSDs) (Ballabio and Gieselmann, 2009; Nixon, 2013; Settembre et al., 2008; Wong and Cuervo, 2010). Several studies supported the idea that enhancing the lysosomal-autophagic pathway could improve disease prognosis (Harris and Rubinsztein, 2012). With recent discovery of TFEB and its function in cellular clearance, targeting TFEB has been an appealing therapeutic strategy for treating common neurodegenerative diseases. As an example, TFEB gene delivery in a mouse model of Parkinson's disease ameliorated tissue pathology (Settembre et al., 2013b).

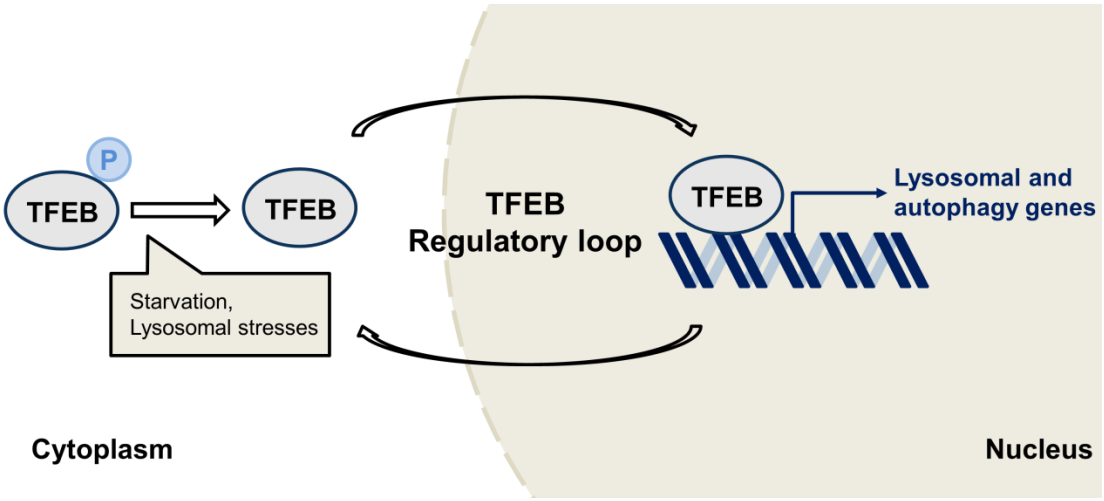

Figure I-3. Illustration of TFEB regulation and functions during starvation
In the presence of sufficient nutrients, TFEB is phosphorylated and localized in the cytoplasm. During starvation, TFEB is no longer phosphorylated and translocates into the nucleus. Once in the nucleus, TFEB regulates the expression of genes involved in the lysosomal–autophagy pathway

I-5. Autophagy

5.1 The autophagy pathway

Autophagy is an intracellular process that allows the degradation of cytoplasmic proteins and organelles by lysosome (Deter et al., 1967; Klionsky, 2007; Mizushima, 2007). It occurs at low basal levels in all cells to perform homeostatic functions. However, it is rapidly upregulated in response to stress including nutrient and energy starvation. The ability of cells to respond to nutrient withdrawal is essential for the maintenance of metabolic homeostasis and survival (Choi et al., 2013; Rabinowitz and White, 2010). For a long time, autophagy has been viewed as a relatively unspecific process where random portions of the cytoplasm are sequestered and delivered to lysosomes for degradations. However, accumulating evidence has led to revisit that notion. Indeed, studies have demonstrated that the autophagic machinery can target specific entities in a highly specific manner (Mizushima et al., 2008). At least three types of autophagy have been identified thus far: microautophagy, macroautophagy and chaperone-mediated autophagy (CMA). Both micro- and macroauotphagy have the ability to engulf large structures through both selective and non-selective mechanisms. CMA on the other hand is known to degrade soluble proteins only. Macroautophagy is the major catabolic mechanism that eukaryotic cells use to degrade damaged or long-lived proteins and organelles.

The earliest step of autophagy is characterized by the formation (vesicle nucleation) and expansion (vesicle elongation) of an isolation membrane called phagophore. The

edges of the phagophore then fuse (vesicle completion) to form a double-membraned vesicle called autophagosome and sequester cytoplasmic cargo. This is followed by fusion of the autophagosome with a lysosome to form an autolysosome where the captured cytoplasmic constituents, together with the inner membrane, are degraded (Fig. I-4).

5.2 Methods in mammalian autophagy research

There are three principal methods used to monitor autophagy: transmission electron microscopy (TEM), biochemical detection and fluorescence microscopy of the membrane-associated form of microtubule-associated protein light chain 3 (LC3) (Klionsky et al., 2012).

TEM was used in the 1950s to discover the process of autophagy and is still considered as the most classical method for monitoring autophagy. As the definition is straightforward, it is usually easy to identify autophagosomes, undigested cytoplasmic contents and autolysosomes. However, although TEM is a powerful tool, it is not perfect and other methods should be accompanied for proper interpretation.

In mammalian cells, most autophagy (ATG) proteins are observed on isolation membranes but not on complete autophagosomes (Longatti and Tooze, 2009). Only LC3, the mammalian homolog of yeast ATG8, is known to exist on autophagosomes. Therefore, LC3 protein serves as a widely used marker of autophagy occurrence and it is widely accepted that the number of LC3-II correlates well with the number of

autophagosomes (Mizushima and Yoshimori, 2007). To assess the number of autophagosomes endogenous conversion of LC3-I to LC3-II can be detected by immunoblot. As another widely used method, GFP-LC3 construct is visualized by fluorescence microscopy. GFP-LC3 is seen as a diffuse cytoplasmic pool or as punctate structures that primarily represent autophagosomes.

Although the number of GFP-LC3 puncta is usually an accurate measure of the autophagosome number, results could lead to misinterpretations of autophagy flux. Indeed, the accumulation of autophagosomes is not always indicative of autophagy induction but could be the results from increased generation of autophagosomes and/or block in autophagosome maturation and completion of the autophagy pathway. For proper interpretation of autophagy occurrence, autophagy flux should be monitored by LC3 turnover assay using autophagy inhibitors and degradation of autophagy substrates such as p62, also known as SQSTM1.

There are many available techniques and methods to monitor autophagy in mammalian cells. It is thus important to use several different methods to accurately assess the status and functions of autophagy activity in a given biological setting.

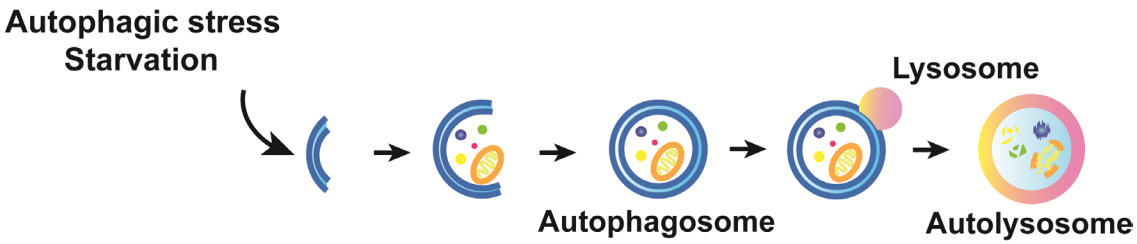

Figure I-4. Illustration of mammalian autophagy

Autophagy is triggered by starvation and starts with the stepwise engulfment of cytoplasmic material by the phagophore, which matures into a double-membrane-bound vesicle called autophagosome. Autophagosome then undergoes maturation by fusion with lysosomes to create autolysosomes. In the autolysosomes, the inner membrane and cargo inside are degraded by lysosomal enzymes.

5.3 Epigenetic and transcriptional regulation of autophagy

Many transcription factors regulating autophagy-related genes have been identified thus far, including forkhead box O (FOXO), p53, hypoxia inducible factor (HIF)-1α, and transcription factor EB (TFEB) (Eijkelenboom and Burgering, 2013; Maiuri et al., 2010; Mazure and Pouysségur, 2010; Pietrocola et al., 2013; Settembre and Ballabio, 2011).

Autophagy is mainly seen as a cytoplasmic event, but recent studies revealed that transcriptional regulation happening in the nucleus is critical for the fine tuning of the autophagy process (de Narvajas et al., 2013; Eisenberg et al., 2009; Füllgrabe et al., 2014b; Shao et al., 2004). Histone post-translational modifications (PTMs) including lysine acetylation, arginine and lysine methylation, phosphorylation, SUMOylation, and ubiquitination, serve as key regulatory marks for the control of transcription and chromatin architecture (Bannister and Kouzarides, 2011; Li et al., 2007). Histone PTMs, carried out by numerous modifying enzymes, need to be tightly regulated as mis-regulation is often a key factor in the development of diseases.

Studies on epigenetic modifications associated with autophagy have just begun and only few histone PTMs linked to autophagy have been reported. As an example, a decrease in lysine 16 of histone H4 acetylation (H4K16Ac) upon autophagy stimuli has been shown to be involved in the repression of key autophagy-regulated genes (Füllgrabe et al., 2013).

An increasing body of evidence suggests that epigenetic modifications influence the overall chromatin structure and have clear functional consequences in cellular processes including autophagy (Füllgrabe et al., 2014a). However, fine-tuning of autophagy

through epigenetic modifications has been mainly focused on acetylation and deacetylation of histone and non-histone proteins, whereas little has been known about other PTMs, including arginine methylation.

CHAPTER II

Increased H3R17 dimethylation by CARM1 is critical for starvation-induced autophagy

II-1. Summary

Autophagy is an intracellular process that allows the degradation of cytoplasmic proteins and organelles by lysosome in response to stress including nutrient starvation (Klionsky, 2007; Mizushima, 2007). Although autophagy is mainly seen as a cytoplasmic event, recent studies revealed that transcriptional regulation happening in the nucleus is critical for the autophagy process (de Narvajas et al., 2013; Eisenberg et al., 2009; Füllgrabe et al., 2014b; Shao et al., 2004). However, little has been known about the fine-tuning molecular basis of autophagy through epigenetic modifications.

To explore the importance of nuclear events in autophagy, I first hypothesized that specific histone marks are involved in the epigenetic and transcriptional regulation of autophagy in the nucleus leading to the fine-tuning of the autophagy process. Here, I found a dramatic increase in histone H3R17 dimethylation (H3R17me2) when autophagy was induced by various starvations. The induction in H3R17me2 resulted from the increase in nuclear CARM1 expression, the sole enzyme responsible for this epigenetic mark. Interestingly, I found that upon starvation CARM1 is stabilized whereas it is constantly degraded in the nucleus by SKP2-SCF E3 ligase complex under nutrient-rich condition. This regulation occurs mainly in the nucleus due to SKP2 exclusive nuclear localization. Further, I defined the detailed molecular mechanism of AMPK-mediated SKP2 downregulation and subsequent CARM1 stabilization upon glucose starvation. Together, I first define the new signaling axis of AMPK-SKP2-CARM1 in autophagy.

II-2. Intoduction

The ability of cells to respond to nutrient withdrawal is essential for the maintenance of metabolic homeostasis and survival (Choi et al., 2013; Rabinowitz and White, 2010). Autophagy-related genes (ATG) that are required for the formation of autophagosome and subsequent autophagy process are highly conserved among species (Mizushima, 2007; Mizushima and Komatsu, 2011; Yang and Klionsky, 2010). Studies using conditional KO mice of various ATG proteins have implicated autophagy in many physiological and pathological processes including neurodegenerative diseases and cancer (Kondo et al., 2005; Levine and Kroemer, 2008; Nixon, 2013; Wong and Cuervo, 2010).

Autophagy process may occur in three phases: a rapid response entirely mediated by post-translational protein modifications in the cytoplasm, followed by a delayed response where the expression of genes encoding proteins that regulate the autophagic flux are upregulated through activation of specific transcriptional machinery in the nucleus (Füllgrabe et al., 2014b; Kroemer et al., 2010). The last phase is characterized by transcriptional repression of autophagy genes to avoid prolonged and sustained autophagy that can potentially be lethal.

Autophagy is mainly seen as a cytoplasmic event, but activation of specific epigenetic and transcriptional programs has emerged as indispensable event for a sustained response to autophagy (de Narvajas et al., 2013; Eisenberg et al., 2009; Füllgrabe et al., 2014b; Shao et al., 2004). Transcriptional regulation of autophagy genes is coupled to

changes in histone modifications to consistently replenish the materials of autophagy machinery and sustain autophagy. Histone post-translational modifications (PTMs) carried out by numerous modifying enzymes, on the other hand, need to be tightly regulated as mis-regulation is often a key factor in the development of diseases. Studies on epigenetic modifications associated with autophagy have just begun and only few histone PTMs linked to autophagy have been reported (Füllgrabe et al., 2013; de Narvajas et al., 2013). An increasing body of evidence suggests that epigenetic modifications influence the overall chromatin structure and have clear functional consequences in cellular processes, including autophagy (Füllgrabe et al., 2014a). Indeed, it is now well-accepted that the nucleus is a major regulator of autophagy and that the autophagic process encompasses epigenetic and transcriptional programs. Studies of the nucleus in autophagy research are on-going as little is known about PTMs on histones and non-histone proteins other than phosphorylation and acetylation.

II-3. Results

Starvation-induced autophagy is accompanied by an increase in histone H3R17 dimethylation

To explore the importance of nuclear events in autophagy, I first hypothesized that specific histone marks are involved in the epigenetic and transcriptional regulation of autophagy in the nucleus leading to the fine-tuning of the autophagy process. I induced autophagy in mouse embryonic fibroblasts (MEFs) by glucose starvation and sought to identify altered specific histone marks. Surprisingly, I observed an increase of histone H3R17dimethylation (H3R17me2) among other histone modification marks tested in response to glucose starvation (Fig. II-1A). Since H3R17me2 is a transcriptional activation mark that is solely mediated by CARM1 arginine methyltransferase, I checked for CARM1 protein levels in cells deprived of glucose. Concomitant with an increase in H3R17me2 levels, levels of CARM1 protein were increased in various human cell lines including HepG2 and HeLa cells under glucose starvation (Fig. II-1B).

To examine whether this H3R17me2 increase along with CARM1 induction is related to the occurrence of autophagy, I analyzed LC3 conversion by immunoblot as an increased ratio of the lipidated LC3-II form to the unlipidated LC3-I is a commonly used biological marker of autophagy (Mizushima and Yoshimori, 2007). The increase of CARM1 protein levels was concomitant with an increase in LC3 conversion, and LC3-II accumulation was significantly decreased upon CARM1 depletion (Fig. II-1C-D). To confirm that the decrease in LC3-II reflects the decrease of functional autophagic

degradation, autophagy flux was also analyzed using the levels of autophagy-associated p62 (also known as SQSTM1), a common autophagosome cargo whose degradation reflects the levels of autophagy flux (Bjørkøy et al., 2009; Mizushima et al., 2010). The accumulation of p62 when CARM1 is depleted further supports that autophagy is blocked (Fig. II-1D).

To further examine whether the enzymatic activity of CARM1 is important in autophagy induction, *Carm1* knockin (KI) MEFs expressing the enzymatic activity-deficient mutant of CARM1 were analyzed for LC3 conversion and p62 degradation. Glucose starvation induced LC3-II accumulation and p62 degradation in WT MEFs but not in *Carm1* KO and KI MEFs (Fig. II-1D). It has been previously reported that *Carm1* KI mice phenocopy *Carm1* KO mice, emphasizing the importance of its enzymatic activity for *in vivo* function (Kim et al., 2010a). Consistent with these findings, *Carm1* KO and KI MEFs showed similar defect of autophagy induction upon glucose starvation.

To evaluate the role of CARM1 in the autophagy process, the formation of GFP-LC3 positive autophagosome was examined by confocal microscopy. The increase in GFP-LC3 punctate cells was strikingly attenuated in *Carm1* KO MEFs compared to WT MEFs upon glucose starvation (Fig. II-1E). Further, autophagosome/autolysosome formation was analyzed by electron microscopy in WT, *Carm1* KO and KI MEFs. Glucose starvation increased the number of autophagic vesicles in WT MEFs, but such double-membrane structures did not appear in *Carm1* KO and KI MEFs (Fig. II-1F).

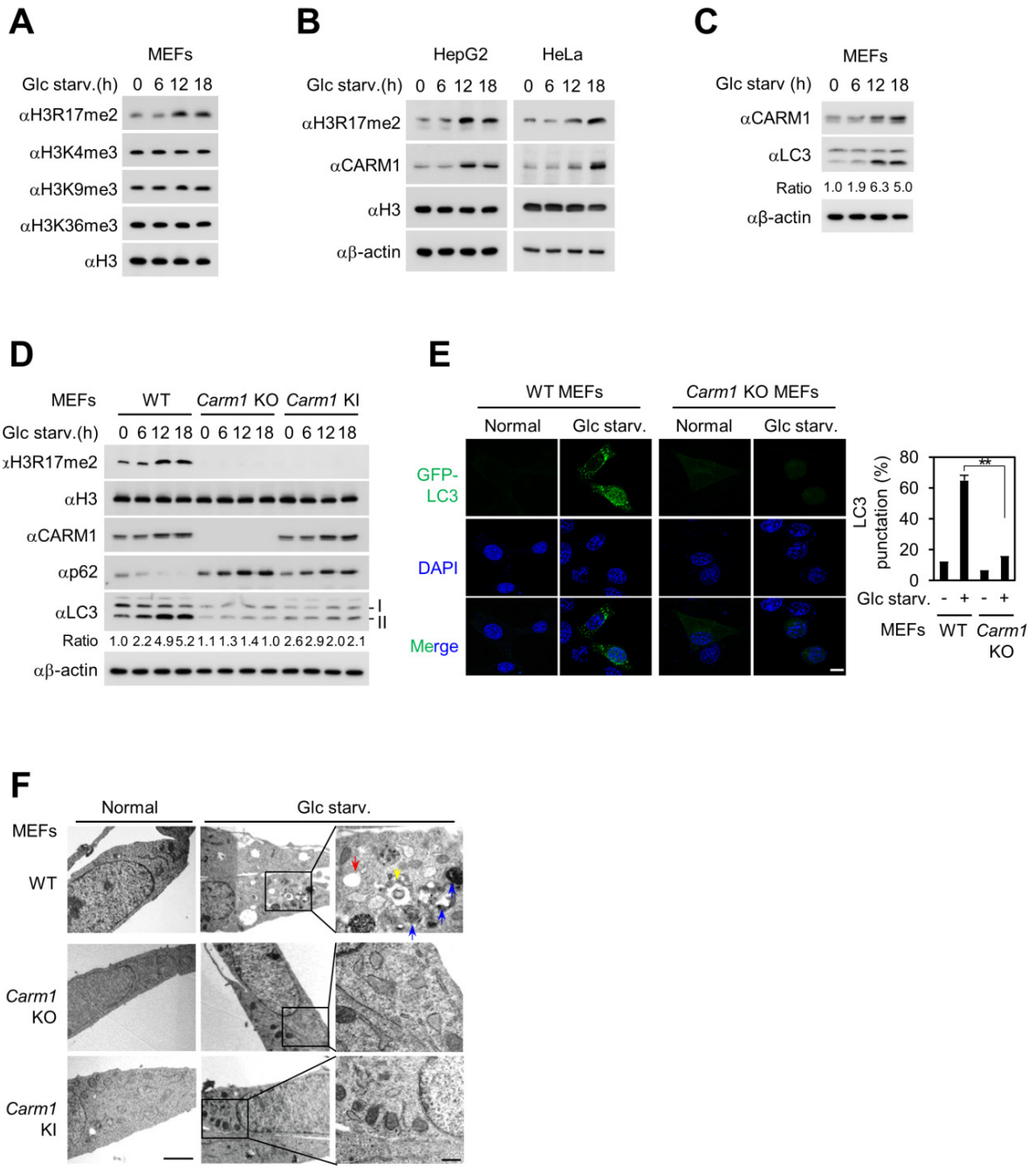
A
MEFs
Glc starv.(h) 0 6 12 18
αH3R17me2
αH3K4me3
αH3K9me3
αH3K36me3
αH3
B
HepG2
HeLa
Glc starv.(h) 0 6 12 18 0 6 12 18
αH3R17me2
αCARM1
αH3
αβ-actin
C
MEFs
Glc starv (h) 0 6 12 18
αCARM1
αLC3
Ratio 1.0 1.9 6.3 5.0
αβ-actin
D
MEFs WT Carm1 KO Carm1 KI
Glc starv.(h) 0 6 12 18 0 6 12 18 0 6 12 18
αH3R17me2
αH3
αCARM1
αp62
αLC3
I
II
Ratio 1.0 2.2 4.9 5.2 1.1 1.3 1.4 1.0 2.6 2.9 2.0 2.1
αβ-actin
E
WT MEFs
Carm1 KO MEFs
Normal
Glc starv.
Normal
Glc starv.
GFP-LC3
DAPI
Merge
LC3 punctation (%)
80
60
40
20
0
**
Glc starv. - + - +
MEFs WT Carm1 KO
F
Normal
Glc starv.
MEFs
WT
Carm1 KO
Carm1 KI

Figure II-1. Increased H3R17 dimethylation by CARM1 is critical for proper autophagy

(**A**) Immunoblot analysis of various histone marks in MEFs in response to glucose (Glc) starvation for indicated times. h=hours. (**B**) Increase in H3R17me2 and CARM1 protein levels in HepG2 and HeLa cells in response to Glc starvation as assessed by immunoblot analysis. (**C**) Immunoblot analysis of CARM1 and lipidated LC3 (LC3-II) upon Glc starvation in MEFs. LC3-II/LC3-I ratio is indicated. (**D**) Cell lysates of WT, *Carm1* KO or KI MEFs starved of Glc for indicated times were subject to immunoblot analysis with the indicated antibodies. LC3-II/LC3-I ratio is indicated. (**E**) GFP-LC3 was transfected in WT or *Carm1* KO MEFs and the formation of GFP-LC3-positive autophagosomes was examined by confocal microscopy. GFP-LC3 (green); DAPI (blue). Scale bar, 10 μm. The graph shows quantification of LC3-positive punctate cells (right). ** $p<0.01$. Statistics by one-tailed *t*-test. (**F**) Representative transmission electron micrograph (TEM) images of WT, *Carm1* KO or KI MEFs after 18 hours (hrs) of Glc starvation. Scale bar, 2 μm. High magnification of boxed areas are shown on the right. Scale bar, 0.5 μm. Blue arrows represent autophagosomes, red arrows represent autolysosomes and yellow arrow represents multilamellar body.

Autophagy flux analysis confirmed the autophagic defect caused by CARM1 loss

I performed LC3 flux analysis in MEFs by knockdown of CARM1 or in WT and *Carm1* KO MEFs using Bafilomycin A1, an inhibitor of the late phase of autophagy, which prevents maturation of autophagic vacuoles by inhibiting fusion between autophagosomes and lysosomes (Yamamoto et al., 1998). Immunoblot analysis in *Carm1* knockdown or KO MEFs indicates a defect in autophagy flux as there was no accumulation of LC3-II when treated with Bafilomycin A1 (Fig. II-2A-B). Moreover, imaging experiments with the mCherry-GFP-LC3 construct which provides a simultaneous readout of autophagosome formation (mCherry-positive and GFP-positive) and maturation (mCherry-positive and GFP-negative) further validated autophagy defect upon CARM1 loss. Indeed, inhibiting lysosomal acidification by Bafilomycin A1 prevented GFP quenching and resulted in merged yellow puncta signals upon glucose starvation in WT MEFs, but not in *Carm1* KO MEFs (Fig. II-2C). Taken altogether, these findings indicate that the autophagic defect caused by CARM1 loss is the result of defect from the initiation step.

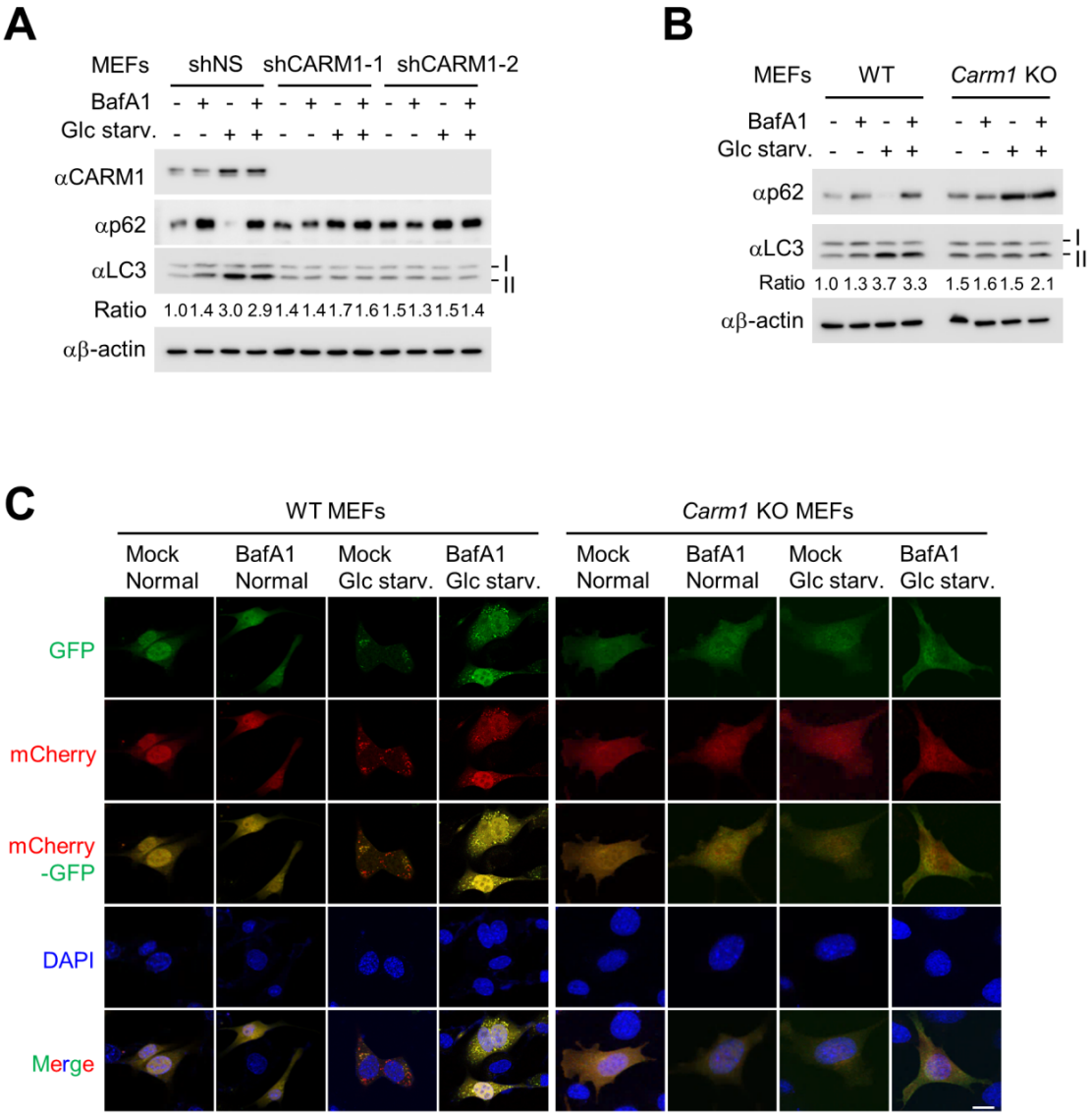
A
MEFs
shNS
shCARM1-1
shCARM1-2
BafA1
Glc starv.
αCARM1
αp62
αLC3
I
II
Ratio
1.0 1.4 3.0 2.9 1.4 1.4 1.7 1.6 1.5 1.3 1.5 1.4
αβ-actin
B
MEFs
WT
Carm1 KO
BafA1
Glc starv.
αp62
αLC3
I
II
Ratio
1.0 1.3 3.7 3.3 1.5 1.6 1.5 2.1
αβ-actin
C
WT MEFs
Carm1 KO MEFs
Mock Normal
BafA1 Normal
Mock Glc starv.
BafA1 Glc starv.
GFP
mCherry
mCherry -GFP
DAPI
Merge

Figure II-2. Autophagy flux analysis after CARM1 loss

(**A**) MEFs infected with lentiviruses expressing nonspecific shRNA (shNS) or CARM1 shRNAs (shCARM1-1 and -2) were deprived of Glc for 18 hours (hrs) in the absence or presence of Bafilomycin A1 (BafA1; 200 nM, 2 hrs). Immunoblot analysis was performed with the indicated antibodies. LC3-II/LC3-I ratio is indicated. (**B**) LC3 flux was analyzed in WT and *Carm1* KO MEFs after cells were Glc starved in the absence or presence of BafA1. LC3-II/LC3-I ratio is indicated. (**C**) mCherry-GFP-LC3 was transfected in WT and *Carm1* KO MEFs and the formation of autophagosome (mCherry-positive; GFP-positive) and autolysosome (mCherry-positive; GFP-negative) were examined. Scale bar, 20 μm.

Increased H3R17me2 by CARM1 occurs in amino-acid starvation-induced autophagy

To determine whether the increase of H3R17me2 mark also occurs when autophagy is triggered by other types of starvation, I induced autophagy by amino acid starvation or rapamycin, an inhibitor of the kinase mammalian target of rapamycin (mTOR) in MEFs. Increase in H3R17me2 and induction of CARM1 was also observed when cells were subject to amino acid starvation or rapamycin treatment (Fig. II-3A-C). CARM1 is a critical component in proper autophagy occurrence in response to these upstream signals as increase of LC3-II and degradation of p62 were severely compromised in *Carm1* KO or KI MEFs (Fig. II-3D). The lack of GFP-LC3 positive puncta in *Carm1* KO MEFs further validated the importance of CARM1 induction and subsequent increase in H3R17me2 in amino acid starvation-mediated autophagy (Fig. II-3E).

Together, these data indicate that the induction of CARM1 in association with increased H3R17me2 is required for the proper progression of the autophagy process.

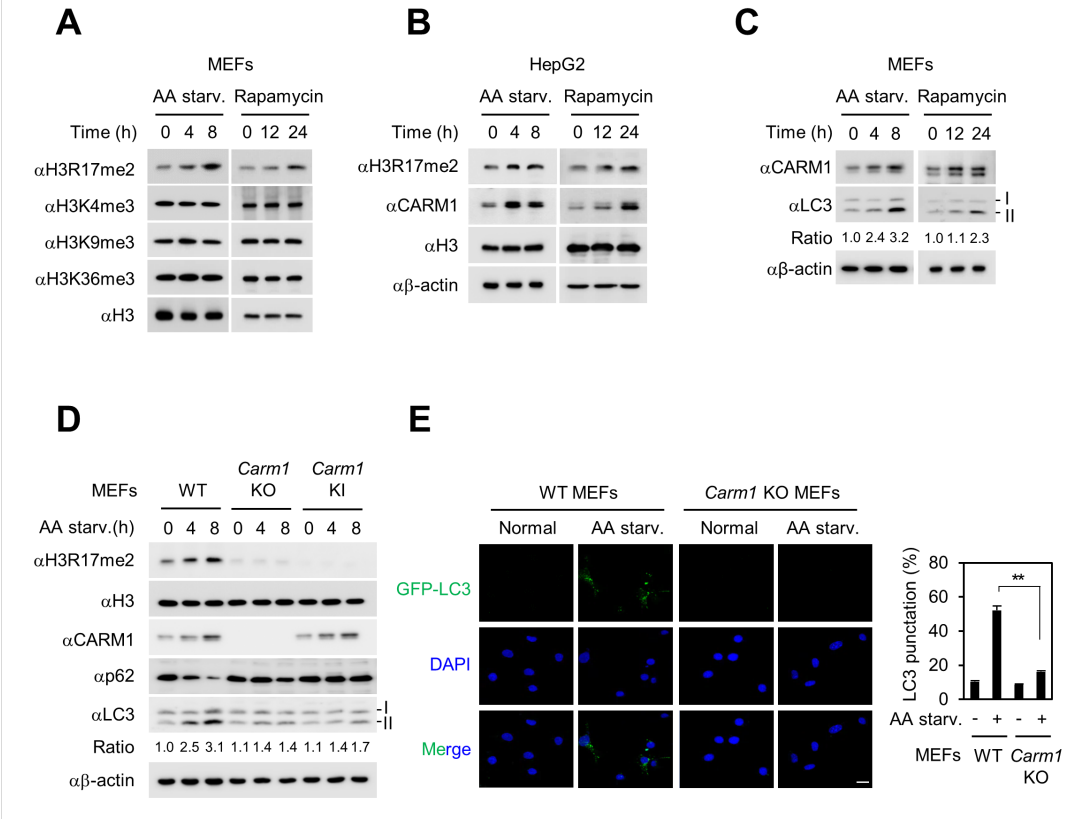

Figure II-3. Increased H3R17me2 by CARM1 in amino-acid starvation-induced autophagy

(**A**) Immunoblot analysis of various histone marks in MEFs in response to amino acid (AA) starvation or rapamycin (100 nM) for indicated times. h=hours. (**B**) Increase in H3R17me2 and CARM1 protein levels in HepG2 cells in response to AA starvation and rapamycin as assessed by immunoblot analysis. (**C**) Immunoblot analysis of CARM1 and lipidated LC3 (LC3-II) upon AA starvation or rapamycin treatment in MEFs. (**D**) Cell lysates of WT, *Carm1* KO or KI MEFs starved of AA for indicated times were subject to immunoblot analysis with the indicated antibodies. (**E**) GFP-LC3 was transfected in WT or *Carm1* KO MEFs and the formation of GFP-LC3-positive autophagosomes was examined by confocal microscopy. GFP-LC3 (green); DAPI (blue). Scale bar, 20 μm. The graph shows quantification of LC3-positive punctate cells (right). **p<0.01. Statistics by one-tailed *t*-test.

Ellagic acid impairs starvation-induced autophagy

Ellagic acid, a naturally occurring polyphenol, selectively inhibits H3R17me2 (Selvi et al., 2010). Decrease in H3R17me2 by ellagic acid was confirmed by immunoblot (Fig. II-4A and C). Then, to examine whether CARM1-mediated increase of H3R17me2 is critical for autophagy occurrence, GFP-LC3 was introduced in MEFs to monitor GFP-LC3 positive autophagic vesicles when cells were treated with ellagic acid along with autophagy induction. Decrease in H3R17me2 by ellagic acid greatly reduced the number of GFP-LC3 positive punctate cells (Fig. II-4B and D). I treated cells with ellagic acid when nutrient deprived and checked for changes in autophagy markers. Treatment of ellagic acid dramatically reduced LC3-II level and blocked p62 degradation (Fig. II-4A and C), indicating that the autophagy process is compromised. These findings substantiate the model that increase in H3R17me2 in nutrient deprived state is critical for proper autophagy occurrence.

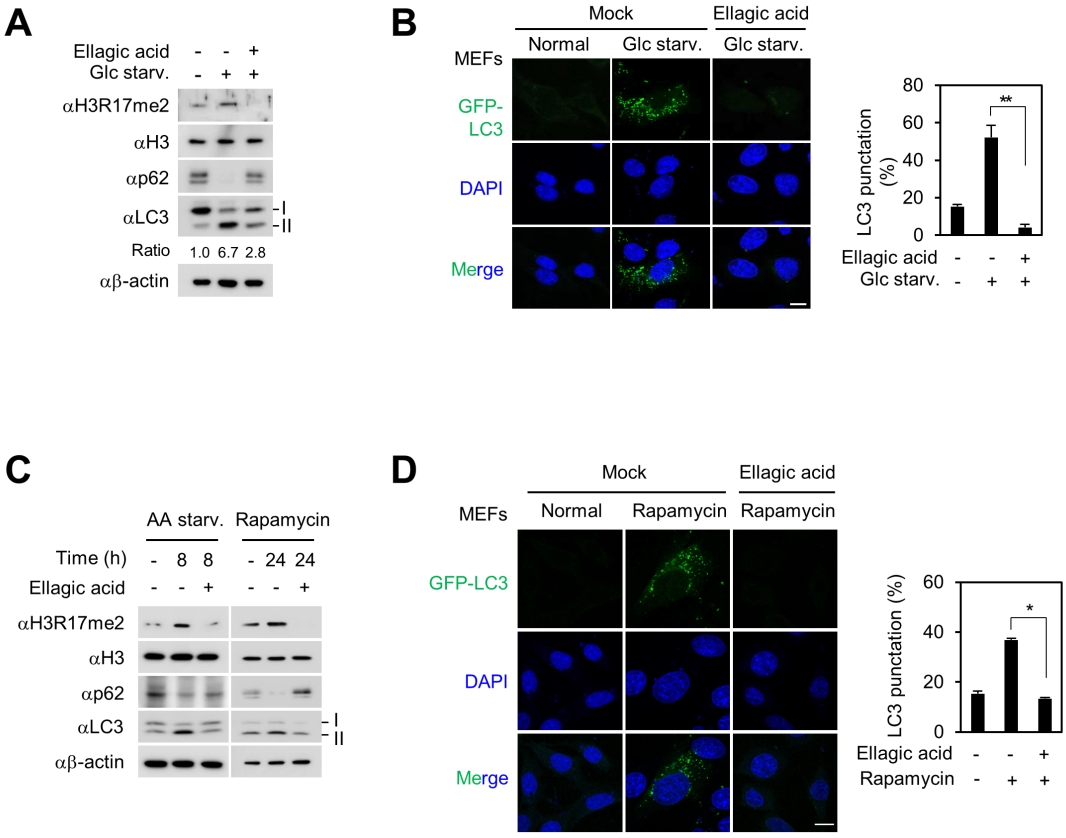
A
Ellagic acid - - +
Glc starv. - + +
αH3R17me2
αH3
αp62
αLC3
I
II
Ratio 1.0 6.7 2.8
αβ-actin
B
Mock
Ellagic acid
MEFs
Normal
Glc starv.
Glc starv.
GFP-LC3
DAPI
Merge
LC3 punctation (%)
80
60
40
20
0
**
Ellagic acid - - +
Glc starv. - + +
C
AA starv.
Rapamycin
Time (h) - 8 8 - 24 24
Ellagic acid - - + - - +
αH3R17me2
αH3
αp62
αLC3
I
II
αβ-actin
D
Mock
Ellagic acid
MEFs
Normal
Rapamycin
Rapamycin
GFP-LC3
DAPI
Merge
LC3 punctation (%)
60
40
20
0
*
Ellagic acid - - +
Rapamycin - + +

Figure II-4. Ellagic acid impairs starvation-induced autophagy

(**A**) Immunoblot analysis in MEFs deprived of Glc in the absence or presence of ellagic acid (100 μM) was performed with the indicated antibodies. (**B**) MEFs transfected with GFP-LC3 were deprived of Glc in the absence or presence of ellagic acid (100 μM) and GFP-LC3 puncta formation was observed with a confocal microscopy. GFP-LC3 (green); DAPI (blue). Scale bar, 10 μm. The graph shows quantification of LC3-positive punctate cells (below). ** $p<0.01$. Statistics by one-tailed *t*-test. **(C)** MEFs were either AA starved or treated with rapamycin for indicated times in the absence or presence of ellagic acid. Immunoblot analysis was performed with the indicated antibodies. h=hours. (**D**) MEFs transfected with GFP-LC3 were treated with rapamycin in the absence or presence of ellagic acid (100 μM) and GFP-LC3 puncta formation was observed with a confocal microscopy. GFP-LC3 (green); DAPI (blue). Scale bar, 10 μm. The graph shows quantification of LC3-positive punctate cells (left). *$p<0.05$. Statistics by one-tailed *t*-test.

Regulation of CARM1 stability by SKP2-SCF E3 ubiquitin ligase-dependent degradation in the nucleus

Since CARM1 turned out to be critical for autophagy occurrence, I examined how CARM1 induction is regulated upon glucose starvation. Unexpectedly, I found that CARM1 protein level is increased only in the nucleus, but not in the cytoplasm, upon glucose starvation (Fig. II-5A, left panel). To examine whether CARM1 protein levels are regulated by 26S proteasome-dependent degradation in the nucleus, I treated cells with MG132, a 26S proteasome inhibitor. MG132 treatment restored CARM1 expression in the nucleus (Figure II-5A, right panel). Ubiquitination site prediction software predicted lysine 471 site of CARM1 as an ubiquitination site (Chen et al., 2013) and I performed site-directed mutagenesis of lysine 471 to arginine and compared its expression with CARM1 WT. CARM1 K471R mutant exhibited comparable expression levels in the nucleus with or without MG132 treatment (Fig. II-5B). Further, ubiquitination of CARM1 K471R mutant was dramatically reduced in the nucleus compared to WT, indicating that K471 site is the ubiquitination targeting site (Fig. II-5C). It is noteworthy that ubiquitination-dependent regulation of CARM1 stability occurs mainly in the nucleus.

In order to identify the E3 ubiquitin ligase responsible for CARM1 ubiquitination, I employed affinity chromatography in the presence of MG132 to block ubiquitin-dependent degradation pathway. CARM1 interacting proteins were then identified by liquid chromatography mass spectrometry/mass spectrometry (LC-MS/MS). Intriguingly, S-phase kinase 2 (SKP2), an F-box protein of the SCF E3 ubiquitin ligase

complex was identified as CARM1 binding protein along with cullin1 (CUL1) (Fig. II-5D). Interaction between CARM1 and SKP2 was confirmed by endogenous co-immunoprecipitation assay and SKP2 exhibited specific binding to CARM1, but not to other arginine methyltransferases (Fig. II-5E).

Since CARM1 is stabilized upon glucose starvation, I checked for endogenous SKP2 protein level changes upon glucose starvation. Interestingly, reduction of SKP2 protein and increase of CARM1 protein levels were observed in glucose-starved MEFs and HepG2 cells (Fig. II-5F). CUL1 protein levels on the other hand were not affected by glucose starvation (Fig. II-5F). Decreased levels of SKP2 under glucose starvation resulted in the stabilization of other known SKP2-SCF substrates including p21, p27 and cyclin E (Fig. II-5G).

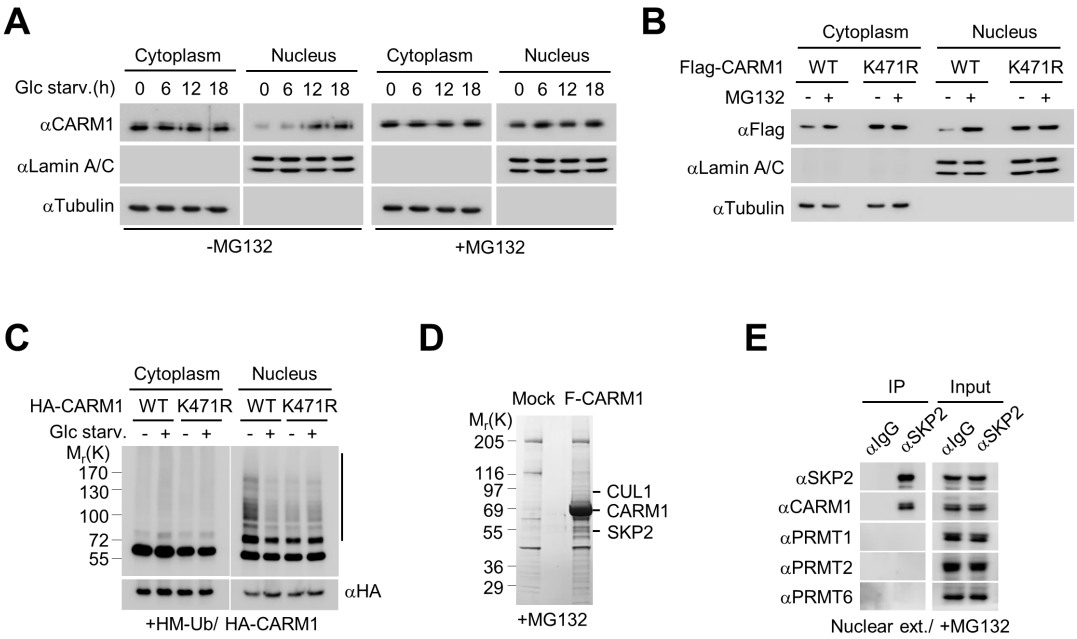
A
Cytoplasm
Nucleus
Cytoplasm
Nucleus
Glc starv.(h) 0 6 12 18 0 6 12 18 0 6 12 18 0 6 12 18
αCARM1
αLamin A/C
αTubulin
-MG132
+MG132
B
Cytoplasm
Nucleus
Flag-CARM1 WT K471R WT K471R
MG132 - + - + - + - +
αFlag
αLamin A/C
αTubulin
C
Cytoplasm
Nucleus
HA-CARM1 WT K471R WT K471R
Glc starv. - + - + - + - +
Mr(K)
170
130
100
72
55
αHA
+HM-Ub/ HA-CARM1
D
Mock F-CARM1
Mr(K)
205
116
97
69
55
36
29
CUL1
CARM1
SKP2
+MG132
E
IP
Input
αIgG αSKP2 αIgG αSKP2
αSKP2
αCARM1
αPRMT1
αPRMT2
αPRMT6
Nuclear ext./ +MG132
F
HepG2
MEFs
Glc starv.(h) 0 6 12 18 0 6 12 18
αSKP2
αCARM1
αCUL1
αLamin A/C
G
HepG2
MEFs
Glc Starv.(h) 0 6 12 18 0 6 12 18
αp21
αp27
αCyclinE
αLamin A/C

Figure II-5. CARM1 is ubiquitinated at K471 site and interacts with SKP2-SCF E3 ligase in the nucleus under nutrient-rich condition

(A) MEFs were deprived of Glc for indicated times in the absence (left) or presence (right) of 5 μg/ml MG132, a proteasome inhibitor. Immunoblot analysis was performed after subcellular fractionation with the indicated antibodies. h=hours. (**B**) CARM1 WT and ubiquitination-defective mutant K471R were analyzed for their expression in MEFs after MG132 treatment. (**C**) *In vivo* ubiquitination assay of CARM1 WT or ubiquitination-defective mutant K471R was conducted in HepG2 cells. After 48 hrs of transfection with HA-CARM1 WT or K471R and HisMax-ubiquitin, HepG2 cells were treated with MG132 for 4 hours (hrs) and harvested for subcellular fractionation. Cytoplasmic and nuclear fractions were pulled down with Ni^{2+}-NTA beads and CARM1 was visualized by immunoblot with anti-HA antibody. (**D**) CARM1-interacting proteins were purified from HEK293T cells expressing Flag-CARM1 in the presence of MG132 by immunoprecipitation with Flag-M2 agarose bead. Bound proteins were eluted, resolved by SDS-PAGE, and prepared for LC-MS/MS analysis. (**E**) MEFs cells were treated with MG132 for 4 hrs and nuclear fraction was subject to immunoprecipitation against control IgG or anti-SKP2 antibody at endogenous expression level. Co-immunoprecipitation of CARM1 and other PRMTs were detected by immunoblot analysis. (**F**) HepG2 cells and WT MEFs were Glc starved for indicated times and nuclear fraction was analyzed for SKP2, CARM1, and CUL1 expression. (**G**) Nuclear fractions of HepG2 and MEFs cells were analyzed for the expression of known SKP2-SCF substrates.

CARM1 is degraded by SKP2-containing SCF E3 ligase in the nucleus under nutrient-rich condition

To determine whether SKP2 is responsible for CARM1 ubiquitination and degradation, I checked for changes in CARM1 ubiquitination upon knockdown of SKP2. Knockdown of SKP2 by shRNA attenuated CARM1 ubiquitination in the nucleus, with no apparent change in the cytoplasm (Fig. II-6A). I then measured the half-life of the CARM1 protein with cycloheximide (CHX) treatment. Knockdown of SKP2 significantly increased the half-life of CARM1 protein (Fig. II-6B). In contrast, overexpression of SKP2 WT, but not SKP2 ΔF mutant which is not able to form a SKP2-SCF complex (Carrano et al., 1999), increased CARM1 ubiquitination in the nucleus upon glucose starvation (Fig. II-6C). Consistently, overexpression of SKP2 WT, but not the ΔF mutant, decreased the half-life of CARM1 protein upon glucose starvation (Fig. II-6D). These data indicate that SKP2 is a crucial player for regulating CARM1 stability in the nucleus. I speculate that exclusive nuclear localization of SKP2 results in selective CARM1 ubiquitination in the nucleus under nutrient rich condition. Further, immunocytochemistry showed that introduction of SKP2 WT, but not SKP2 ΔF mutant, decreased CARM1 protein level in cells deprived of glucose (Fig. II-6E). Collectively, these data indicate that SKP2-containing SCF E3 ligase complex is responsible for CARM1 degradation in the nucleus under nutrient rich condition (Fig. II-6F).

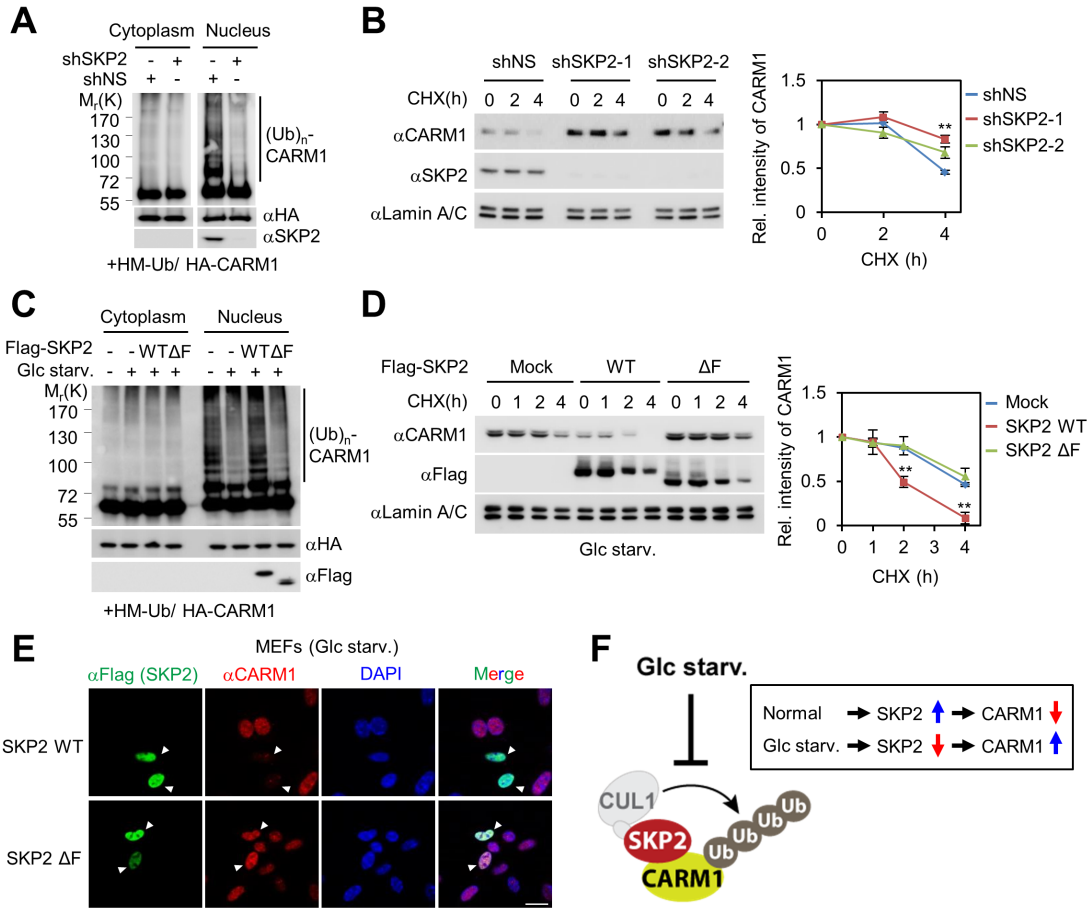
A
Cytoplasm
Nucleus
shSKP2 - + - +
shNS + - + -
Mr(K)
170
130
100
72
55
(Ub)n-CARM1
αHA
αSKP2
+HM-Ub/ HA-CARM1
B
shNS
shSKP2-1
shSKP2-2
CHX(h) 0 2 4 0 2 4 0 2 4
αCARM1
αSKP2
αLamin A/C
Rel. intensity of CARM1
1.5
1
0.5
0
0
2
4
CHX (h)
shNS
shSKP2-1
shSKP2-2
C
Cytoplasm
Nucleus
Flag-SKP2 - - WT ΔF - - WT ΔF
Glc starv. - + + + - + + +
Mr(K)
170
130
100
72
55
(Ub)n-CARM1
αHA
αFlag
+HM-Ub/ HA-CARM1
D
Flag-SKP2
Mock
WT
ΔF
CHX(h) 0 1 2 4 0 1 2 4 0 1 2 4
αCARM1
αFlag
αLamin A/C
Glc starv.
Rel. intensity of CARM1
1.5
1
0.5
0
0
1
2
3
4
CHX (h)
Mock
SKP2 WT
SKP2 ΔF
E
MEFs (Glc starv.)
αFlag (SKP2)
αCARM1
DAPI
Merge
SKP2 WT
SKP2 ΔF
F
Glc starv.
Normal → SKP2 ↑ → CARM1 ↓
Glc starv. → SKP2 ↓ → CARM1 ↑
CUL1
SKP2
CARM1
Ub
Ub
Ub
Ub

Figure II-6. CARM1 is degraded by SKP2-containing SCF E3 ligase in the nucleus under nutrient-rich condition

(A) HepG2 cells were infected with SKP2 shRNA lentivirus and *in vivo* ubiquitination assay of CARM1 was performed. (**B**) HepG2 cells were infected with 2 different SKP2 shRNA lentiviruses and treated with cycloheximide (CHX, 50 μg/ml) for indicated times. Nuclear fraction was then analyzed for indicated antibodies. The protein half-life of CARM1 was quantitatively defined (right). **p<0.01. Statistics by one-tailed *t*-test. h=hours. (**C**) HepG2 cells were transiently transfected with indicated plasmids and subject to Glc starvation for 18 hrs. Cells were treated with MG132 for 4 hrs prior harvesting and *in vivo* ubiquitination assay of CARM1 was performed. (**D**) HepG2 cells were transiently transfected with SKP2 WT or ΔF mutant, Glc starved and treated with CHX for indicated times. Nuclear fraction was then analyzed for indicated antibodies. Protein half-life of CARM1 was quantitatively defined (right). **p<0.01. Statistics by one-tailed *t*-test. (**E**) MEFs were transfected with Flag-SKP2 WT or ΔF mutant and Glc starved for 18 hrs. Cells were fixed for immunocytochemistry and examined by confocal microscopy. Flag-SKP2 (green); CARM1 (red); DAPI (blue). Scale bar 20 μm. (**F**) Schematics of SKP2-SCF E3 ligase complex-dependent degradation of CARM1 (left). Schematics of newly identified SKP2-CARM1 signaling axis in starvation-induced autophagy (left).

CARM1 is degraded by SKP2/CUL1-containing SCF E3 ligase in the nucleus under nutrient-rich condition

Among E3 ubiquitin ligase family members, there are cullin family (CUL1, 2, 3, 4A, 4B, 5 and 7) and each cullin allows interaction with specific adaptors by acting as a scaffold (Petroski and Deshaies, 2005). Since SKP2 is part of the SCF complex and CUL1 was identified as a binding partner of CARM1 (Fig. II-5D), I checked whether CARM1 could bind CUL1. Interestingly, among cullin family members tested, CARM1 specifically bound CUL1 (Fig. II-7A). More importantly, as a result of SKP2 down-regulation, the interaction between CUL1 and CARM1 was significantly decreased upon glucose starvation (Fig. II-7B). To examine whether CUL1 is responsible for CARM1 ubiquitination as a component of the SKP2-containing SCF E3 ligase complex, I performed ubiquitination assay by knockdown of CUL1. CUL1 depletion attenuated CARM1 ubiquitination in the nucleus (Fig. II-7C). In contrast, overexpression of CUL1 WT, but not CUL1 K720R mutant which has impaired E3 ubiquitin ligase activity, increased CARM1 ubiquitination in the nucleus (Fig. II-7D). Consistently, knockdown of CUL1 increased the protein half-life of CARM1 (Fig. II-7E), whereas overexpression of CUL1 WT, but not the K720R mutant, decreased the half-life of CARM1 (Fig. II-7F). Collectively, these data indicate that SKP2- and CUL1-containing SCF E3 ligase complex is responsible for CARM1 degradation in the nucleus under nutrient rich condition (Fig. II-6F).

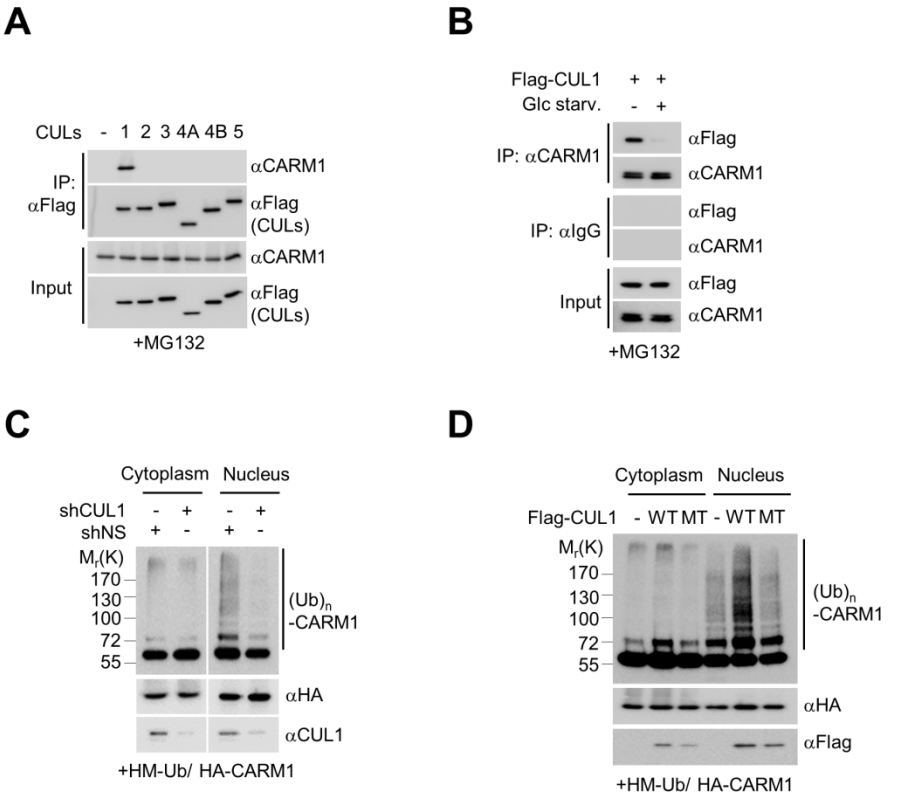
A
CULs - 1 2 3 4A 4B 5
IP: αFlag
αCARM1
αFlag (CULs)
Input
αCARM1
αFlag (CULs)
+MG132
B
Flag-CUL1 + +
Glc starv. - +
IP: αCARM1
αFlag
αCARM1
IP: αIgG
αFlag
αCARM1
Input
αFlag
αCARM1
+MG132
C
Cytoplasm Nucleus
shCUL1 - + - +
shNS + - + -
Mr(K)
170
130
100
72
55
(Ub)n -CARM1
αHA
αCUL1
+HM-Ub/ HA-CARM1
D
Cytoplasm Nucleus
Flag-CUL1 - WT MT - WT MT
Mr(K)
170
130
100
72
55
(Ub)n -CARM1
αHA
αFlag
+HM-Ub/ HA-CARM1
E
shNS shCUL1-1 shCUL1-2
CHX (h) 0 2 4 0 2 4 0 2 4
αCARM1
αCUL1
αLamin A/C
Rel. intensity of CARM1
1.5
1
0.5
0
0 2 4
CHX (h)
shNS
shCUL1-1
shCUL1-2
F
Flag-CUL1 Mock WT MT
CHX (h) 0 1 2 4 0 1 2 4 0 1 2 4
αCARM1
αFlag
αLamin A/C
Rel. intensity of CARM1
1
0.5
0
0 1 2 3 4
CHX (h)
Mock
CUL1 WT
CUL1 MT

Figure II-7. CARM1 is degraded by SKP2/CUL1-containing SCF E3 ligase in the nucleus under nutrient-rich condition

(A) HepG2 cells were transiently transfected with Flag-tagged CULs. Cells were treated with MG132 for 4 hrs prior harvesting and Flag-CUL 1, 2, 3, 4A, 4B or 5 was immunoprecipitated with anti-Flag antibody and co-immunoprecipitated CARM1 was detected by immunoblot analysis against anti-CARM1 antibody. (**B**) HepG2 cells transfected with Flag-CUL1 were deprived of Glc for 18 hrs and treated with MG132 prior harvesting. Interaction between CARM1 and CUL1 was analyzed. (**C**) HepG2 cells were infected with either nonspecific shRNA (shNS) or CUL1 shRNA (shCUL1) lentivirus and *in vivo* ubiquitination assay of CARM1 was performed. (**D**) *In vivo* ubiquitination assay of CARM1 using CUL1 WT or K720R mutant (MT). (**E**) HepG2 cells infected with 2 different CUL1 shRNA lentiviruses were subject to cycloheximide (CHX) experiment (left). Protein half-life of CARM1 was quantitatively defined (right). (**F**) CHX experiment in HepG2 expressing CUL1 WT or K720R MT (left). Protein half-life of CARM1 was quantitatively defined (right).*p< 0.05, **p<0.01. Statistics by one-tailed *t*-test.

AMPKα2 accumulates in the nucleus and is transcriptionally induced upon glucose starvation

It has been shown that AMP-activated protein kinase (AMPK) is activated during glucose starvation and leads to starvation-induced autophagy (Hardie, 2011; Inoki et al., 2012; Mihaylova and Shaw, 2011). AMPK activates autophagy through its ability to inactivate mTOR (Gwinn et al., 2008; Inoki et al., 2003) and by direct phosphorylation of ULK1 (Egan et al., 2011; Kim et al., 2011) and other autophagy components (Kim et al., 2013b), all of which occur in the cytoplasm. As the role of nuclear AMPK in the outcome of autophagy has not been defined thus far, I aim to examine whether AMPK is involved in transcriptional response to autophagy. Intriguingly, I found that unlike AMPKα1, AMPKα2 protein level and phosphorylated AMPK, the activated form of AMPK, increased in the nucleus upon glucose starvation along with CARM1 (Fig. II-8A). Increased AMPKα2 protein level resulted from the transcription induction rather than post-translational regulation (Fig. II-8B-C). AMPKα2 has been shown to be preferentially expressed in the nucleus (Jakub et al., 1998), suggesting that it is possible to perform distinct roles in the nucleus. To test the possibility that AMPK directly binds and/or phosphorylates CARM1 and SKP2, I performed co-immunoprecipitation and *in vitro* kinase assays. Co-immunoprecipitation assay showed that AMPK and CARM1 do not bind at endogenous expression level in the nucleus upon glucose starvation (Fig. II-8D). *In vitro* kinase assay revealed that AMPK does not directly phosphorylate SKP2 (Fig. II-8E).

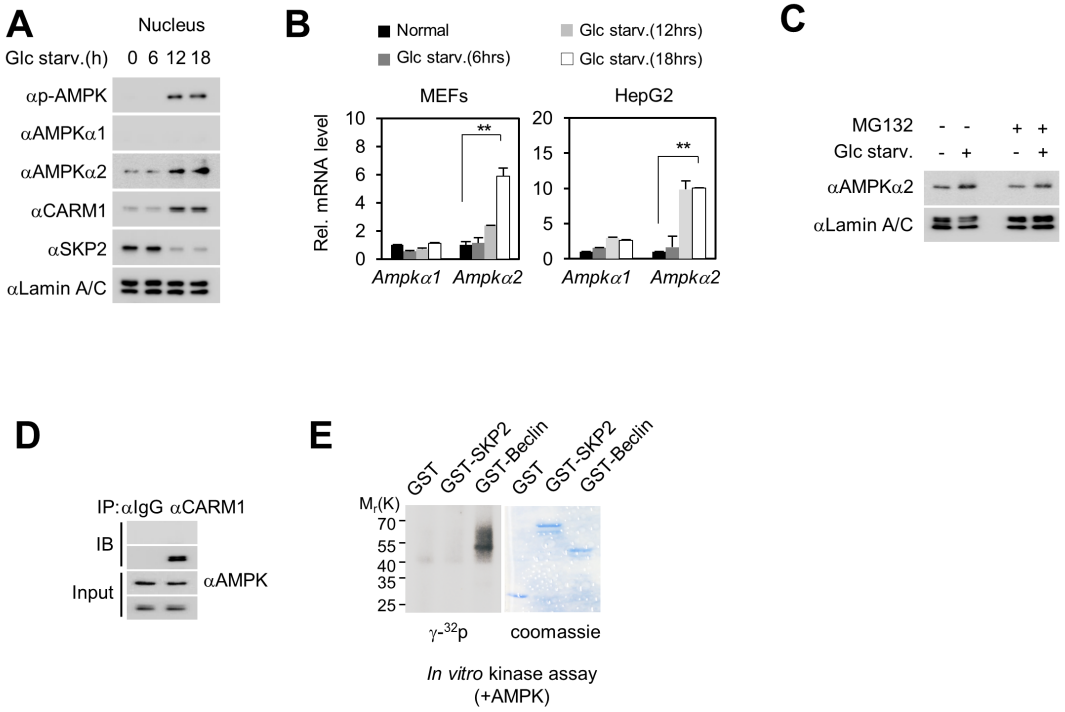

Figure II-8. AMPKα2 accumulates in the nucleus

(A) MEFs were deprived of Glc for the indicated times and nuclear fraction was analyzed with indicated antibodies. h=hours. (**B**) qRT-PCR of *Ampkα1* and *Ampkα2* in MEFs (right) and HepG2 cells (left). **p<0.01. Statistics by one-tailed *t*-test. (**C**) Nuclear expression of AMPKα2 was analyzed after MG132 treatment. (**D**) Co-immunoprecipitation assay between CARM1 and AMPK from nuclear extract of MEFs after 18 hrs of Glc starvation. (**E**) *In vitro* kinase assay. AMPK was immunopurified from transfected HEK293T cells and GST-tagged proteins were purified from *E.coli*. GST-SKP2 or GST-Beclin were incubated with AMP and [γ-^{32}p]ATP for *in vitro* phosphorylation by AMPK. GST-Beclin was used as positive control.

AMPKα2 accumulated in the nucleus leads to repression of SKP2 and stabilization of CARM1 under nutrient-starved condition.

Since the phosphorylated form of AMPK increased about 12 hours after glucose starvation in the nucleus (Fig. II-8A), the involvement of AMPK in the regulation of CARM1 stability in the nucleus was assessed using two well-characterized AMPK activators, aminoimidazole carboxamide ribonucleotide (AICAR) and phenformin. AMPK activation resulted in the increase of CARM1 and reduction of SKP2 (Fig. II-9A). Next, I co-treated glucose starved cells with Compound C, an AMPK inhibitor. Interestingly, increase in CARM1 and reduction of SKP2 were compromised when AMPK activity was blocked by Compound C treatment (Fig. II-9B).

I then used WT and *Ampkα1*- and *Ampkα2*-double knockout (DKO) MEFs to check for the expression of SKP2 and CARM1. Interestingly, reduction of SKP2 protein level upon glucose starvation was not observed in *Ampk* DKO MEFs (Fig. II-9C). In the nucleus, CARM1 was induced by glucose starvation in WT MEFs, but this induction was abrogated in *Ampk* DKO MEFs (Fig. II-9C). In parallel, the half-life of the CARM1 protein in the nucleus was decreased in *Ampk* DKO MEFs compared to WT MEFs upon glucose starvation (Fig. II-9D). Introduction of AMPKα2 WT, but not the dominant-negative (DN) form of AMPKα2, in *Ampk* DKO MEFs recovered the expression pattern of SKP2 and CARM1 similar to WT MEFs when glucose starved (Fig. II-9E). Since SKP2 is responsible for CARM1 degradation, I performed knockdown of SKP2 in *Ampk* DKO MEFs to see whether CARM1 level is recovered. SKP2 depletion led to increased CARM1 protein levels, indicating that reduction of CARM1 expression in

Ampk DKO MEFs is mediated by SKP2 (Fig. II-9F). Since the binding of CARM1 to CUL1 is mediated by SKP2, knockdown of SKP2 or decrease in SKP2 expression upon glucose starvation in WT MEFs almost completely abrogated mutual binding of CARM1 and CUL1(Fig. II-9G). However, their binding was still maintained in *Ampk* DKO MEFs upon glucose starvation as SKP2 failed to decrease (Fig. II-9G). Taken altogether, I was able to conclude that decrease of SKP2 and subsequent increase of CARM1 upon glucose starvation is AMPK-dependent.

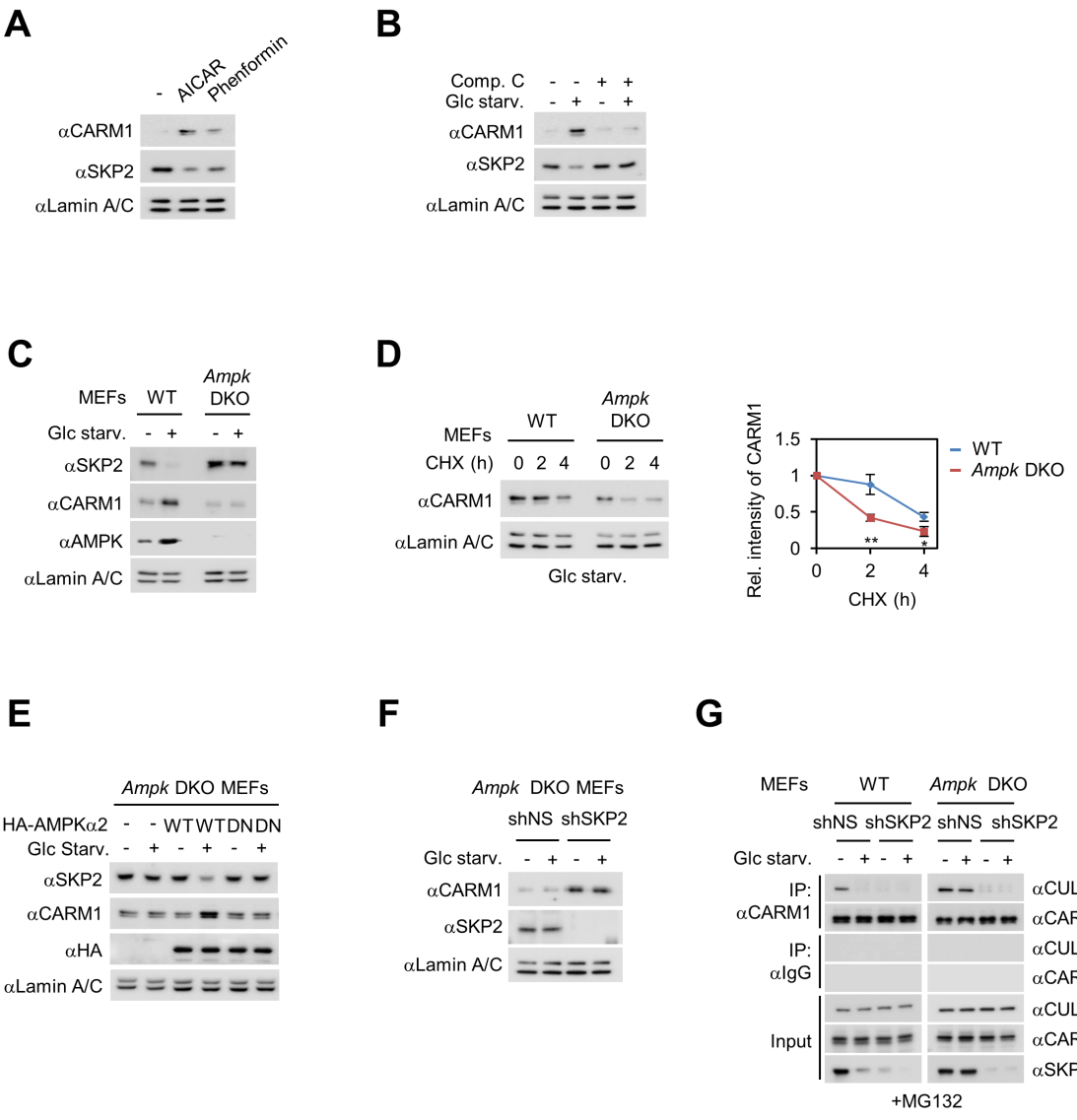
A
- AICAR Phenformin
αCARM1
αSKP2
αLamin A/C
B
Comp. C - - + +
Glc starv. - + - +
αCARM1
αSKP2
αLamin A/C
C
MEFs WT Ampk DKO
Glc starv. - + - +
αSKP2
αCARM1
αAMPK
αLamin A/C
D
MEFs WT Ampk DKO
CHX (h) 0 2 4 0 2 4
αCARM1
αLamin A/C
Glc starv.
Rel. intensity of CARM1
1.5
1
0.5
0
0 2 4
CHX (h)
WT
Ampk DKO
**
*
E
Ampk DKO MEFs
HA-AMPKα2 - - WT WT DN DN
Glc Starv. - + - + - +
αSKP2
αCARM1
αHA
αLamin A/C
F
Ampk DKO MEFs
shNS shSKP2
Glc starv. - + - +
αCARM1
αSKP2
αLamin A/C
G
MEFs WT Ampk DKO
shNS shSKP2 shNS shSKP2
Glc starv. - + - + - + - +
IP: αCARM1
αCUL1
αCARM1
IP: αIgG
αCUL1
αCARM1
Input
αCUL1
αCARM1
αSKP2
+MG132

Figure II-9. Decrease of SKP2 and subsequent increase in CARM1 upon glucose starvation is AMPK dependent

(A) MEFs were treated with AICAR (1 mM) or phenformin (2 mM) for 4 hrs. Nuclear fraction was subject to immunoblot analysis with the indicated antibodies. (**B**) MEFs were deprived of Glc in the absence or presence of 10 μM Compound C, an AMPK inhibitor, and nuclear fraction was analyzed with indicated antibodies. (**C**) WT and *Ampk* DKO MEFs were Glc starved and nuclear fraction was analyzed with indicated antibodies. (**D**) WT and *Ampk* DKO MEFs were deprived of Glc for 12 hrs and treated with cycloheximide (CHX) for indicated times. Nuclear CARM1 expression was analyzed after subcellular fractionation (left). Protein half-life of CARM1 was quantitatively defined (right). *$p<0.05$, **$p<0.01$. Statistics by one-tailed *t*-test. (**E**) *Ampk* DKO MEFs were transfected with AMPKα2 WT or dominant-negative (DN) mutant and deprived of Glc for 18 hrs. Immunoblot analysis with the indicated antibodies was performed after nuclear fractionation. (**F**) *Ampk* DKO MEFs were infected with SKP2 shRNA lentivirus and deprived of Glc for 18 hrs. Immunoblot analysis was performed from nuclear fraction with the indicated antibodies. (**G**) CARM1-CUL1 interaction was analyzed after SKP2 knockdown in WT and *Ampk* DKO MEFs

AMPK-dependent SKP2 downregulation is mediated by FOXO transcription factor

Reduction of SKP2 expression upon glucose starvation is not mediated by proteasomal degradation (Fig. II-10A), but rather regulated at transcription level (Fig. II-10B), as SKP2 mRNA level decreased upon glucose starvation in MEFs and HepG2 cells. Glucose starvation failed to decrease *Skp2* mRNA level in *Ampk* DKO MEFs, but reconstitution of AMPKα2 WT, but not AMPKα2 DN mutant, restored reduction of *Skp2* mRNA level (Fig. II-10C). Therefore, I prompted to search for a possible regulatory mechanism of SKP2 down-regulation by AMPKα2. Interestingly, *Skp2* promoter analysis revealed a highly conserved FOXO response element (Fig. II-10D). FOXO transcription factors are a subgroup of the Forkhead family involved in diverse functions including tumor suppression, energy metabolism, aging, and autophagy (Maiese et al., 2008; Salih and Brunet, 2008; van der Horst and Burgering, 2007). Recent studies have emphasized the AMPK-FOXO axis as a highly conserved nutrient-sensing pathway critical for cellular and organismal homeostasis (Eijkelenboom and Burgering, 2013). FOXO3a is directly modulated by AMPK as AMPK directly phosphorylates FOXO3a and regulates FOXO3a transcriptional activity without affecting its subcellular localization (Greer et al., 2007). Although mainly known as transcriptional activators, FOXO proteins function as transcriptional repressors as well (Lam et al., 2013; Potente et al., 2005; Wang and Li, 2010; Yang et al., 2014). Therefore, I hypothesized that FOXO might function as a transcriptional repressor of SKP2. To examine whether the FOXO response element is functional on *Skp2* promoter, I

performed luciferase reporter assay driven by *Skp2* promoter. Glucose starvation attenuated *Skp2* promoter-luciferase activity, but *Skp2* promoter in which I replaced the core FOXO consensus response element GTAAACTA into GTGGGGTA showed no change in luciferase activity upon glucose starvation (Fig. II-10D), indicating that the FOXO response element of *Skp2* promoter is functional. In *Foxo1/3/4* triple KO (TKO) MEFs, *Skp2* mRNA level failed to decrease upon glucose starvation (Fig. II-10E). Reconstitution of FOXO3a WT in *Foxo1/3/4* TKO MEFs significantly reduced *Skp2* mRNA level (Fig. II-10F), indicating that FOXO3a functions as a critical transcription repressor of SKP2. In contrasts, neither FOXO3a H212R (HR) DNA-binding mutant (Tsai et al., 2007) nor FOXO3a SA mutant which is not phosphorylated by AMPK (Greer et al., 2007) reduced *Skp2* mRNA level (Fig. II-10F).

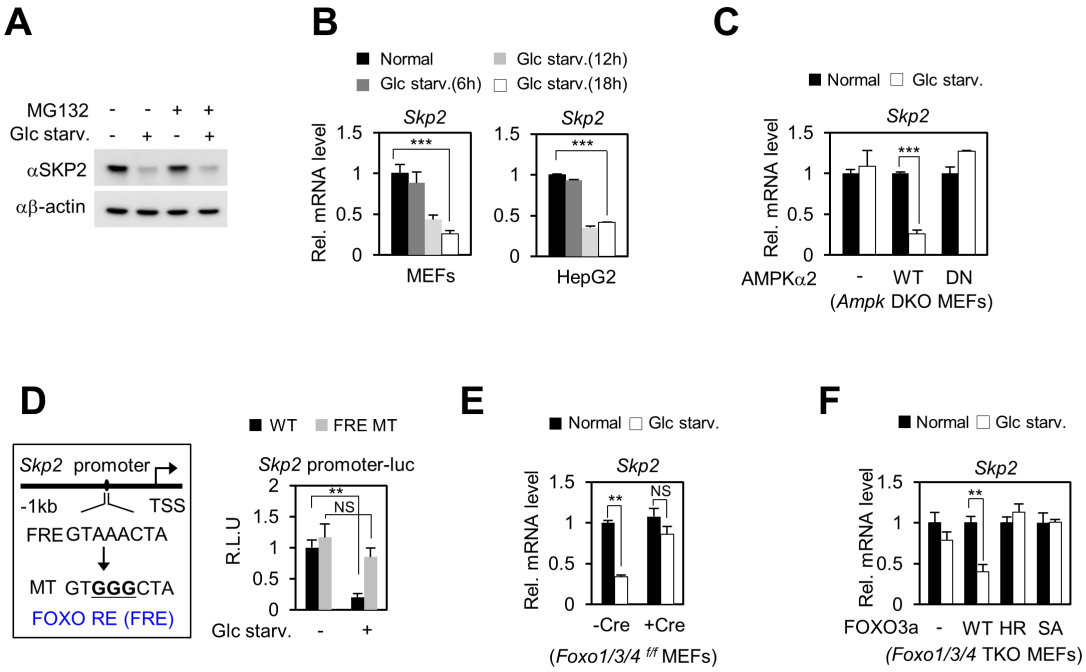

Figure II-10. AMPK-dependent SKP2 downregulation is mediated by FOXO transcription factor

(A) Immunoblot analysis with the indicated antibodies after Glc starvation in the absence or presence of MG132.(**B**) Quantitative RT-PCR (qRT-PCR) of *Skp2* following Glc starvation in MEFs and HepG2 cells. *** p<0.001. Statistics by one-tailed *t*-test. (**C**) *Ampk* DKO MEFs were transfected with AMPKα2 WT or DN mutant and analyzed for *Skp2* mRNA level. *** p<0.001. Statistics by one-tailed *t*-test. (**D**) Schematics of *Skp2* promoter (left). Luciferase activities of *Skp2* WT promoter and FOXO response element mutant (FRE MT) were measured in MEFs after Glc starvation (right). ** p<0.01, NS=Non-Significant. Statistics by one-tailed *t*-test. (**E**) *Foxo1/3/4* $^{f/f}$ MEFs were infected with Cre virus and analyzed for *Skp2* mRNA level. ** p<0.01, NS=Non-Significant. Statistics by one-tailed *t*-test. (**F**) *Foxo1/3/4* $^{f/f}$ MEFs were infected with Cre virus and transfected with indicated plasmids. *Skp2* mRNA level was analyzed.
** p<0.01. Statistics by one-tailed *t*-test.

AMPK-mediated FOXO phosphorylation is critical in SKP2 transcriptional repression

Glucose starvation resulted in FOXO3a phosphorylation which was abolished in *Ampk* DKO cells (Fig. II-11A). Since AMPKα2 has been shown to be preferentially expressed in the nucleus (Jakub et al., 1998), I performed ChIP assay on *Skp2* promoter to examine for possible recruitment of AMPKα2 and phosphorylated FOXO3a. ChIP assay revealed increased co-recruitment of AMPKα2 and phosphorylated FOXO3a on *Skp2* promoter upon glucose starvation (Fig. II-11B). Next, I rescued AMPKα2 WT or AMPKα2 DN mutant in *Ampk* DKO MEFs and performed ChIP assays to further validate the recruitment of AMPKα2-dependent phosphorylated FOXO3a on *Skp2* promoter upon glucose starvation. Phosphorylated FOXO3a recruitment was accompanied by a decrease in RNA pol II level, indicating transcription repression of SKP2 (Fig. II-11C). Next, I reconstituted FOXO3a WT or SA mutant in *Foxo1/3/4* TKO cells and performed ChIP assay on *Skp2* promoter. Upon glucose starvation, phosphorylated FOXO3a is recruited on the *Skp2* promoter along with decreased RNA pol II level, but FOXO3s SA mutant failed to be recruited to the *Skp2* promoter upon glucose starvation (Fig. II-11D), indicating that AMPK-dependent FOXO3a phosphorylation is crucial for the recruitment of FOXO3a on *Skp2* promoter. FOXO3a SA mutant exhibited comparable expression level to FOXO3a WT but SKP2 expression failed to decrease and autophagy occurrence was impaired in FOXO3a SA mutant-reconstituted *Foxo1/3/4* TKO MEFs (Fig. II-11E).

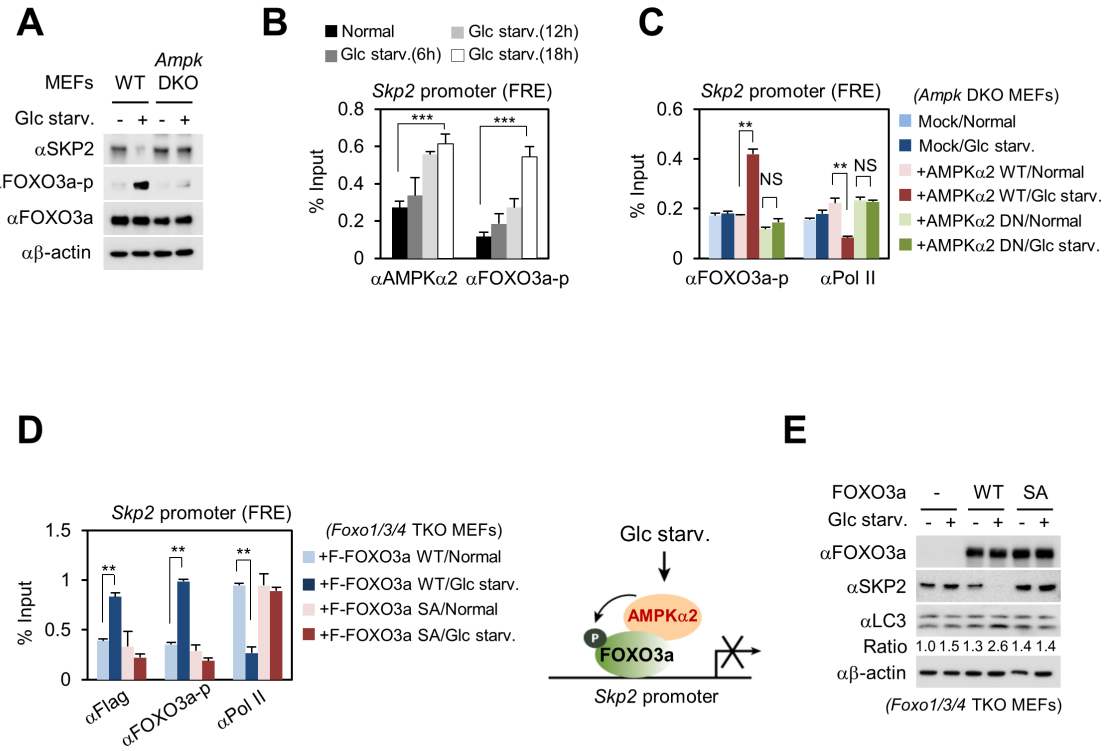

Figure II-11. AMPK-mediated FOXO phosphorylation is critical in SKP2 transcriptional repression

(A) Immunoblot analysis with the indicated antibodies in WT and *Ampk* DKO MEFs after Glc starvation. (**B**) ChIP assays on *Skp2* promoter in WT MEFs following Glc starvation. *** $p<0.001$. Statistics by one-tailed *t*-test. (**C**) ChIP assays in *Ampk* DKO MEFs reconstituted with AMPKα2 WT or DN mutant. ** $p<0.01$, NS=Non-Significant. Statistics by one-tailed *t*-test. (**D**) *Foxo 1/3/4* TKO MEFs were transfected with indicated plasmids and ChIP assay of *Skp2* promoter was performed (left). ** $p<0.01$. Statistics by one-tailed *t*-test. Schematics of SKP2 regulation by AMPK-FOXO axis (right). (**E**) Immunoblot analysis with the indicated antibodies in *Foxo1/3/4* TKO MEFs transfected with FOXO3a WT or SA mutant.

SKP2 knockdown or CARM1 overexpression partially recover autophagy in *Ampk* DKO MEFs

Given that CARM1 failed to increase in *Ampk* DKO MEFs after glucose starvation but is completely restored after SKP2 knockdown, I sought to examine the autophagy occurrence in *Ampk* DKO MEFs. Confocal microscopy showed that the number of GFP-LC3 positive punctate cells strikingly increased upon glucose starvation in *Ampk* DKO MEFs after knockdown of SKP2 (Fig. II-12A). In parallel, I examined whether knockdown of SKP2 in *Ampk* DKO MEFs can restore the increase in LC3 conversion. Compared to WT MEFs, glucose starvation-induced LC3 conversion was minimal in *Ampk* DKO MEFs, but knockdown of SKP2 in *Ampk* DKO MEFs significantly restored the increase in LC3 conversion upon glucose starvation (Fig. II-12B).

I also tested whether CARM1 overexpression could restore autophagy induction in *Ampk* DKO MEFs. GFP-LC3 puncta analysis showed that in *Ampk* DKO MEFs, introduction of CARM1 WT or ubiquitination-defective K471R mutant restored the number of GFP-LC3 punctate cells, whereas enzymatic-dead mutant CARM1 R169A failed to do so (Fig. II-12C), indicating that enzymatic activity of CARM1 is required for autophagy induction.

Together, I found a new signaling axis in autophagy induction where glucose starvation activates AMPKα2 in the nucleus leading to the transcriptional repression of SKP2 via FOXO3a phosphorylation. Reduction of SKP2 expression in turn leads to increased CARM1 expression along with H3R17me2 signal resulting in autophagy induction (Fig.II-12D).

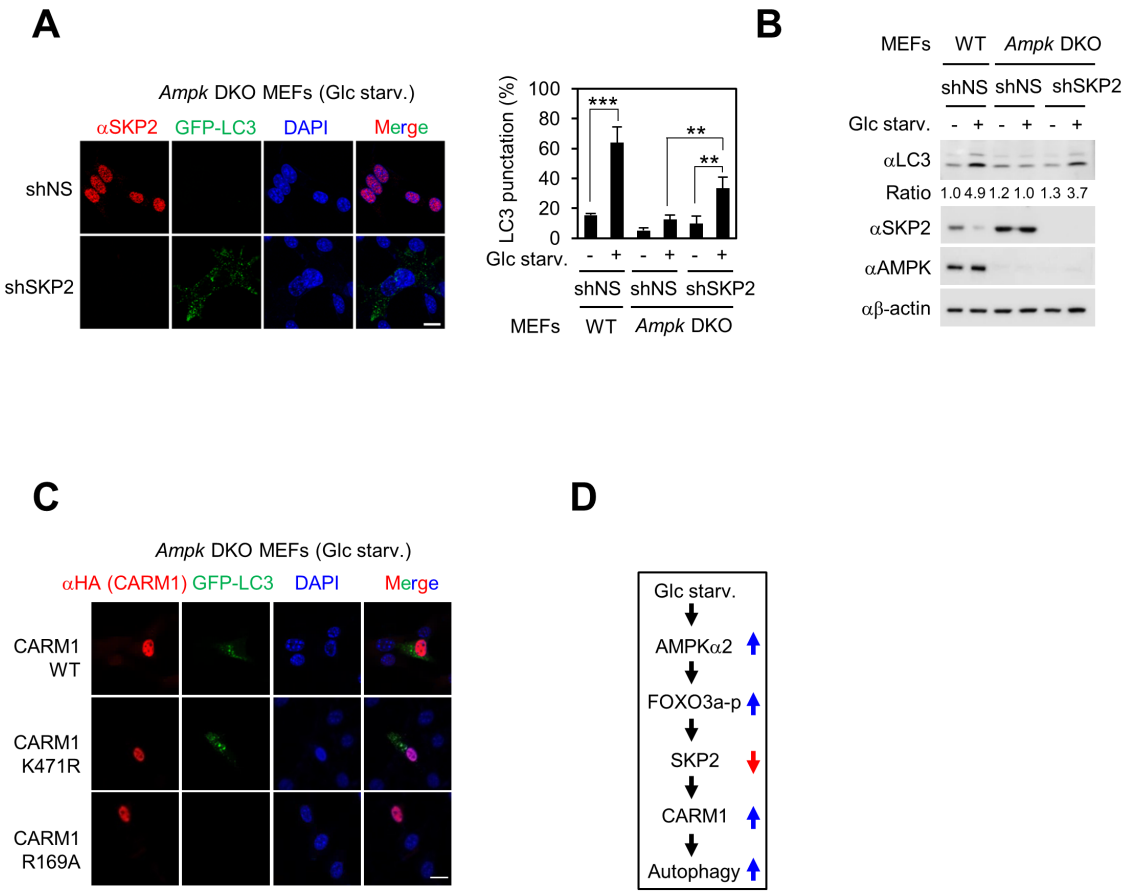
A
Ampk DKO MEFs (Glc starv.)
αSKP2 GFP-LC3 DAPI Merge
shNS
shSKP2
LC3 punctation (%)
100
80
60
40
20
0
***
**
**
Glc starv. - + - + - +
shNS shNS shSKP2
MEFs WT Ampk DKO
B
MEFs WT Ampk DKO
shNS shNS shSKP2
Glc starv. - + - + - +
αLC3
Ratio 1.0 4.9 1.2 1.0 1.3 3.7
αSKP2
αAMPK
αβ-actin
C
Ampk DKO MEFs (Glc starv.)
αHA (CARM1) GFP-LC3 DAPI Merge
CARM1 WT
CARM1 K471R
CARM1 R169A
D
Glc starv.
AMPKα2
FOXO3a-p
SKP2
CARM1
Autophagy

Figure II-12. SKP2 knockdown or CARM1 overexpression partially recover autophagy in *Ampk* DKO MEFs

(**A**) *Ampk* DKO MEFs infected with lentiviruses expressing nonspecific shRNA (shNS) or SKP2 shRNA (shSKP2) were transfected with GFP-LC3 and the formation of GFP-LC3-positive autophagosomes was examined by confocal microscopy. SKP2 (red); GFP-LC3 (green); DAPI (blue). Scale bar, 20 μm. The graph shows quantification of LC3-positive punctate cells (left). ** $p<0.01$, *** $p<0.001$. Statistics by one-tailed *t*-test. (**B**) WT and *Ampk* DKO MEFs infected with shNS or shSKP2 were deprived of Glc for 18 hrs. Immunoblot analysis was performed from whole extracts with the indicated antibodies. (**C**) *Ampk* DKO MEFs were transfected with CARM1 WT, ubiquitination-defective mutant K471R or enzymatic mutant R169A along with GFP- LC3 and the formation of GFP-LC3-positive autophagosomes was examined by confocal microscopy. CARM1 (red); GFP-LC3 (green); DAPI (blue). Scale bar, 20 μm. *$p<0.05$, ** $p<0.01$. Statistics by one-tailed *t*-test. **(D)** Schematics of newly identified AMPK-FOXO3a-SKP2-CARM1 signaling cascade in starvation-induced autophagy.

II-4. Discussion

In this study, I identify the histone arginine methyltransferase CARM1 as a novel component and subsequent histone H3R17 dimethylation as critical epigenetic mark in starvation-induced autophagy. Interestingly, I found that CARM1 is stabilized upon starvation and degraded by SKP2-SCF E3 ligase complex under nutrient-rich condition in the nucleus, but not in the cytoplasm. Further, I defined the molecular mechanism underlying CARM1 stability. Indeed, starvation led to AMPKα2 activation in the nucleus, and AMPKα2 directly phosphorylated FOXO3a for transcriptional repression of SKP2. ChIP assay showed that phosphorylated FOXO3a is recruited on *Skp2* promoter containing FOXO binding element. Down-regulated SKP2 leads to the stabilization of CARM1 and subsequent induction of autophagy.

It is important to note that CARM1 stability is regulated primarily in the nucleus due to the exclusive nuclear localization of SKP2. It is plausible that basal level of CARM1 expression in the nucleus is required for efficient and rapid induction of CARM1 in response to glucose starvation. I speculate that this type of stabilization of histone modifiers in the nucleus might be an efficient way to regulate target gene expression and could be a prototype of protein stabilization in specific compartments of the cells in starvation-induced autophagy.

Taken together, my finding provides evidence of CARM1 induction as a critical nuclear event of autophagy and further supports the need to view autophagy that encompasses both cytoplasmic and nuclear events for complete understanding of the process.

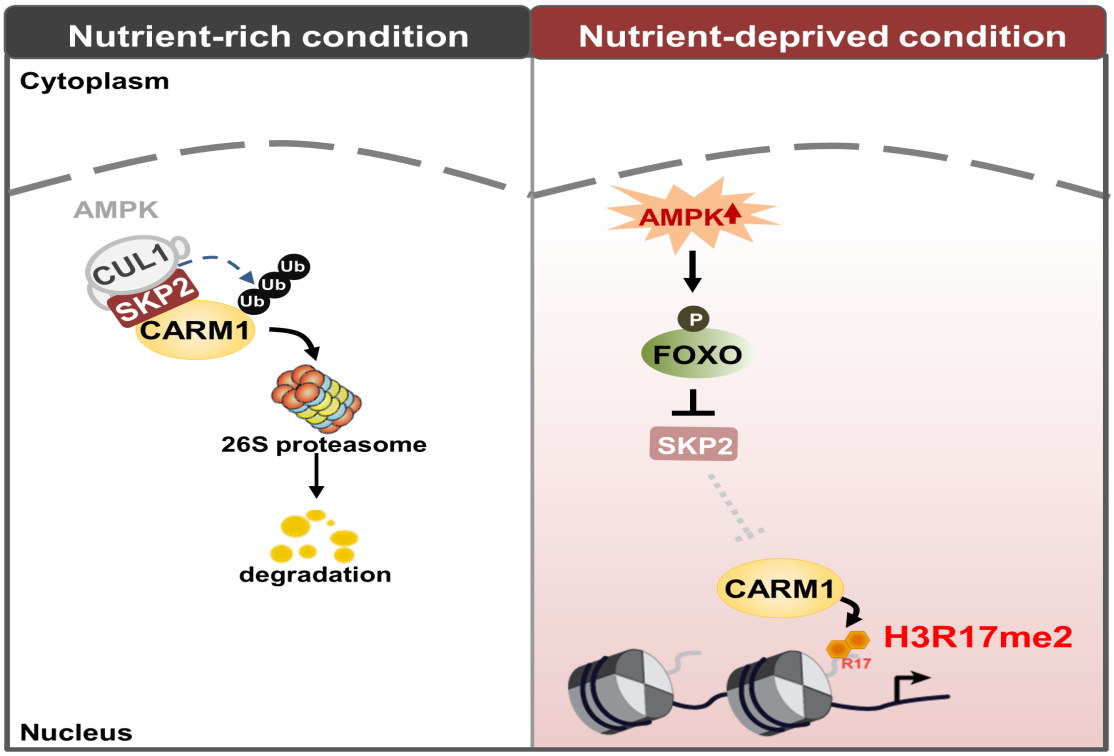

Figure II-13. Schematic model of the newly identified AMPK-FOXO3a-SKP2-CARM1 signaling cascade in starvation-induced autophagy

Under nutrient-rich condition, CARM1 is degraded by SKP2-SCF E3 ubiquitin ligase in the nucleus. Under nutrient-deprived condition, activated AMPK directly phosphorylates FOXO which in turn transcriptionally represses SKP2. Stabilized CARM1 then increases histone H3R17 dimethylation (H3R17me2).

II-5. Materials and Methods

Antibodies

The following commercially available antibodies were used: Anti-AMPKα1 (ab110036), anti-AMPKα2 (ab3760), anti-FOXO3a (ab12162), anti-histone H3 (ab1791), anti-H3R17me2 (ab8284), anti-H3K4me3 (ab8580), anti-H3K9me3 (ab8898), and anti-H3K36me3 (ab9050) antibodies were purchased from Abcam. Anti-AMPK (#2532), anti-CARM1 (#3379 for IB, #12495 for IP), anti-LC3 (#2775), anti-phospho-AMPKα T172 (#2535), anti-phospho-FOXO3a S413 (#8174), and anti-SQSTM1/p62 (#5114) antibodies were from Cell Signaling technology. Anti-SKP2 (sc-7164), anti-CUL1 (sc-17775), anti-Tubulin (sc-8035), and anti-Lamin A/C (sc-6215) were from Santa Cruz biotechnology. Anti-Flag (F3165), and anti-β-actin (A1978) antibodies were from Sigma, anti-HA antibody (#MMS-101R) and anti-RNA-Polymerase II (8WG16) (#MMS-126R) from Covance, and anti-tubulin antibody (LF-PA0146A) from Abfrontier. The following chemicals were used in this study: rapamycin (R-5000) was purchased from LC laboratories, cycloheximide (C4859), AICAR (A9978) and phenformin (P7045) from Sigma, Bafilomycin A1 (#11038) and ellagic acid from Cayman (#10569), Compound C from Calbiochem (#171260), and MG132 (M-1157) from A.G. Scientific.

Cell culture and generation of shRNA knockdown cells

HEK293T, HeLa, HepG2 cells, WT, *Carm1* KO, *Ampk* DKO, *Foxo1.3.4 f/f* MEFs were

cultured at 37°C in Dulbecco's modified Eagle's medium (DMEM) containing 10 % fetal bovine serum (FBS) and antibiotics in a humidified incubator with 5 % CO_2. All cell lines used in the study were regularly tested for mycoplasma contamination. For glucose starvation, cells were washed with PBS, then incubated with glucose-free DMEM supplemented with 10 % dialyzed FBS. Transfection was performed with Turbofect (Fermentas) or Lipofectamine 3000 (Invitrogen) according to manufacturer's protocol. To generate knockdown cells, lentiviral shRNA constructs were first transfected along with viral packaging plasmids (psPAX2 and pMD2.G) into HEK293T cells. Three days post-transfection, viral supernatant was filtered through 0.45-μm filter and infected into targeting cells. Infected cells were then selected with 5 μg/ml puromycin. The targeting sequences of shRNAs are as follows.

mCARM1-1; 5'-TCAGGGACATGTCTGCTTATT-3',

mCARM1-2; 5'-GCCTGAGCAAGTGGACATTAT-3',

mSKP2; 5'-GCAAGACTTCTGAACTGCTAT-3',

hCUL1-1; 5'-GATTTGATGGATGAGAGTGTA-3',

hCUL1-2; 5'- CCCGCAGCAAATAGTTCATGT-3',

hSKP2-1; 5'-TTCCGCTGCCCACGATCATTT-3',

hSKP2-2; 5'-AGTCGGTGCTATGATATAATA-3'.

Cre-retrovirus infection

PT67 packaging cells (Clontech) transfected with retroviral plasmid expressing Cre

recombinase were grown in puromycin selection media, and the clone producing high-titer virus particle (PT67-Cre) was obtained. *Foxo1.3.4*$^{f/f}$ MEFs were incubated with culture supernatants containing PT67-Cre virus overnight in the presence of 4 μg/ml polybrene (Sigma). Cells were then treated with 5 μg/ml of puromycin for 48 hr for selection.

Whole-cell lysate preparation and subcellular fractionation

All cells were briefly rinsed with ice-cold PBS before collection. For whole-cell lysates, the cells were resuspended in RIPA buffer (150 mM NaCl, 1 % Triton X-100, 1 % Sodium deoxycholate, 0.1 % SDS, 50 mM Tris-HCl [pH 7.5], and 2 mM EDTA [pH 8.0]) supplemented with protease inhibitors and sonicated using a Branson Sonifier 450 at output 3 and a duty cycle of 30 for 5 pulses. For cytosolic and nuclear fractions, cells were lysed in harvest buffer (10 mM HEPES [pH 7.9], 50 mM NaCl, 0.5 M sucrose, 0.1 mM EDTA, 0.5 % Triton X-100 and freshly added DTT, PMSF and protease inhibitors), incubated on ice for 5 min and spun at 1,000 rpm for 10 min at 4°C. The supernatant (cytosolic fraction) was removed to a separate tube. The nuclear pellet was rinsed twice with 500 μl of buffer A (10 mM HEPES [pH 7.9], 10 mM KCl, 0.1 mM EDTA, and 0.1 mM EGTA) and spun down at 1,000 rpm for 10 min at 4°C. The supernatant was discarded and the pellet (nuclear fraction) were resuspended in RIPA buffer and sonicated as for the whole-cell lysates. All lysates were quantified by the Bradford method and analyzed by SDS-PAGE.

Immunofluorescence

Immunocytochemistry was performed as previously described (Kim et al., 2012). Cells grown on coverslips at a density of 7 x 10^4 cells were washed three times with PBS and then fixed with 2 % paraformaldehyde in PBS for 10 min at RT. Fixed cells were permeabilized with 0.1 % Triton X-100 in PBS (PBS-T) for 10 min at RT. Blocking was performed with 3 % bovine serum in PBS-T for 30 min. For staining, cells were incubated with antibodies for 2 hrs at RT, followed by incubation with fluorescent labeled secondary antibodies for 1 hr (Invitrogen). Cells were mounted and visualized under a confocal microscope (Zeiss, LSM700). For autophagy studies, MEF cells were transfected with GFP-LC3 and sub-cultured onto coverslips. The following day, cells were incubated with either complete media or glucose starvation media for 18 hrs. Cells were treated with rapamycin for 24 hrs and ellagic acid for 18 hrs.

Electron microscopy

Cells were fixed in 0.1 M sodium cacodylate containing 4 % glutaraldehyde, 1 % paraformaldehyde for 1 hr at room temperature (RT). After washing three times with 0.1 M sodium cacodylate, cells were dehydrated through a gradient series of ethanol, 20 min each step, starting from 50 % ethanol and ending with 100 % ethanol. Afterwards, cells were incubated with progressively concentrated propylene oxide dissolved in ethanol then infiltrated with increasing concentration of Eponate 812 resin. Samples were baked in a 65 °C oven overnight then sectioned using Ultra microtome. Sections

were viewed with an energy filtering TEM unit (LEO-192AB OMEGA, Carl Zeiss) at the Korean Basic Science Institute, South Korea.

Site-directed mutagenesis

To generate the CARM1 ubiquitination mutant (K471R), CUL1 mutant (K720R), FOXO-response element(FRE) mutant in *SKP2*-promoter luciferase construct, FOXO3a DNA-binding mutant (H212R) and FOXO3a SA mutant site-directed mutagenesis assay by PCR was performed using the following primers.

mCARM1 K471R Forward(Fwd): 5'- ccagtaacctgctggatctaaggaacccttcttcagg -3'

mCARM1 K471R Reverse(Rev): 5'- cctgaagaaggggttccttagatccagcaggttactgg -3'

hCUL1 K720R Fwd: 5'- catcgtgagaatcatgaggatgaggaaggttctg -3'

hCUL1 K720R Rev: 5' - cagaaccttcctcatcctcatgattctcacgatg -3'

mSkp2 promoter_FREmut Fwd: 5'- cctttcctcacttgtgggctaggctcgaggacg -3'

mSkp2 promoter_FREmut Rev: 5'- cgtcctcgagcctagcccacaagtgaggaaagg -3'

FOXO3a T179A Fwd: 5'- cggacaaacggctagctctgtcccagatc -3'

FOXO3a T179A Rev: 5'- gatctgggacagagctagccgtttgtccg -3'

FOXO3a S399A Fwd: 5' - cacgctcccgccggcccagccatcgccc -3'

FOXO3a S399A Rev: 5' - gggcgatggctgggccggcgggagcgtg -3'

FOXO3a S413A Fwd: 5'- catgcagcggagctcagctttcccgtatacc - 3'

FOXO3a S413A Rev: 5' - ggtatacgggaaagctgagctccgctgcatg - 3'

FOXO3a S555A Fwd: 5' - ccttgtcgaattctgtcgccaacatgggcttgag - 3'

FOXO3a S555A Rev: 5' - ctcaagcccatgttggcgacagaattcgacaagg - 3'

FOXO3a S588A Fwd: 5’ – cctctcggactctctcgcaggatcctccttgtactc - 3’

FOXO3a S588A Rev: 5’- gagtacaaggaggatcctgcgagagagtccgagagg - 3’

FOXO3a S626A Fwd: 5’ – ggaatgtgacatggaggccattatccgtag - 3’

FOXO3a S626A Rev: 5’ – ctacggataatggcctccatgtcacattcc - 3’

FOXO3a H212R Fwd: 5’- gaactccatccggcgcaacctgtcactgc - 3’

FOXO3a H212R Rev: 5’ – gcagtgacaggttgcgccggatggagttc -3’

The amplified fragments were treated with *DpnI* and were transformed to *E. coli*. All mutants were verified by sequencing.

Ubiquitination assay

Cells were transfected with combinations of plasmids including HisMax-tagged ubiquitin. After incubation for 48 hrs, cells were treated with 5 μg/ml of MG132 for 4 hrs, lysed in buffer A (6 M guanidinium-HCl, 0.1 M Na_2HPO_4/NaH_2PO_4, 0.01 M Tris-HCl [pH 8.0], 5 mM imidazole, and 10 mM β-mercaptoethanol), and incubated with Ni^{2+}-NTA beads (QIAGEN) for 4 hrs at RT. The beads were sequentially washed with buffer A, buffer B (8 M urea, 0.1 M Na_2PO_4/NaH_2PO_4, 0.01 M Tris-HCl [pH 8.0], and 10 mM β-mercaptoethanol), and buffer C (8 M urea, 0.1 M Na_2PO_4/NaH_2PO_4, 0.01 M Tris-HCl [pH 6.3], and 10 mM β-mercaptoethanol). Bound proteins were eluted with buffer D (200 mM imidazole, 0.15 M Tris-HCl [pH 6.7], 30 % glycerol, 0.72 M β-mercaptoethanol, and 5 % SDS), and subject to immunoblot analysis. Ubiquitination site prediction software was used for CARM1 ubiquitination site prediction (Chen et al., 2013).

***In vitro* kinase assay**

GST-SKP2 and Beclin (1-148 amino acids) were transformed in Rosetta *E.coli*, purified with glutathione beads (GE Healthcare) and eluted in elution buffer (50 mM Tris-HCl [pH 8.0], 100 mM NaCl, 10 mM L-glutathione reduced (SIGMA). HA-AMPKα1 constitute active (CA) were co-transfected in HEK293T with Flag-AMPKβ and HA-AMPKγ, and the complex was immunoprecipitated using Flag-M2 bead (SIGMA) and eluted through 3X-Flag peptide in elution buffer (0.1 mg/ml in TBS). 1 μg of each substrate was reacted with AMPK complexes in kinase reaction buffer containing 20 mM HEPES [pH 7.4], 5 mM $MgCl_2$, 1 mM EGTA, 0.4 mM EDTA, and 0.05 mM DTT as previously described (Kim et al., 2013b). Reactions were incubated with 150 μM AMP and 2 μCi of radiolabeled [γ-^{32}p]ATP at 30°C for 15 min. The reactions were terminated by adding SDS sampling buffer, and phosphorylation was detected by SDS-PAGE and autoradiography.

Construction of reporter plasmids and luciferase assays

The *Skp2* promoter region (from 1 kb upstream of transcription start site to 200 bp downstream) was cloned into pGL2-luciferase reporter vector (Promega). FOXO response element (FRE) mutant on *Skp2* promoter was constructed by site-directed mutagenesis. MEFs were transiently transfected with luciferase reporter plasmids and luciferase activity was measured 36 hrs post-transfection and normalized by β-galactosidase expression.

Quantitative RT-PCR

Total RNAs were extracted using Trizol (Invitrogen) and reverse transcription was performed from 2.5 μg total RNAs using the M-MLV cDNA Synthesis kit (Enzynomics). The abundance of mRNA was detected by an ABI prism 7500 system or BioRad CFX384 with SYBR TOPreal qPCR 2x PreMix (Enzynomics). The quantity of mRNA was calculated using ddCt method and HPRT, GAPDH and β-actin were used as controls. All reactions were performed as triplicates.

The following mouse primers were used in this study.

β-actin Fwd: 5' – TAGCCATCCAGGCTGTGCTG - 3'

β-actin Rev: 5' – CAGGATCTTCATGAGGTAGTC - 3'

Gapdh Fwd: 5' - CATGGCCTTCCGTGTTCCTA - 3'

Gapdh Rev: 5' – CCTGCTTCACCACCTTCTTGA - 3'

Hprt Fwd: 5' - GCTGGTGAAAAGGACCTCTCG - 3'

Hprt Rev: 5' – CCACAGGACTAGAACACCTGC - 3'

Skp2 Fwd: 5' - CCTCCAAGGAAACGAGTCAAG - 3'

Skp2 Rev: 5' – CAGGAGACACCTGGAAAGTTC - 3'.

Ampkα1 Fwd: 5' – GTCAAAGCCGACCCAATGATA - 3'

Ampkα1 Rev: 5' - CGTACACGCAAATAATAGGGGTT - 3'

Ampkα2 Fwd: 5' - CAGGCCATAAAGTGGCAGTTA - 3 '

Ampkα2 Rev: 5' - AAAAGTCTGTCGGAGTGCTGA - 3'

The following human primers were used in this study.

ACTB Fwd: 5′-ATTGCCGACAGGATGCAGAA-3′

ACTB Rev: 5'-ACATCTGCTGGAAGGTGGACAG-3′

GAPDH Fwd: 5′-CGACCACTTTGTCAAGCTCA-3′

GAPDH Rev: 5′-AGGGGAGATTCAGTGTGGTG-3′

HPRT Fwd: 5'-TGACACTGGCAAAACAATGCA-3',

HPRT Rev: 5'-GGTCCTTTTCACCAGCAAG CT-3'

SKP2 Fwd: 5' - ATGCCCCAATCTTGTCCATCT -3'

SKP2 Rev: 5' - CACCGACTGAGTGATAGGTGT - 3'

AMPKA1 Fwd: 5' -TTTGCGTGTACGAAGGAAGAAT -3'

AMPKA1 Rev: 5'- CTCTGTGGAGTAGCAGTCCCT -3'

AMPKA2 Fwd: 5'- CTGTAAGCATGGACGGGTTGA -3'

AMPKA2 Rev: 5' - AAATCGGCTATCTTGGCATTCA -3'

ChIP assays and qRT-PCR analyses

Cells were crosslinked with 1% formaldehyde for 10 min at room temperature. After glycine quenching, the cell pellets were lysed in buffer containing 50mM Tris-HCl (pH8.1), 10mM EDTA, 1% SDS, supplemented with complete protease inhibitor cocktail (Roche), and sonicated. Chromatin extracts containing DNA fragments with an average of 250bp were then diluted tem times with dilution buffer containing 1% Triton X-100, 2mM EDTA, 150mM NaCl, 20mM Tris-HCl (pH 8.1) with complete protease inhibitor cocktail, pre-cleared with protein A/G sepharose and subjected to immunoprecipitations for

overnight at 4°C. Immunocomplexes were captured by incubating 45ul of protein A/G sepharose for 2 hours at 4°C. Beads were washed with low-salt wash buffer (0.1% SDS, 1% Triton X-100, 2mM EDTA, 20mM Tris-HCl (pH 8.1), 150mM NaCl), high-salt wash buffer (0.1% SDS, 1% Triton X-100, 2mM EDTA, 20mM Tris-HCl (pH 8.1), 500mM NaCl), buffer III buffer (0.25M LiCl, 1% NP-40, 1% deoxycholate, 10mM Tris-HCl (pH 8.1), 1mM EDTA), TE buffer (10mM Tris-HCl (pH 8.0), 0.5M EDTA) and eluted in elution buffer (1% SDS, 0.1M NaHCO3). The supernatant was incubated overnight at 65°C to reverse-crosslink, digested with RNase A for 2 hours at 37°C and proteinase K for 2 hours at 55°C. ChIP and input DNA were then purified and analyzed for qRT-PCR analysis.

Quantitative PCR (qPCR) was used to measure enrichment of bound DNA, and the value of enrichment was calculated by relative amount to input and ratio to IgG. All reactions were performed in triplicates. The following primers were used in ChIP assays.

mSkp2 (FRE) Fwd: 5' - CCTTAGGACTGGGTCTGTGG - 3'

mSkp2 (FRE) Rev: 5' - GCACGCTGATTTGATCTTCA - 3'

Statistical analysis

All experiments were performed independently at least three times. For GFP-LC3 puncta counting, five random confocal images were chosen and the number of cells with GFP-positive dots was counted. An average of 80 cells was examined for each group and *p*-values were calculated using one-tailed *t*-test. Values are expressed as mean ± s.e.m. A *p*-

value of less than 0.05 was considered statistically significant.

NS=Non-Significant, *p<0.05, **p<0.01, ***p<0.001.

CHAPTER III

CARM1 exerts transcriptional coactivator function on autophagy-related and lysosomal genes though TFEB

III-1. Summary

Autophagy is an evolutionary conserved process that promotes the degradation of cytoplasmic proteins and organelles by lysosome. Besides operating as a quality control mechanism in steady-state conditions, autophagy is triggered in response to stress including nutrient starvation (Klionsky, 2007; Mizushima, 2007). Autophagy is commonly seen as a cytoplasmic event but accumulating evidence has unveiled the importance of epigenetic and transcriptional network that regulates autophagy. It is now widely accepted that prolonged autophagic response relied on the activation of specific transcriptional programs (Füllgrabe et al., 2014b). Although major transcription factors in autophagy have been defined and extensively studied, little is known on the nuclear dynamics of autophagy and the network between transcription and histone modifications in autophagy. Here, I provide evidence that nutrient starvation-induced CARM1 functions as a critical transcriptional coactivator of autophagy-related and lysosomal genes through Transcription Factor EB (TFEB). Furthermore, ellagic acid treatment that block H3R17 dimethylation almost completely abolished CARM1-induced autophagy occurrence *in vivo* suggesting that increase in histone H3R17 dimethylation from increased CARM1 expression directly regulates the outcome of autophagy. Taken together, our findings provide evidence of CARM1-dependent histone arginine methylation as a critical nuclear event of epigenetic and transcriptional regulation in autophagy and shed light on a potential therapeutic targeting of a new signaling axis of AMPK-SKP2-CARM1 in autophagy-related diseases.

III-2. Introduction

The class I enzyme PRMT4, commonly called CARM1, methylates histones and several non-histone proteins and influences many cellular processes including signal transduction, RNA processing and transcriptional regulation (Wolf, 2009). It is known to enhance transcriptional activation through interaction with the coactivators CBP, p300 and p160 and methylation of histone H3R17 (H3R17me2) (Lee and Stallcup, 2009). CARM1 methylation sites on histone substrates have been mapped to H3R17 and H3R26 but biochemical studies revealed that CARM1 preferentially methylation H3R17 over H3R26 (Jacques et al., 2016). CARM1 methylation of histones is thought to promote active transcription through the recruitment of chromatin-remodeling complexes and transcriptional elongation complexes but the functional significance of H3R17me2 has not yet been elucidated.

Many transcription factors regulating autophagy genes have been reported thus far but TFEB is the only transcription factor that controls the transcription of both autophagy-related and lysosomal genes. Indeed, TFEB appears to have a much broader activity since it controls genes involved in multiple crucial steps of the autophagy pathway such as autophagosome formation, autophagosome-lysosome fusion and lysosome-mediated degradation of the autophagosomal content. TFEB is localized in the cytoplasm and rapidly translocates into the nucleus upon starvation or lysosomal stress. This change in subcellular localization, essentially mediated by phosphorylation, simultaneously promotes lysosomal biogenesis, autophagy induction as well as expression of critical

mitochondrial and metabolic regulators (Martina et al., 2012; Roczniak-Ferguson et al., 2012; Settembre et al., 2013a; Settembre et al., 2011; Settembre et al., 2012). Although regulation of TFEB by phosphorylation has been extensively studied, the mechanism of TFEB regulation in the nucleus is far unknown. Epigenetic regulation and transcription complex of TFEB as well as transcriptional cofactors involved in TFEB target gene activation have not been defined yet.

Activation of TFEB leads to an increased number of autophagosomes and autophagic flux, biogenesis of new lysosomes, and clearance of storage material in several lysosomal storage disorders and neurodegenerative diseases (Settembre et al., 2011; Settembre et al., 2013b). Since autophagy dysfunction has been linked to several disorders, understanding the mechanism of TFEB activation and transcriptional induction of its target genes would enlarge therapeutic strategies to modulate cellular clearance and disease progression.

III-3. Results

Identification of CARM1 target genes by RNA-sequencing

To gain insight on the role of CARM1 in chromatin and transcriptional regulation of autophagy in a genome-wide scale, I performed RNA-sequencing (RNA-seq) experiments in WT and *Carm1* KO MEFs following glucose starvation (Fig. III-1A). By comparing the transcriptome in WT and *Carm1* KO MEFs subject to either nutrient rich condition or glucose starvation, I identified a total of 4,998 differentially expressed genes (DEGs) that can be classified into six groups by unsupervised hierarchical cluster analysis (Fig. III-1B). Among these genes, I was particularly interested in the pools that are activated upon glucose starvation in WT MEFs but failed to be so in *Carm1* KO MEFs (Cluster 1), as CARM1 is a transcriptional coactivator. As *Carm1* KO MEFs are autophagy defective, I aimed to examine the contribution of CARM1 in transcriptional regulation of autophagy. The process of autophagy relies on the cooperation of autophagosomes and lysosomes, and lysosomal biogenesis and function are highly dependent on transcription (Laplante and Sabatini, 2013; Settembre et al., 2013b). Using a comprehensive list of 246 known autophagy-related genes and 348 known lysosomal genes (Table III-1), I found that potential CARM1 target genes (Cluster 1) are significantly enriched for autophagy-related genes and lysosomal genes (Fig. III-1C). Among them are critical components of autophagy initiation (*Ulk1, Atg13*), vesicle nucleation (*PIk3c3/Vps34, Atg14*), elongation (*Atg12, Map1lc3*) and lysosomes (*Vps11, Ctsf*).

I examined whether glucose starvation affects genes regulated by specific transcription factors such as Transcription Factor EB (TFEB), p53, FOXO, and hypoxia-inducible factor (HIF), which have been previously reported to modulate transcription upon energy deprived condition (Pietrocola et al., 2013). I investigated the enrichment of the motif of these factors at the promoter region of the genes in Cluster 1. The analysis indicates that TFEB may be a major transcription factor for CARM1 upon glucose starvation (Fig. III-1D). I further validated CARM1 dependency of the autophagy-related genes and lysosomal genes in WT and *Carm1* KO MEFs with or without glucose starvation by individual qRT-PCR analysis (Fig. III-1E). These data indicate that upon glucose starvation, CARM1 regulates the autophagy process through transcriptional activation of key autophagy-related genes and lysosomal genes in the nucleus.

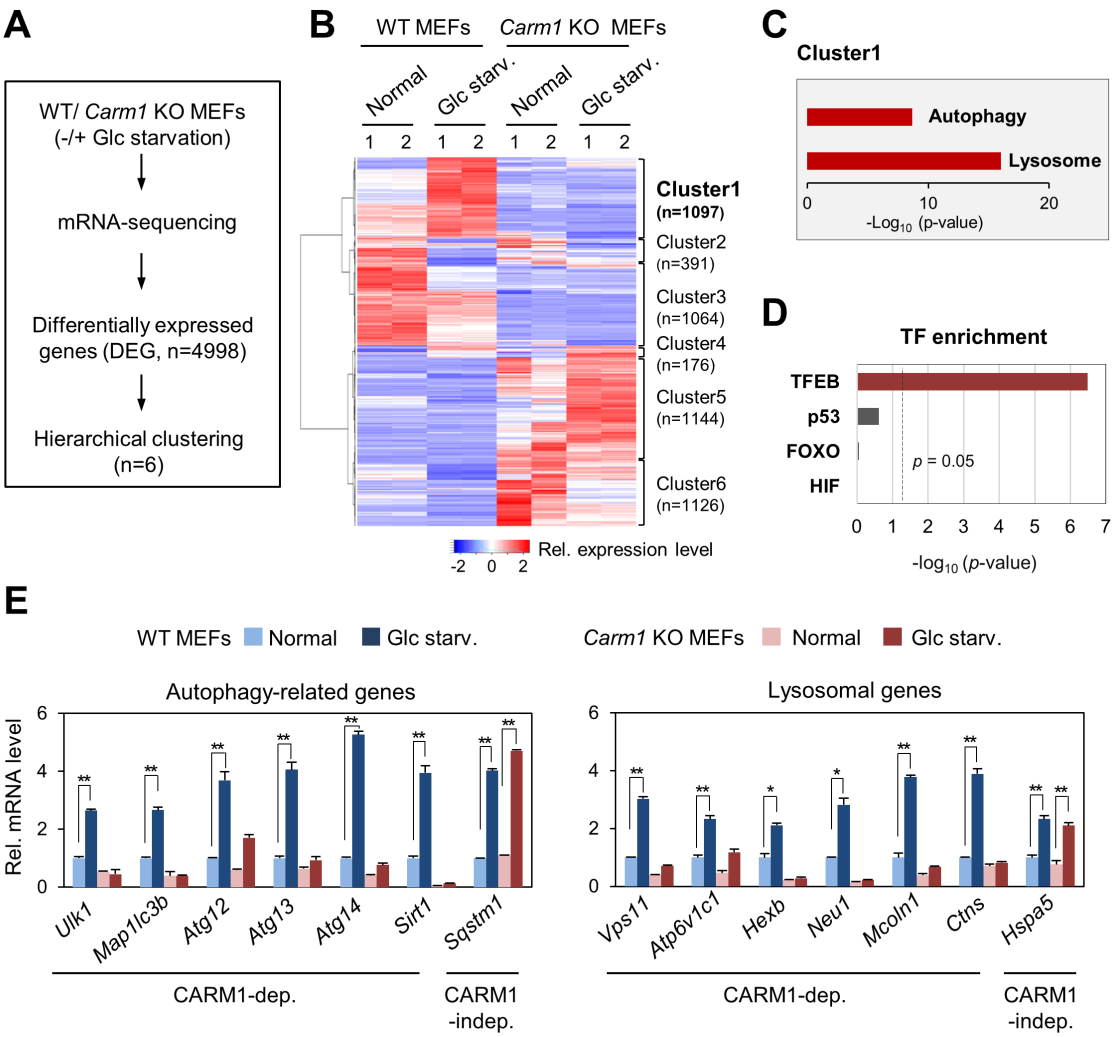
A
WT/ Carm1 KO MEFs
(-/+ Glc starvation)
mRNA-sequencing
Differentially expressed
genes (DEG, n=4998)
Hierarchical clustering
(n=6)
B
WT MEFs
Carm1 KO MEFs
Normal
Glc starv.
Normal
Glc starv.
1 2 1 2 1 2 1 2
Cluster1
(n=1097)
Cluster2
(n=391)
Cluster3
(n=1064)
Cluster4
(n=176)
Cluster5
(n=1144)
Cluster6
(n=1126)
Rel. expression level
-2 0 2
C
Cluster1
Autophagy
Lysosome
0
10
20
-Log10 (p-value)
D
TF enrichment
TFEB
p53
FOXO
HIF
p = 0.05
0 1 2 3 4 5 6 7
-log10 (p-value)
E
WT MEFs Normal Glc starv.
Carm1 KO MEFs Normal Glc starv.
Autophagy-related genes
Rel. mRNA level
Ulk1
Map1lc3b
Atg12
Atg13
Atg14
Sirt1
Sqstm1
CARM1-dep.
CARM1
-indep.
Lysosomal genes
Vps11
Atp6v1c1
Hexb
Neu1
Mcoln1
Ctns
Hspa5
CARM1-dep.
CARM1
-indep.

Figure III-1. Identification of CARM1 target genes by RNA-seq analysis

(**A**) Flow chart showing the strategy of RNA-seq analysis. A total of 4,998 differentially expressed genes (DEGs) are identified using a pairwise comparison between WT and *Carm1* KO MEFs under Normal or Glc starvation. (**B**) Hierarchical clustering results applied to 4,998 DEGs identified 6 Clusters including Cluster 1, where Glc starvation up-regulates gene expression levels only in WT MEFs, indicating CARM1-dependent target genes. (**C**) Autophagy-related genes and lysosomal genes significantly observed in Cluster 1. Hyper-geometric *p*-values were calculated using the genes from the human autophagy database (http://autophagy.lu) and the mouse autophagy database (http://www.tanpaku.org/autophagy) as well as the human lysosome gene database (http://lysosome.unipg.it/). (**D**) Genes from cluster 1 were analyzed for transcription factor (TF) motif enrichment of TFEB, p53, FOXO, and HIF, which are all known TFs involved in autophagy and lysosomal biogenesis at their promoter region (-500~100). Hypergeometric p-values were calculated. **(E**) qRT-PCR analysis showing mRNA levels of CARM1-dependent autophagy-related genes and lysosomal genes in WT and *Carm1* KO MEFs in response to Glc starvation. Data represent mean ± s.e.m. NS = Non-Significant; *p<0.05, ** p<0.01. Statistics by one-tailed *t*-test.

Autophagy genes (n=246)						
Akt1	Brsk1	Dclk2	Hif1a	Nampt	Rab5a	Ulk1
Akt2	Brsk2	Ddit3	Hsp90ab1	Nbr1	Rac1	Ulk2
Akt3	Calcoco1	Dlc1	Hspa5	Nckap1	Raf1	Ulk3
Ambra1	Calcoco2	Dnajb1	Hspa8	Nfe2l2	Rb1	Usp10
Arnt	Camk1	Dnajb9	Hspb8	Nfkb1	Rb1cc1	Uvrag
Arsa	Camk1d	Dram1	Ifng	Nkx2-3	Rela	Vamp3
Arsb	Camk1g	Edem1	Ikbkb	Nlrc4	Rgs19	Vegfa
Atf4	Camk2a	Eef2	Ikbke	Npc1	Rheb	Wdfy3
Atf6	Camk2b	Eef2k	Il24	Nrg1	Rock1	Wdr45
Atg10	Camk2d	Egfr	Itga3	Nrg2	Rps6kb1	Wipi1
Atg12	Camk2g	Eif2ak2	Itga6	Nrg3	Rps6kb2	Wipi2
Atg13	Camkk2	Eif2ak3	Itgb1	Nuak1	Rptor	Zfyve1
Atg16l1	Canx	Eif2s1	Itgb4	Nuak2	Sar1a	
Atg16l2	Capn1	Eif4ebp1	Itpr1	P4hb	Sesn2	
Atg2a	Capn10	Eif4g1	Kif15	Park2	Sgk1	
Atg2b	Capn2	Erbb2	Kif5b	Parp1	Sgk2	
Atg3	Capns1	Ern1	Klhl24	Pelp1	Sgk3	
Atg4a	Casp1	Ero1l	Lamp1	Pex14	Sh3glb1	
Atg4b	Casp3	Fadd	Lamp2	Pex3	Sik1	
Atg4c	Casp4	Fas	Map1lc3a	Phldb2	Sik2	
Atg4d	Casp8	Fkbp1a	Map1lc3b	Pik3c3	Sirt1	
Atg5	Ccl2	Fkbp1b	Map2k7	Pik3r4	Sirt2	
Atg7	Ccr2	Fos	Mapk1	Pink1	Snrk	
Atg9a	Cd46	Foxo1	Mapk3	Pkd1l3	Sphk1	
Atg9b	Cdkn1a	Foxo3	Mapk8	Plk3	Spns1	
Atic	Cdkn1b	Gaa	Mapk8ip1	Plk4	Sqstm1	
Bag1	Cdkn2a	Gabarap	Mapk9	Pnck	St13	
Bag3	Cflar	Gabarapl1	Mark1	Ppp1r15a	Stk11	
Bak1	Chd9	Gabarapl2	Mark2	Prkaa1	Stk33	
Bax	Chmp2b	Gapdh	Mark3	Prkaa2	Stk36	
Bcl2	Chmp4b	Gnai3	Mark4	Prkab1	Tbk1	
Bcl2l1	Cln3	Gnb2l1	Mbtps2	Prkar1a	Thoc5	
Becn1	Ctsb	Gopc	Mlst8	Prkcd	Tm9sf1	
Bid	Ctsd	Grid1	Mtmr14	Prkcq	Tmem74	
Birc5	Cx3cl1	Grid2	Mtor	Pten	Tnfsf10	
Birc6	Cxcr4	Harbi1	Muc6	Ptk6	Tpr	
Bnip1	Dapk1	Hdac1	Myc	Rab11a	Tsc1	
Bnip3	Dapk2	Hdac6	Myo18a	Rab24	Tsc2	
Bnip3l	Dclk1	Hgs	Naf1	Rab33b	Tusc1	

Lysosomal genes (n=348)								
Abca2	Atp5b	Cts7	Fnbp1	Hyal1	Mcoln1	Pld3	Slc17a5	Tpcn2
Abca5	Atp6ap1	Ctsa	Fth1	Hyal2	Mfsd8	Plekhf1	Slc26a11	Tpp1
Abcb9	Atp6v0a1	Ctsb	Ftl1	Hyal3	Mlc1	Plod1	Slc29a3	Trim23
Acp2	Atp6v0a2	Ctsc	Fuca1	Ids	Mmd	Pnpla7	Slc31a1	Trip10
Acp5	Atp6v0a4	Ctsd	Fuca2	Idua	Mmp13	Pon2	Slc36a1	Tspan1
Acpp	Atp6v0b	Ctse	Fyco1	Ifi30	Mpo	Ppt1	Slc48a1	Unc13d
Ada	Atp6v0c	Ctsf	Gaa	Ifitm3	Mt1	Ppt2	Smpd1	Unc93b1
Adam8	Atp6v0d1	Ctsg	Gabarap	Igf2r	Mtor	Pqlc2	Smpdl3a	Uvrag
Aga	Atp6v0d2	Ctsh	Galc	Il4i1	Myh1	Prcp	Snap23	Vamp8
Aldob	Atp6v1g1	Ctsj	Galns	Irgm1	Myo7a	Prdx6	Snapin	Vma21
Ank3	Atp6v1h	Ctsk	Gba	Itm2c	Naaa	Prf1	Snx16	Vps11
Ankrd27	Bcl10	Ctsl	Gc	Kcne1	Naga	Prss16	Sort1	Vps18
Anxa11	Calcrl	Ctsm	Gga1	Kcne2	Naglu	Psap	Spaca3	Vps33a
Ap1b1	Cat	Ctso	Gga2	Kif2a	Nagpa	Psapl1	Sphk2	Vps33b
Ap1g1	Ccdc115	Ctsr	Gga3	Lamp1	Napsa	Psen1	Spns1	Vps36
Ap1g2	Cckar	Ctss	Ggh	Lamp2	Nbr1	Psen2	Src	Vps39
Ap1m1	Ccz1	Ctsw	Gimap5	Lamp3	Ncstn	Rab14	Srgn	Vps4b
Ap1m2	Cd164	Ctsz	Gja1	Lamtor1	Neu1	Rab27a	Stx3	Wdr48
Ap1s1	Cd1d1	Cubn	Gla	Lamtor2	Neu4	Rab7	Stx7	Znrf1
Ap1s2	Cd1d2	Cxcr2	Glb1	Laptm4a	Ngp	Rab9	Stx8	Znrf2
Ap1s3	Cd300lh	Dirc2	Gm2a	Laptm4b	Nos1	Rilp	Stxbp2	
Ap3b1	Cd63	Dnase2a	Gnptab	Laptm5	Npc1	Rnase6	Sult1c2	
Ap3b2	Cd68	Dnase2b	Gnptg	Ldlr	Npc2	Rnaset2a	Sumf1	
Ap3d1	Cd74	Doc2a	Gns	Lgmn	Nppa	Rnaset2b	Syt7	
Ap3m1	Ces1d	Dpp4	Got1	Lhcgr	Nup62-il4i1	Rnf13	Tcirg1	
Ap3m2	Ces2e	Dpp7	Gpc3	Lipa	Oca2	Rnf152	Tecpr1	
Ap3s1	Ces3b	Dram1	Gpr137b	Litaf	Ostm1	Rptor	Thbs1	
Ap3s2	Chid1	Dram2	Gpr143	Lmbrd1	P2ry2	Rraga	Tlr7	
Ap4b1	Chit1	Ear14	Grn	Lpl	P4hb	Rragb	Tlr9	
Ap4e1	Clcn7	Ear4	Gusb	Lrba	Pax2	Rragc	Tm9sf1	
Ap4m1	Cln3	Eif5a	H2-Aa	Ltf	Pcsk9	Rragd	Tmbim1	
Ap4s1	Cln5	Elane	H2-DMa	M6pr	Pcyox1	Scarb2	Tmem106b	
Aqp2	Clta	Enpep	H2-DMb2	Man2b1	Pdgfrb	Scpep1	Tmem192	
Arl8a	Cltb	Entpd4	H2-Eb1	Man2b2	Pdia3	Selenbp2	Tmem55a	
Arl8b	Cltc	Epdr1	H2-Ob	Manba	Pf4	Sgsh	Tmem55b	
Arsa	Creg1	Fam20c	Hck	Manf	Pla2g15	Siae	Tmem63a	
Arsb	Crhbp	Fasl	Hexa	March1	Pla2g4e	Sidt2	Tmem74	
Arsg	Cst3	Fgb	Hexb	March2	Pla2g4f	Slc11a1	Tmem9	
Asah1	Ctbs	Fgfr3	Hgsnat	March3	Plb1	Slc11a2	Tmem97	
Ass1	Ctns	Flot1	Hps4	March8	Plbd1	Slc15a3	Tnfaip3	
Atp13a2	Ctrb1	Flot2	Hpse	March9	Plbd2	Slc15a4	Tpcn1	

Table III-1. List of autophagy-related genes and lysosomal genes.
Lysosomal genes were obtained from lysosomal gene database http://lysosome.unipg.it. Autophagy genes were combined from the human autophagy database (http://autophagy.lu) and the mouse autophagy database (http://www.tanpaku.org/autophagy).

Identification of CARM1 target genes by ChIP-sequencing

I performed chromatin immunoprecipitation (ChIP)-sequencing analysis against anti-H3R17me2 antibody in WT MEFs upon glucose starvation. I observed active promoters were enriched for H3R17me2 as well as activating H3K4me3 signal (Fig. III-2A). On the other hand, H3R17me2 signals were missing at distally (<2.5 kbp from annotated transcription start sites) bound CBP (Visel et al., 2009) or Med12 (Kagey et al., 2010) in MEFs, indicating that H3R17me2 signal is predominantly enriched to active promoters similar to H3K4me3, but not at enhancer regions (Fig. III-2A). Upon glucose starvation, H3R17me2 peaks were globally increased as exemplified by *Map1lc3b* (Fig. III-2B-C), confirming the increased H3R17me2 levels under nutrient deprived state. Using the previously defined autophagy-related genes and lysosomal genes, I found that H3R17me2 increase is observed at promoters of 127 autophagy-related genes (127/246, 51.6%) and 190 lysosomal genes (190/348, 54.6%) (Table III- 2).

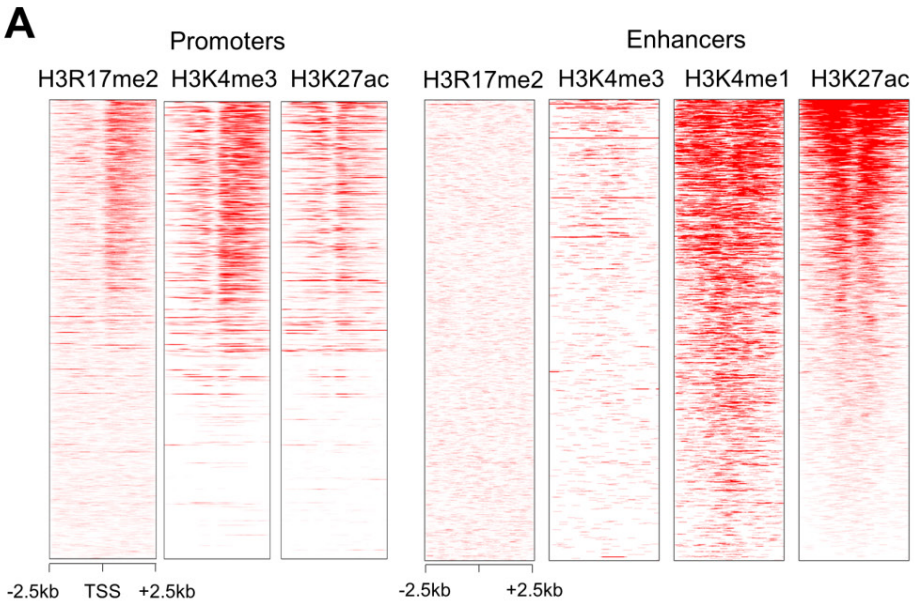
A
Promoters
H3R17me2
H3K4me3
H3K27ac
-2.5kb
TSS
+2.5kb
Enhancers
H3R17me2
H3K4me3
H3K4me1
H3K27ac
-2.5kb
+2.5kb

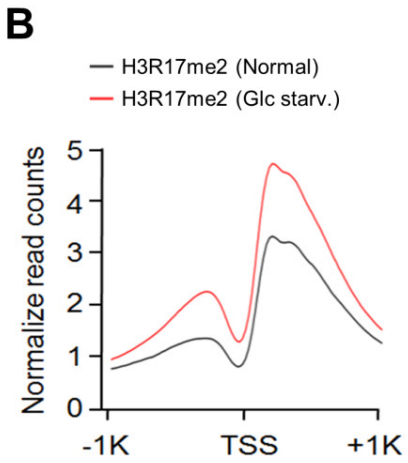
B
H3R17me2 (Normal)
H3R17me2 (Glc starv.)
Normalize read counts
5
4
3
2
1
0
-1K
TSS
+1K

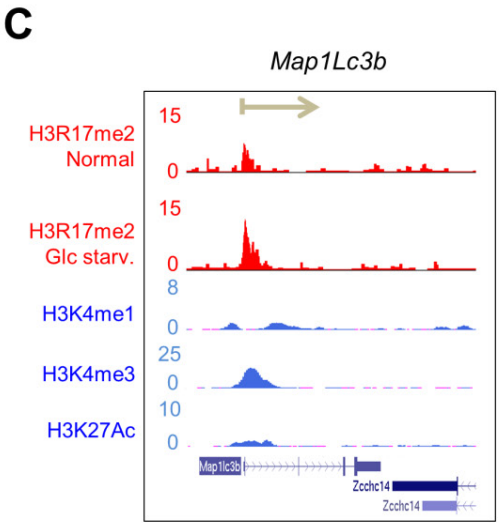
C
Map1Lc3b
H3R17me2
Normal
15
0
H3R17me2
Glc starv.
15
0
H3K4me1
8
0
H3K4me3
25
0
H3K27Ac
10
0
Map1lc3b
Zcchc14
Zcchc14

Figure III-2. Identification of CARM1 target genes by ChIP-sequencing

(**A**) Enrichment of H3R17me2 at promoters (left) and enhancers (right). At promoters, genes were sorted based on the expression levels, indicating that H3R17me2 as well as H3K4me3 were enriched at active promoters. We used 8,398 distal (<2.5 kbp from annotated TSSs) CBP and Med12 binding sites for enhancers, which were sorted based on H3K27ac levels. H3R17me2 was not detected at enhancers. The data on H3R17me2, H3K4me1, H3K4me3, and H3K27ac were obtained from MEFs under normal condition. (**B**) Increase in H3R17me2 at promoters of genes from cluster 1 after Glc starvation. (**C**), Increased H3R17me2 levels in response to 18 hours of Glc starvation at the autophagy-related gene, *Map1lc3b*. The direction of transcription is indicated by the arrow and the beginning of the arrow indicates the TSS. The data on H3K4me1, H3K4me3, and H3K27ac were obtained from MEFs under normal condition.

Autophagy genes (n=127)			
Akt1	Dclk2	Mtmr14	Stk36
Ambra1	Ddit3	Mtor	Tmem74
Arsb	Dlc1	Myc	Tsc1
Atf6	Dnajb9	Nbr1	Tusc1
Atg10	Egfr	Nfe2l2	Ulk1
Atg12	Eif2ak2	Nfkb1	Ulk3
Atg13	Eif4ebp1	Nuak1	Usp10
Atg16l1	Eif4g1	Park2	Vamp3
Atg2a	Fadd	Parp1	Vegfa
Atg4a	Fos	Pelp1	Wdr45
Atg4b	Foxo3	Pik3r4	Wipi1
Atic	Gaa	Pink1	Wipi2
Bag1	Gabarap	Plk3	Zfyve1
Bag3	Gabarapl1	Plk4	
Bax	Gabarapl2	Ppp1r15a	
Bcl2	Gapdh	Prkab1	
Bcl2l1	Gnai3	Prkar1a	
Becn1	Grid1	Prkcd	
Bid	Harbi1	Ptk6	
Birc5	Hdac6	Rab24	
Bnip1	Hgs	Rab33b	
Calcoco1	Hif1a	Rab5a	
Camk1	Hsp90ab1	Raf1	
Camk1d	Hspb8	Rela	
Camk2a	Ikbkb	Rps6kb1	
Camk2b	Ikbke	Rps6kb2	
Camk2g	Itga3	Rptor	
Camkk2	Itpr1	Sar1a	
Capn1	Klhl24	Sesn2	
Capn10	Lamp1	Sik1	
Cd46	Lamp2	Sik2	
Cdkn1a	Map2k7	Sirt1	
Cdkn2a	Mapk1	Sirt2	
Cflar	Mapk3	Snrk	
Chd9	Mapk8ip1	Sphk1	
Chmp2b	Mapk9	Spns1	
Cln3	Mark1	Sqstm1	
Ctsd	Mark2	St13	

Lysosomal genes (n=190)				
Abca5	Creg1	Gpr137b	Naga	Sidt2
Abcb9	Crhbp	Grn	Naglu	Slc15a4
Acp2	Cst3	Gusb	Nagpa	Slc26a11
Ada	Ctns	H2-Aa	Nbr1	Slc31a1
Adam8	Cts7	H2-DMa	Neu1	Slc36a1
Anxa11	Ctsa	H2-Eb1	Nup62-il4i1	Slc48a1
Ap1g1	Ctsc	Hexa	Oca2	Smpd1
Ap1g2	Ctsd	Hexb	Ostm1	Snap23
Ap1m1	Ctsf	Hgsnat	P2ry2	Sort1
Ap1s3	Ctsj	Hps4	Pcyox1	Sphk2
Ap3b2	Cubn	Hpse	Pdgfrb	Spns1
Ap3m1	Dnase2a	Hyal2	Pdia3	Srgn
Ap3s2	Doc2a	Hyal3	Pf4	Stx3
Ap4m1	Dpp7	Ids	Pla2g15	Stx7
Ap4s1	Dram2	Idua	Pld3	Stx8
Arl8a	Ear14	Ifitm3	Plod1	Stxbp2
Arl8b	Ear4	Igf2r	Pnpla7	Sult1c2
Arsb	Elane	Kcne1	Pon2	Sumf1
Arsg	Entpd4	Lamp1	Ppt1	Syt7
Asah1	Fam20c	Lamp2	Ppt2	Tcirg1
Ass1	Fasl	Lamtor1	Pqlc2	Tecpr1
Atp13a2	Fgfr3	Lamtor2	Prcp	Thbs1
Atp6v0a1	Flot1	Laptm4a	Psap	Tlr9
Atp6v0a2	Flot2	Lgmn	Psen1	Tmem74
Atp6v0b	Fth1	Lipa	Psen2	Tmem9
Atp6v0c	Ftl1	Lrba	Rab27a	Tpcn1
Atp6v0d1	Fuca2	Man2b1	Rab7	Tpp1
Atp6v1g1	Fyco1	Man2b2	Rilp	Trim23
Atp6v1h	Gaa	Manba	Rnaset2a	Unc13d
Calcrl	Gabarap	Manf	Rnaset2b	Vamp8
Cckar	Galc	March2	Rnf152	Vps11
Cd63	Gba	March9	Rptor	Vps18
Cd74	Gga2	March8	Rraga	Vps33a
Chid1	Ggh	Mfsd8	Rragc	Vps33b
Chit1	Gimap5	Mmp13	Rragd	Vps39
Cln3	Gja1	Mtor	Scarb2	Wdr48
Cln5	Gns	Myh1	Scpep1	Znrf1
Cltb	Got1	Naaa	Sgsh	Znrf2

Table III-2. List of autophagy-related genes and lysosomal genes with increase in H3R17me2 upon glucose starvation

List of genes with “H3R17me2 peak Tag counts GS18h / H3R17me2 peak Tag count GS 0h > 1.5” are listed

CARM1 binds with TFEB upon glucose starvation

TFEB, a member of the microphthalmia-associated transcription factor (MITF) subfamily (Steingrímsson et al., 2004), functions as a master regulator of lysosomal biogenesis and autophagy (Sardiello et al., 2009; Settembre et al., 2011). TFEB was identified as the transcription factor of target genes involved in lysosomal biogenesis and autophagy under nutrient starvation or lysosomal dysfunction. Under basal conditions, it is mainly located and sequestered in the cytoplasm whereas it rapidly moves into the nucleus to function as a transcription factor in stress conditions (David, 2011; Settembre and Ballabio, 2011). In order to ascertain the involvement of TFEB for the transcriptional regulation of CARM1 target genes, I first checked the binding of TFEB to CARM1. Upon glucose starvation, CARM1 and TFEB exhibited mutual binding from nuclear fractions (Fig. III-3A). Immunocytochemistry data revealed that TFEB translocated into the nucleus and co-localized with CARM1 upon glucose starvation (Fig. III-3B). Bimolecular fluorescence complementation (BiFC) assays showed that TFEB-CARM1 interaction happens mainly in the nucleus (Fig. III-3C). I have further analyzed the binding between CARM1 and TFEB and performed domain analysis to see which domains are important for their binding. CARM1 binds to transcriptional activation domain of TFEB (Fig. III-3D) and TFEB on the other hand binds to the methyltransferase domain of CARM1 (Fig. III-3E).

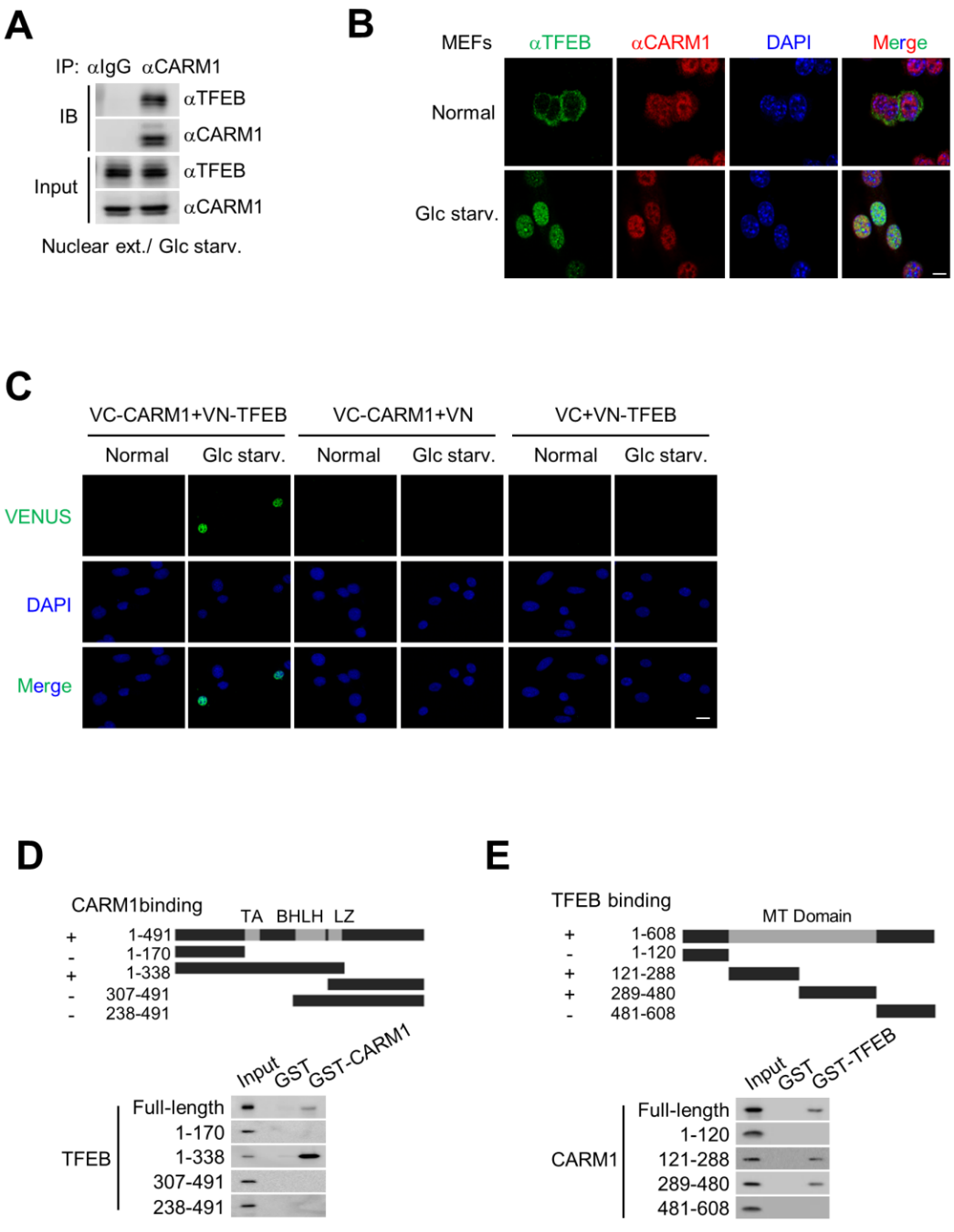
A
IP: αIgG αCARM1
IB
αTFEB
αCARM1
Input
αTFEB
αCARM1
Nuclear ext./ Glc starv.
B
MEFs
αTFEB
αCARM1
DAPI
Merge
Normal
Glc starv.
C
VC-CARM1+VN-TFEB
VC-CARM1+VN
VC+VN-TFEB
Normal
Glc starv.
Normal
Glc starv.
Normal
Glc starv.
VENUS
DAPI
Merge
D
CARM1binding
TA BHLH LZ
+ 1-491
- 1-170
+ 1-338
- 307-491
- 238-491
Input
GST
GST-CARM1
TFEB
Full-length
1-170
1-338
307-491
238-491
E
TFEB binding
MT Domain
+ 1-608
- 1-120
+ 121-288
+ 289-480
- 481-608
Input
GST
GST-TFEB
CARM1
Full-length
1-120
121-288
289-480
481-608

Figure III-3. Interaction between CARM1 and TFEB

(**A**) Co-immunoprecipitation assay between endogenous CARM1 and TFEB in MEFs after 18 hrs of Glc starvation. (**B**) Immunocytochemistry of Flag-TFEB (green); CARM1 (red); DAPI (blue) in MEFs before and after Glc starvation. Scale bar, 10 μm. (**C**) BiFC analysis of CARM1-TFEB interaction. MEFs were transfected with the indicated combination of split Venus constructs and analyzed by confocal microscopy. Scale bar, 20 μm. (**D**) *In vitro* GST pull-down assay for binding between GST-CARM1 and TFEB deletions. TA: Transcription Activation domain; BHLH: Basic helix-loop-helix; LZ: Leucine Zipper. (**E**) *In vitro* GST pull-down assay for binding between GST-TFEB and CARM1 deletions. MT; Methyltransferase domain.

CARM1 interacts with TFE3, another member of the MITF family

CARM1 also interacts with TFE3, another member of the MiTF family (Fig.III-4A). Recent studies have shown that like TFEB, TFE3 could function as a regulator of lysosomal response and autophagy (Martina et al., 2014). However, knockdown of TFE3 in MEFs had rather mild effect on the transcriptional level of various autophagy-related and lysosomal genes in response to starvation (Fig. III-4B-C). TFEB ablation, on the other hand, dramatically altered their expression (Fig. III-4B-C). Assays were conducted on TFEB as it was the dominant transcription factor in my experimental setting but I suspect that in a biological system where TFE3 plays a critical role, CARM1 functions as an important binding partner and regulator of TFE3 transcriptional activity.

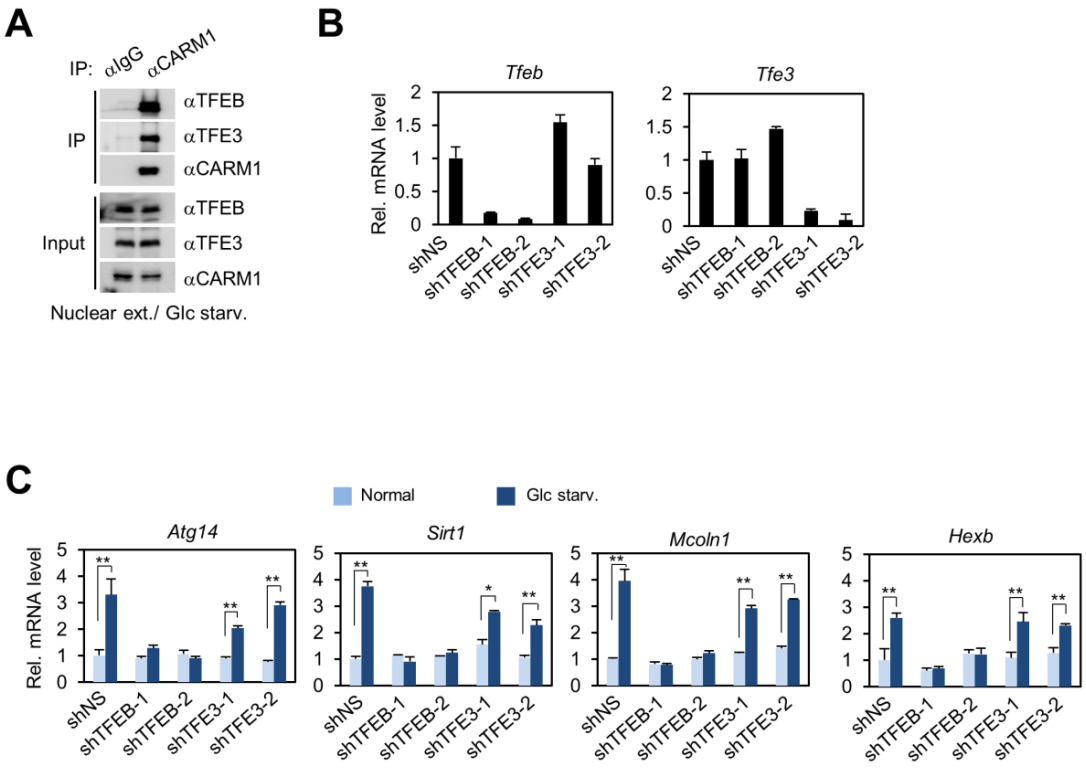

Figure III-4. CARM1 interacts with TFE3, another member of the MiTF family
(**A**) Co-immunoprecipitation assay between CARM1 and TFEB or TFE3 in MEFs after 18 hrs of Glc starvation. (**B**) qRT-PCR analysis of TFEB and TFE3 in MEFs after knockdown with indicated shRNAs. (**C**) qRT-PCR analysis of known TFEB target genes in response to Glc starvation after knockdown of TFEB or TFE3.

CARM1 exerts a transcriptional coactivator function on autophagy-related genes and lysosomal genes through TFEB

Introduction of TFEB increased 2X CLEAR (TFEB binding site)-luciferase reporter activity and overexpression of CARM1 further enhanced its activity (Fig. III-5A), indicating CARM1 functions as a transcriptional coactivator for TFEB. To examine whether the CARM1-dependent target genes identified from my RNA-seq and ChIP-seq analyses are regulated by TFEB, qRT-PCR analysis was performed after knockdown of TFEB. The expression of CARM1-dependent target genes failed to be increased upon glucose starvation after knockdown of TFEB (Fig. III-5B), validating an essential role of TFEB in the transcriptional regulation of CARM1 target genes. I then searched for putative CLEAR (TFEB binding) motif (Table III-3) and performed ChIP assays on CARM1-dependent and -independent target promoters. ChIP assays revealed that the TFEB-dependent, CARM1-dependent genes exhibited recruitment of both TFEB and CARM1 on the promoters accompanied by an increase in H3R17me2 upon glucose starvation (Fig. III-5C-D). However, knockdown of TFEB abolished recruitment of CARM1 on the TFEB-dependent, CARM1-dependent target promoters, subsequently leading to the failure of H3R17me2 induction (Fig. III-5C-D), indicating that recruitment of CARM1 is mediated through TFEB. In contrast, the TFEB-dependent, CARM1-independent promoters did not show CARM1 recruitment with little or no change of H3R17me2 signals (Fig. III-5E).

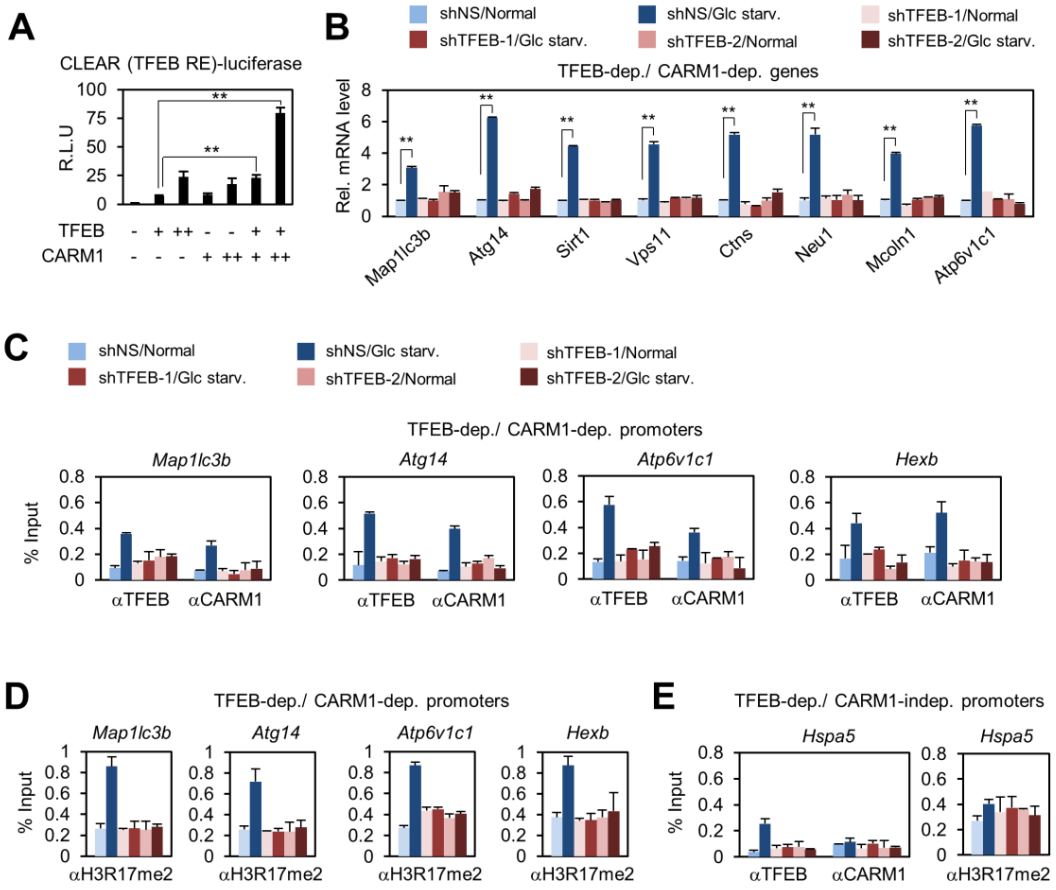
A
CLEAR (TFEB RE)-luciferase
R.L.U
100
75
50
25
0
**
**
TFEB - + ++ - - + +
CARM1 - - - + ++ + ++
B
shNS/Normal
shNS/Glc starv.
shTFEB-1/Normal
shTFEB-1/Glc starv.
shTFEB-2/Normal
shTFEB-2/Glc starv.
TFEB-dep./ CARM1-dep. genes
Rel. mRNA level
8
6
4
2
0
Map1lc3b
Atg14
Sirt1
Vps11
Ctns
Neu1
Mcoln1
Atp6v1c1
C
shNS/Normal
shNS/Glc starv.
shTFEB-1/Normal
shTFEB-1/Glc starv.
shTFEB-2/Normal
shTFEB-2/Glc starv.
TFEB-dep./ CARM1-dep. promoters
Map1lc3b
Atg14
Atp6v1c1
Hexb
% Input
0.8
0.6
0.4
0.2
0
αTFEB
αCARM1
D
TFEB-dep./ CARM1-dep. promoters
Map1lc3b
Atg14
Atp6v1c1
Hexb
% Input
1
0.8
0.6
0.4
0.2
0
αH3R17me2
E
TFEB-dep./ CARM1-indep. promoters
Hspa5
Hspa5
% Input
0.8
0.6
0.4
0.2
0
αTFEB
αCARM1
αH3R17me2

Figure III-5. CARM1 exerts a transcriptional coactivator function on autophagy-related genes and lysosomal genes through TFEB

(**A**) Effect of overexpression of TFEB and CARM1 on 2X CLEAR (TFEB RE)-luciferase reporter. TFEB Response Element (TFEB RE). ** $p<0.01$. Statistics by one-tailed *t*-test. (**B**) qRT-PCR analysis showing mRNA levels of TFEB-dependent and CARM1-dependent autophagy-related genes and lysosomal genes in MEFs in response to Glc starvation after knockdown of TFEB by two different shRNAs. (**C**) ChIP assays were performed using anti-TFEB and anti-CARM1 antibodies on TFEB-dependent, CARM1-dependent promoters after knockdown of TFEB with two different lentivirus shRNAs. CARM1 recruitment is compromised when TFEB is absent. (**D**) ChIP assay using anti-H3R17me2 antibody on TFEB-dependent, CARM1-dependent promoters. (**E**) ChIP assays on *Hspa5* promoter, a TFEB-dependent, CARM1-independent target promoter using anti-TFEB, anti-CARM1, and anti-H3R17me2 antibodies.

Gene name	Chr. location	motif_start (mm9)
1700001L05Rik	chr15	[83197910]
1700007K13Rik	chr2	[28321866]
1700030K09Rik	chr8	[74967716]
2410006H16Rik	chr11	[62416289]
6430548M08Rik	chr8	[122668471]
9430076C15Rik	chr6	[53237246]
Aars	chr8	[113557594]
Abcb9	chr5	[124545833]
Adck3	chr1	[182126397]
Adck4	chr7	[28017882]
Aldh1l2	chr10	[82996926]
Als2	chr1	[59293994]
Armcx1	chrX	[131252472]
Armcx3	chrX	[131291120]
Armcx6	chrX	[131285977]
Arrdc1	chr2	[24791121]
Arsk	chr13	[76236454]
Atg14	chr14	[48188103]
Atp6v1c1	chr15	[38591692]
AW549877	chr15	[3945740, 3945748, 3945764]
B4galnt2	chr11	[95776482]
Bex1	chrX	[132750048]
Bscl2	chr19	[8914529]
C2cd2l	chr9	[44128830]
Calr	chr8	[87371047]
Canx	chr11	[50139094]
Ccdc163	chr4	[116381138]
Ccdc9	chr7	[16872140]
Cdkn1c	chr7	[150647198]
Cenpk	chr13	[105018214]
Chaf1a	chr17	[56179738]
Chmp7	chr14	[70132404]
Cnppd1	chr1	[75139106, 75139288, 75139308]
Cpeb4	chr11	[31770450]
Crebrf	chr17	[26852468, 26852579, 26852597]
Cry1	chr10	[84647852]
Ctns	chr11	[73012542]
Cystm1	chr18	[36508310]
D6Ertd527e	chr6	[87054319]
Dgkq	chr5	[109089828]
Dhps	chr8	[87595598]
Dhtkd1	chr2	[5863815]
Dleu2	chr14	[62301381]
Eaf2	chr16	[36828827]
Eif5a2	chr3	[28680080]
Elovl4	chr9	[83699900]
Epcam	chr17	[88035347]
Fabp3	chr4	[129985935]
Fam178a	chr19	[45005456]
Fam210b	chr2	[172170578, 172170623]

Gene name	Chr. location	motif_start (mm9)
Fam214a	chr9	[74800675]
Fbxl3	chr14	[103499033]
Fbxo10	chr4	[45097484]
Fbxo25	chr8	[13907715]
Flcn	chr11	[59623457]
Fn3k	chr11	[121295883, 121296270]
Fnip1	chr11	[54251604]
Foxred2	chr15	[77787190]
G630090E17Rik	chr10	[39680072]
Garem1	chr5	[30431688]
Gga2	chr7	[129164706]
Glt1d1	chr5	[128112407]
Gm10560	chr4	[155398335]
Gm1141	chrX	[69177683]
Gm16515	chr11	[60727322]
Gng3	chr19	[8914138]
Golga5	chr12	[103707916]
Gpbp1l1	chr4	[116229946]
Gpc2	chr5	[138721565]
Gpnmb	chr6	[48986588]
Gps2	chr11	[69727689]
Hagh	chr17	[24986943, 24987042]
Helq	chr5	[101227613]
Hmgcl	chr4	[135502358]
Hsdl1	chr8	[122099077]
Hsp90b1	chr10	[86168648]
Hspa1a	chr17	[35109576]
Hspbap1	chr16	[35770444]
Ica1	chr6	[8728434]
Ift172	chr5	[31593804]
Ing4	chr6	[124989610]
Irak3	chr10	[119638641]
Kcnip4	chr5	[48901443]
Kdm4b	chr17	[56465246]
Khk	chr5	[31223859]
Klf15	chr6	[90412203, 90412396, 90412565]
Lgals3	chr14	[47993310, 47993623]
Lin52	chr12	[85792453]
Lmtk2	chr5	[144861230]
Lnp	chr2	[74417065]
Lonp1	chr17	[56766355]
Lrrc48	chr11	[60166805]
Lrrc56	chr7	[148381036, 148381111]
Lrrc73	chr17	[46390723]
Lyrm9	chr11	[78639757]
Mamdc4	chr2	[25426761]
Map1lc3b	chr8	[124114336]
Mark1	chr1	[186823628]
Mcoln1	chr8	[3500446, 3500472]
Med4	chr14	[73909485]

Gene name	Chr. location	motif_start (mm9)
Mfsd1	chr3	[67386602, 67386618, 67386652, 67386662, 67386670]
Mfsd7c	chr12	[87087467]
Mocos	chr18	[24811721]
Mpv17	chr5	[31456559, 31456593]
Mtss1l	chr8	[113245325]
Muc2	chr7	[148875737]
Neurl2	chr2	[164659154, 164659259, 164659276]
Nfx1	chr4	[40918004]
Nkpd1	chr7	[20103885]
Nmnat1	chr4	[148859521]
Nol7	chr13	[43493364]
Orc6	chr8	[87823410]
Osbp2	chr11	[3764006]
Osgep	chr14	[51544622]
Palb2	chr7	[129276728]
Pcgf1	chr6	[83028228]
Pcsk6	chr7	[73006726]
Pdhb	chr14	[9005747, 9005863]
Phyhip	chr14	[70857218]
Pim2	chrX	[7454960]
Plagl1	chr10	[12810454]
Plcg2	chr8	[120022153]
Plgrkt	chr19	[29436282]
Pmaip1	chr18	[66618191]
Pnpla7	chr2	[24831575]
Poln	chr5	[34512097]
Ppargc1a	chr5	[51945151, 51945588]
Prrg4	chr2	[104690152]
Ptpdc1	chr13	[48721065]
Ptplad1	chr9	[64869595]
Qtrt1	chr9	[21216231]
Rab24	chr13	[55423332]
Rab5b	chr10	[128133665]
Rad51ap1	chr6	[126889507]
Rad54b	chr4	[11485702, 11485794]
Rcan3	chr4	[134990055]
Rfc4	chr16	[23128139]
Rgs12	chr5	[35341633]
Rnf207	chr4	[151693023]
Rpa1	chr11	[75161946]
Rpl3	chr15	[79914168]
Rsph9	chr17	[46281535]
Rtbdn	chr8	[87470624]
Scnn1a	chr6	[125271305]
Serac1	chr17	[6079729]
Sfn	chr4	[133158117]
Sh3bgrl2	chr9	[83441793]
Shmt1	chr11	[60624701]
Sirt1	chr10	[62801819, 62801891]
Slc22a13b-ps	chr9	[119140991, 119141220]
Slc26a11	chr11	[119216846]
Slc38a7	chr8	[98377418, 98377433]

Gene name	Chr. location	motif_start (mm9)
Slc38a9	chr13	[113450686]
Slc5a8	chr10	[88348494]
Smox	chr2	[131317269]
Smpd2	chr10	[41210333]
Snora21	chr11	[97643319]
Snx32	chr19	[5510650]
Sox21	chr14	[118636162]
Sptbn2	chr19	[4711160]
Tbc1d24	chr17	[24342967]
Tbcel	chr9	[42280339]
Tceal1	chrX	[133242518]
Tmeff2	chr1	[50984316]
Tmem181a	chr17	[6270376, 6270444]
Tmem194	chr10	[127113738]
Tmem246	chr4	[49610686]
Tmem41b	chr7	[117129719, 117129771]
Tom1	chr8	[77557599, 77557633]
Tom1l2	chr11	[60166805]
Trmt1	chr8	[87213163]
Tsc1	chr2	[28496423]
Ttbk1	chr17	[46624808]
Tubg2	chr11	[101017004]
Ubxn11	chr4	[133658412]
Ulk1	chr5	[111239469]
Ung	chr5	[114580088]
Usp11	chrX	[20280697]
Vps11	chr9	[44169746, 44169767]
Wbscr27	chr5	[135408091]
Wdr19	chr5	[65590807]
Wdr62	chr7	[31065831, 31065901, 31065932]
Wisp3	chr10	[38883831]
Ypel5	chr17	[73185640]
Zer1	chr2	[29980593]
Zfp112	chr7	[24896986]
Zfp28	chr7	[6336094]
Zfp296	chr7	[20162677]
Zfp40	chr17	[23330294]
Zfp459	chr13	[67522392]
Zfr2	chr10	[80695511]
Zmym6	chr4	[126754552, 126754589, 126754637]

Table III-3. List of genes from RNA-seq Cluster 1 with potential TFEB motifs
Criteria for a TFEB motif were at most a single mismatch with the 8bp consensus TFEB sequence (TCACGTGA). The motifs were searched within the region from the transcription start site (tss) to 500bp upsteam to 100bp downstream.

A subset of autophagy-related genes and lysosomal genes regulated by TFEB requires CARM1

Given that TFEB knockdown impairs transcription activation and CARM1 recruitment, I sought to examine the effect of CARM1 knockdown on TFEB target genes. qRT-PCR analysis after CARM1 knockdown showed that the expression of a subset of TFEB-dependent autophagy-related genes and lysosomal genes failed to be increased upon glucose starvation (Fig. III-6A). ChIP assay confirmed that knockdown of CARM1 was accompanied by a reduction of H3R17me2 signal on the TFEB-dependent, CARM1-dependent target promoters with little or no effect on TFEB recruitment (Fig. III-6B). However, the TFEB-dependent, CARM1-independent target promoter was not affected by CARM1 knockdown (Fig. III-6C). These data indicate a critical role of CARM1 as a coactivator of TFEB. Finally, to ascertain whether TFEB and CARM1 are co-recruited to the target promoters upon glucose starvation, I performed two-step ChIP assay. Elutes from the first immunoprecipitation reaction with anti-TFEB antibody were re-immunoprecipitated with anti-CARM1 antibody. By using two-step ChIP assay, I confirmed the recruitment of CARM1 at TFEB-bound autophagy-related genes and lysosomal genes (Fig. III-6D). The TFEB-dependent, CARM1-independent target promoter such as *Hspa5* was used as a negative control (Fig. III-6D).

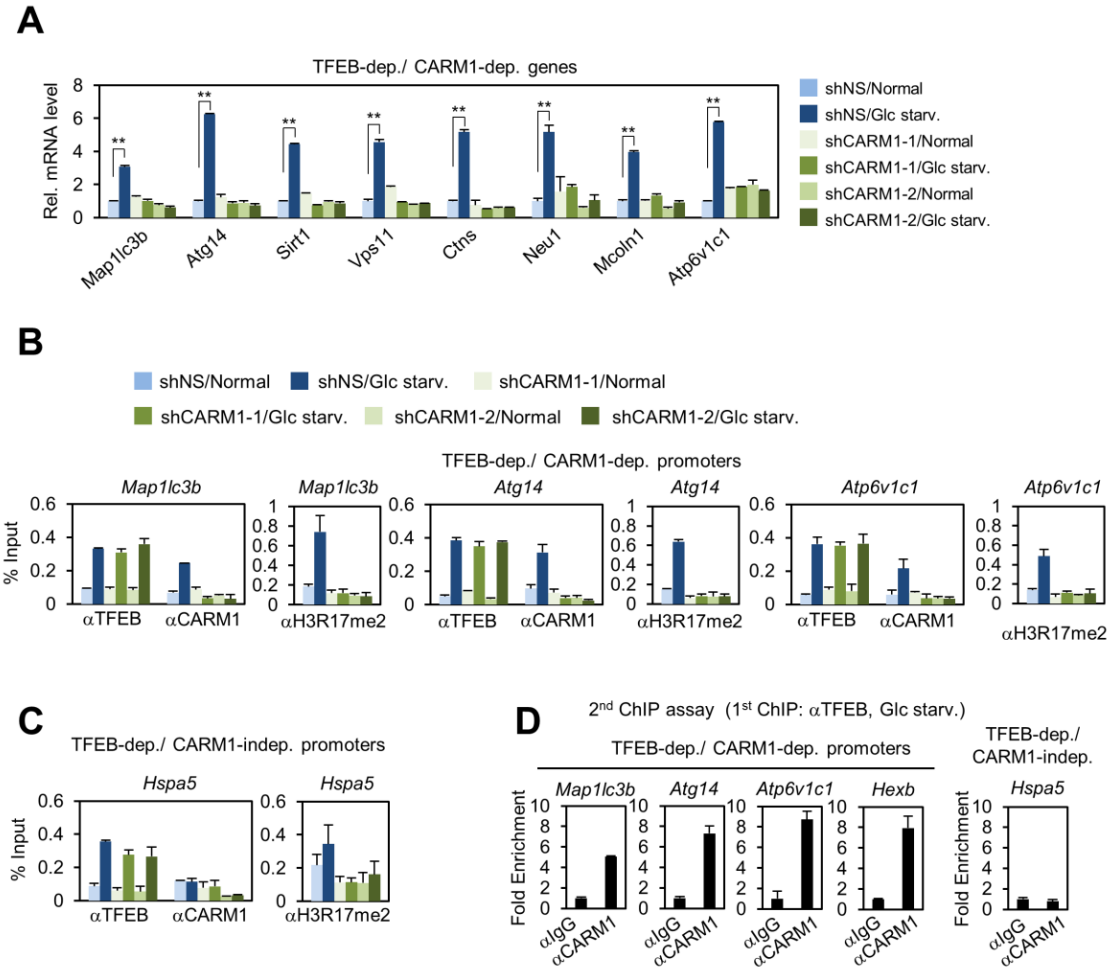
A
TFEB-dep./ CARM1-dep. genes
Rel. mRNA level
shNS/Normal
shNS/Glc starv.
shCARM1-1/Normal
shCARM1-1/Glc starv.
shCARM1-2/Normal
shCARM1-2/Glc starv.
Map1lc3b
Atg14
Sirt1
Vps11
Ctns
Neu1
Mcoln1
Atp6v1c1
B
TFEB-dep./ CARM1-dep. promoters
% Input
αTFEB
αCARM1
αH3R17me2
C
TFEB-dep./ CARM1-indep. promoters
Hspa5
D
2nd ChIP assay (1st ChIP: αTFEB, Glc starv.)
TFEB-dep./ CARM1-dep. promoters
TFEB-dep./ CARM1-indep.
Hexb
Fold Enrichment
αIgG
αCARM1

Figure III-6. A subset of autophagy-related genes and lysosomal genes regulated by TFEB requires CARM1

(**A**) qRT-PCR analysis in MEFs after knockdown of CARM1 by two different shRNAs. ** $p<0.01$. Statistics by one-tailed *t*-test. (**B**) Recruitment of TFEB and CARM1 with increase of H3R17me2 was analyzed by ChIP assays after knockdown of CARM1 with two different lentivirus shRNAs, showing that TFEB recruitment is not affected by CARM1 knockdown. (**C**) ChIP assay using anti-TFEB, anti-CARM1, and anti-H3R17me2 antibodies on TFEB-dependent, CARM1-independent promoters after CARM1 knockdown. (**D**) Two-step ChIP assays were performed on promoters of TFEB-dependent, CARM1- dependent target genes or TFEB-dependent, CARM1-independent target genes in MEFs after 18 hrs of Glc starvation. The chromatin fractions were first subject to pull- down with anti-TFEB antibody, eluted from immunocomplexes and applied for the second pull-down with control IgG or anti-CARM1 antibody

CARM1 is a critical co-activator of TFEB

To ascertain that CARM1 target genes induced by glucose starvation are reflected in their protein expressions, I performed immunoblot analysis of several key autophagy regulators including ULK1, ATG12, ATG13, ATG14, and Vps34 and confirmed that genes that are transcriptionally regulated by CARM1 are induced by glucose starvation in WT MEFs, but not in CARM1 knockdown or *Carm1* KO MEFs (Fig. III-7A).

Previous studies reported overexpression of TFEB increases the formation of autophagosomes and levels of LC3-II (Settembre et al., 2011). Introduction of TFEB in WT MEFs dramatically induced the number of autophagosomes detected by immunofluorescence but not in *Carm1* KO MEFs (Fig. III-7B). Immunoblot analysis of LC3 further showed that increase in LC3-II levels by TFEB overexpression was not observed in *Carm1* KO MEFs (Fig. III-7C). Together, my data demonstrate that CARM1 is a critical cofactor of TFEB and that co-recruitment of TFEB and CARM1 on the target promoters after nuclear localization of TFEB upon glucose starvation is responsible for transcriptional activation of a subset of the autophagy-related genes and lysosomal genes (Fig. III-7D).

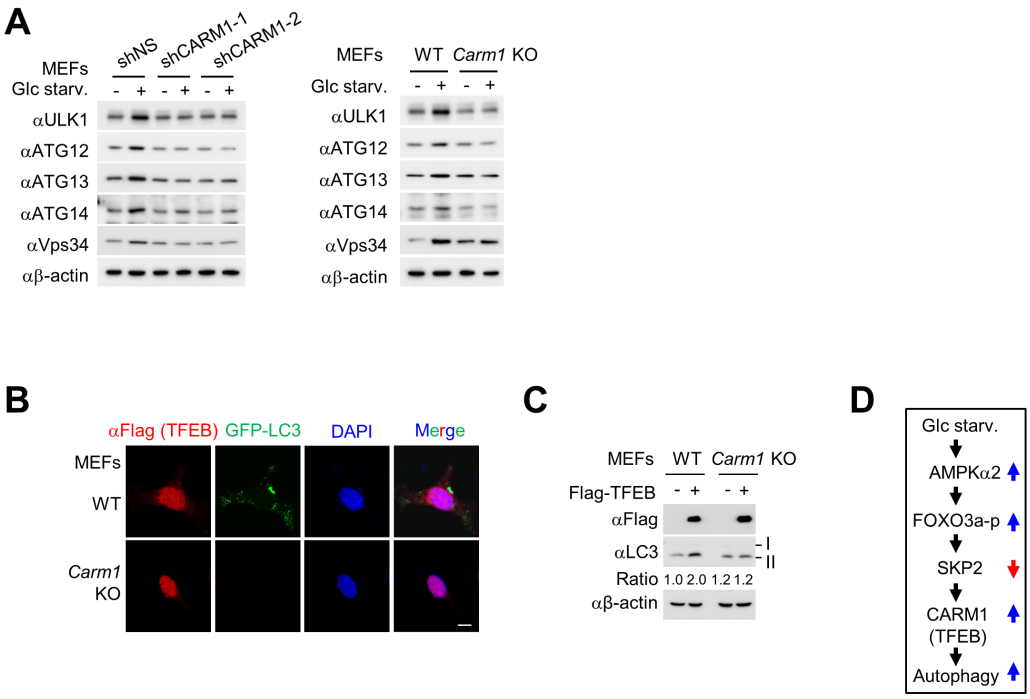

Figure III-7. CARM1 is a critical co-activator of TFEB

(**A**) Immunoblot analysis after knockdown of CARM1 (left) or in WT and *Carm1* KO MEFs (right). (**B**) Flag-TFEB and GFP-LC3 were transiently transfected in WT and *Carm1* KO MEFs and examined by confocal microscopy. Flag-TFEB (red); GFP-LC3 (green); DAPI (blue). Scale bar, 10 μm. (**C**) WT and *Carm1* KO MEFs transiently transfected with Flag-TFEB expressing plasmid were examined by immunoblot for the indicated antibodies. LC3-II/LC3-I ratio is indicated. (**D**) Schematics of newly identified AMPK-SKP2-CARM1 signaling cascade in starvation-induced autophagy.

AMPK is required for activation of TFEB- and CARM1-dependent target genes

As CARM1 failed to increase upon glucose starvation in *Ampk* DKO MEFs, I aimed to analyze for the expression levels of TFEB-dependent, CARM1-dependent target genes in WT and *Ampk* DKO MEFs. qRT-PCR analysis revealed that the increased expression levels of TFEB-dependent, CARM1-dependent target genes in WT MEFs were abrogated in *Ampk* DKO MEFs (Fig. III-8A). Supporting the qRT-PCR results, the recruitment of TFEB was not affected but H3R17me2 was decreased in *Ampk* DKO MEFs (Fig. III-8B). In addition, in *Ampk* DKO MEFs, knockdown of SKP2 significantly increased the mRNA levels of CARM1-dependent autophagy-related and lysosomal genes (Fig. III-8C). I previously showed that SKP2 knockdown partially rescue autophagy in *Ampk* DKO MEFs (Fig. II-12A). It is therefore highly probable that this rescue is due to transcriptional activation of autophagy-related and lysosomal genes resulting from CARM1 recovery.

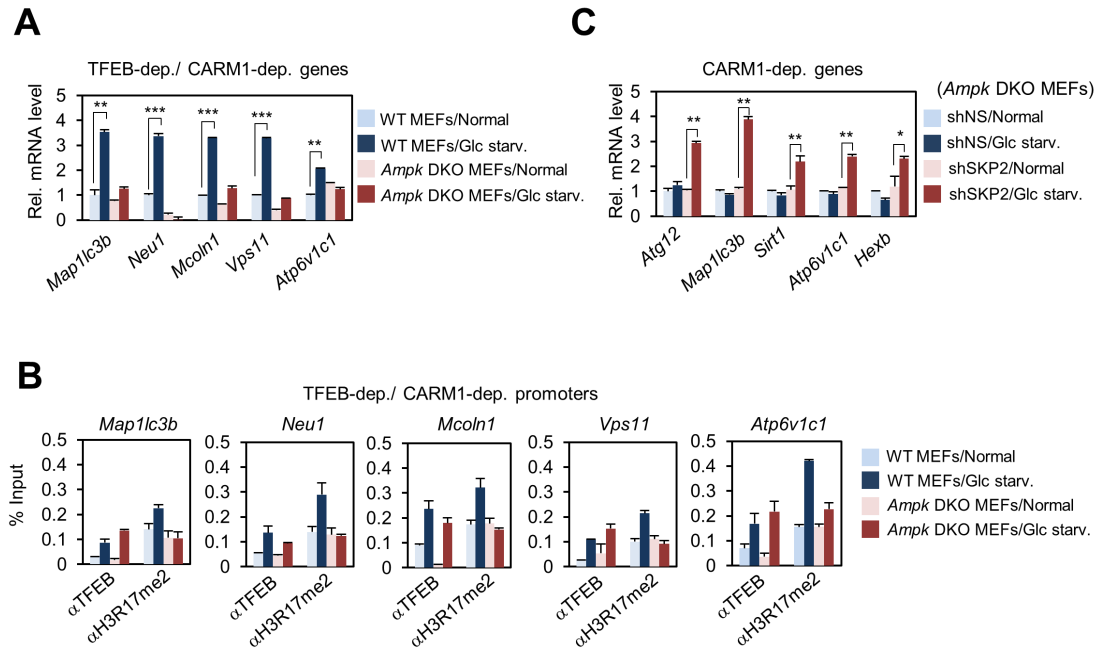

Figure III-8. AMPK is required for activation of TFEB- and CARM1-dependent target genes

(**A**) qRT-PCR analysis showing mRNA levels of TFEB-dependent and CARM1-dependent autophagy-related genes and lysosomal genes in WT and *Ampk* DKO MEFs in response to Glc starvation. (**B**) ChIP assays using anti-TFEB and anti-H3R17me2 antibodies on TFEB-dependent, CARM1-dependent target genes in WT and *Ampk* DKO MEFs. (**C**) qRT-PCR analysis of CARM1-dependent autophagy-related and lysosomal genes after knockdown of SKP2 in *Ampk* DKO MEFs.

Treatment of ellagic acid inhibits CARM1 target gene expression in cells and CARM1-induced autophagy in mice

Given that ellagic acid impaired starvation-induced autophagy, I prompted to examine whether ellagic acid treatment affects the induction of CARM1 target genes. Ellagic acid treatment inhibited the induction of a subset of autophagy-related genes and lysosomal genes regulated by CARM1 with little or no effect on CARM1-independent target genes (Fig. III-9A). Further, I performed ChIP assays on TFEB-dependent, CARM1-dependent or CARM1-independent promoters after ellagic acid treatment. Ellagic acid treatment blocked the recruitment of CARM1, but not TFEB, on the CARM1-dependent promoters, but did not affect CARM1-independent promoters (Fig. III-9B). In parallel, ellagic acid treatment reduced H3R17me2 level on the CARM1-dependent promoters, but not the CARM1-independent promoters (Fig. III-9C).

To examine whether CARM1 and subsequent H3R17me2 are critical for autophagy occurrence *in vivo*, I analyzed for hepatic autophagy in wild-type C57BL/6J mice. Mice were injected with vehicle or ellagic acid then, fed *ad libidum* or fasted overnight. Livers of fasted WT mice showed dramatic increase in CARM1 expression as well as increase in LC3 conversion. However, the LC3 conversion was greatly attenuated in fasted liver pre-injected with ellagic acid (Fig. III-9D). Further, mRNA expression of various CARM1-dependent autophagy-related genes or lysosomal genes was induced in fasted mouse livers but not in the livers of fasted mice treated with ellagic acid (Fig. III-9E).

Taken together, inhibition of H3R17me2 increase by ellagic acid greatly compromises

starvation-induced transcriptional regulation of autophagy and impairs CARM1-mediated autophagy *in vivo*. Given that inhibition of H3R17me2 mark by ellagic acid almost completely blocks CARM1-induced autophagy occurrence *in vivo*, ellagic acid might have a potential to be developed as a therapeutic agent in autophagy-related diseases.

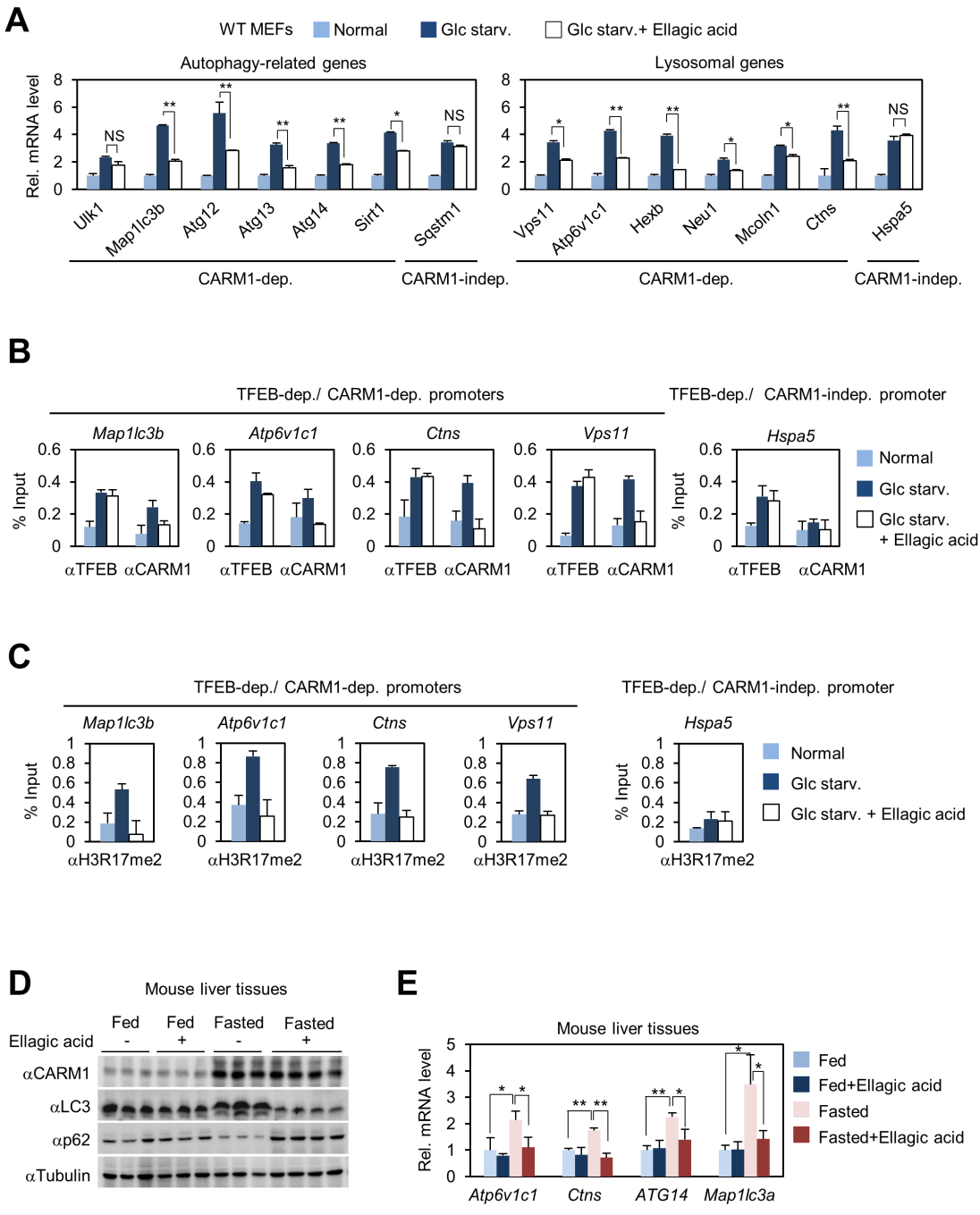
A
WT MEFs
Normal
Glc starv.
Glc starv.+ Ellagic acid
Autophagy-related genes
Lysosomal genes
Rel. mRNA level
Ulk1
Map1lc3b
Atg12
Atg13
Atg14
Sirt1
Sqstm1
Vps11
Atp6v1c1
Hexb
Neu1
Mcoln1
Ctns
Hspa5
CARM1-dep.
CARM1-indep.
B
TFEB-dep./ CARM1-dep. promoters
TFEB-dep./ CARM1-indep. promoter
Map1lc3b
Atp6v1c1
Ctns
Vps11
Hspa5
% Input
αTFEB
αCARM1
Normal
Glc starv.
Glc starv.
+ Ellagic acid
C
TFEB-dep./ CARM1-dep. promoters
TFEB-dep./ CARM1-indep. promoter
αH3R17me2
D
Mouse liver tissues
Fed
Fed
Fasted
Fasted
Ellagic acid
-
+
-
+
αCARM1
αLC3
αp62
αTubulin
E
Mouse liver tissues
Rel. mRNA level
Fed
Fed+Ellagic acid
Fasted
Fasted+Ellagic acid
Atp6v1c1
Ctns
ATG14
Map1lc3a

Figure III-9. Treatment of ellagic acid inhibits CARM1 target gene expression in cells and CARM1-induced autophagy in mice

(**A**) qRT-PCR analysis was performed in MEFs deprived of Glc in the absence or presence of H3R17me2-specific inhibitor, ellagic acid. *p<0.05, ** p<0.01, NS= Non-Significant. Statistics by one-tailed *t*-test. (**B**) Recruitment of TFEB and CARM1 was analyzed by ChIP assays on TFEB-dependent, CARM1-dependent promoters. *Hspa5* promoter was also analyzed as a CARM1-independent promoter. (**C**) ChIP assay using anti-H3R17me2 antibody on the same promoters as in (**B**). Treatment of ellagic acid abolished the increase of H3R17me2 on promoters of TFEB-dependent, CARM1-dependent target genes (**D**) Liver tissues from fed or fasted mice treated with vehicle or ellagic acid were subject to immunoblot analysis. (n=3 per group) (**E**) Expression of autophagy-related genes and lysosomal genes in wild-type mouse livers. Mice were fed or fasted treated with vehicle or ellagic acid (n=3 per group). *p<0.05, ** p<0.01. Statistics by two-tailed *t*-test.

III-4. Discussion

Compared to the cytoplasmic event in autophagy, nuclear events have not been considered of importance for autophagy occurrence thus far. However, my data unveil a critical link between the induction of autophagy and increase of histone H3R17 dimethylation (H3R17me2) through up-regulation of CARM1 leading to the activation of autophagy-related genes and lysosomal genes (Fig. III-10). I report CARM1 as a previously unrecognized coactivator of TFEB, essential in exerting proper transcriptional activity of TFEB. Indeed, the expression of CARM1 is increased upon glucose starvation along with TFEB nuclear translocation and CARM1 is co-recruited on TFEB-dependent target promoters to induce H3R17me2, a transcriptional activation histone mark. The absence of CARM1 significantly dampens TFEB transcriptional activity.

Interestingly, H3R17me2, a modification solely mediated by CARM1 is mainly localized near transcription start site (TSS). Previous studies showed that TFEB is recruited near TSS or within 500bp from TSS (Palmieri et al., 2011). Further, valid CLEAR consensus motifs are significantly enriched in positions from -300 to +100bp from annotated TSSs. Altogether, this supports the idea that TFEB requires CARM1 as a critical coactivator.

The histone arginine methylation on H3R17 appears to directly regulate the outcome of autophagy, as ellagic acid treatment to block H3R17me2 almost completely abolished CARM1-induced autophagy occurrence. Therefore, it is tempting to speculate that there

exist readers of methyl-arginine marks able to recognize histone H3R17 dimethylation and link this histone mark to autophagy program. It will be challenging to screen potential methyl-arginine reader domain-containing proteins to further explore direct functional link of autophagy induction and histone modifications.

AMPK is the upstream kinase responsible for CARM1 stabilization and subsequent transcriptional regulation of TFEB target genes. It is noteworthy that this mechanism is focused on glucose starvation, a signaling that is highly dependent on AMPK. But CARM1 induction and the transcription of lysosomal and autophagy-related genes mediated by TFEB occurred more broadly, for autophagy downstream of a variety of stimuli such as amino acid starvation and rapamycin. This implies that CARM1 induction, subsequent increase in H3R17me2 and the coactivator function of CARM1 on TFEB are well-conserved and important signaling axis in autophagy induction. In parallel, it would be interesting to study for the molecular mechanism underlying CARM1 stabilization independent of AMPK.

Taken together, my findings provide evidence of CARM1-dependent histone arginine methylation as a critical nuclear event for epigenetic regulation in autophagy and shed light on a potential therapeutic targeting of the new signaling axis AMPK-SKP2-CARM1 in autophagy-related diseases.

.

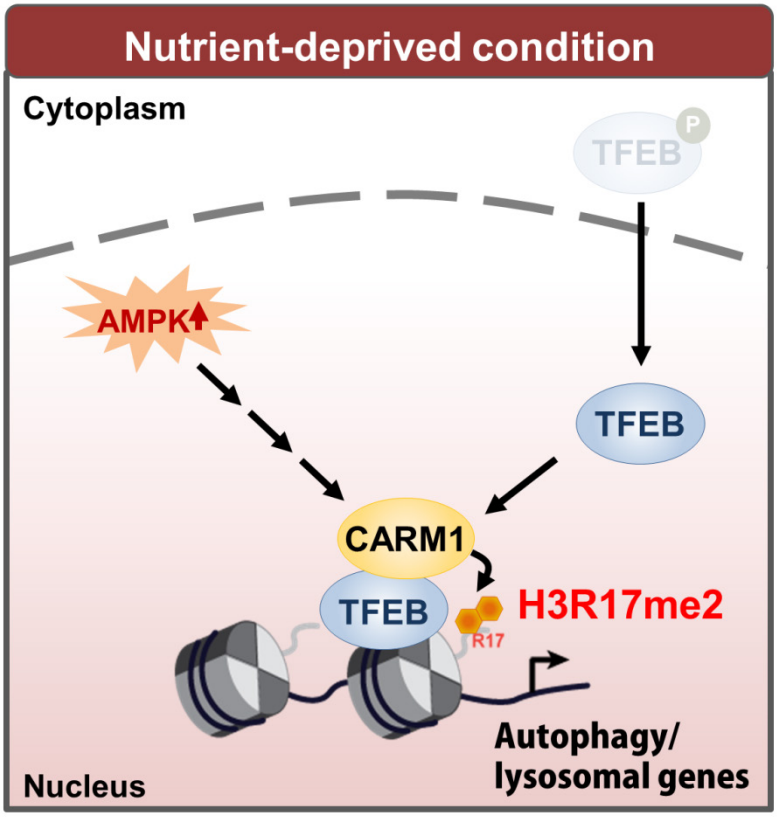

Figure III-10. Schematic model of CARM1-dependent transcriptional regulation of autophagy and lysosomal genes under nutrient-deprived condition

Starvation results in TFEB translocation to the nucleus where it functions as a critical transcription factor of autophagy-related and lysosomal genes. CARM1, stabilized in an AMPK-dependent manner, is co-recruited along with TFEB and functions as its co-activator.

III-5. Materials and Methods

Antibodies

The following commercially available antibodies were used: anti-ATG14 (ab173943), anti-H3R17me2 (ab8284), anti-PI3K Class 3 (ab124905), and anti-TFEB (ab2636) antibodies were purchased from Abcam. anti-ATG12 (#4180), anti-CARM1 (#3379 for IB, #12495 for IP and ChIP), anti-LC3 (#2775), and anti-TFE3 (#14779) antibodies were from Cell Signaling technology. Anti-Flag (F3165), anti-ULK1 (A7481) and anti-β-actin (A1978) antibodies were from Sigma. ellagic acid was from Cayman (#10569).

Cell culture and generation of shRNA knockdown cells

HEK293T, WT, *Carm1* KO and *Ampk* DKO MEFs were cultured at 37°C in Dulbecco's modified Eagle's medium (DMEM) containing 10 % fetal bovine serum (FBS) and antibiotics in a humidified incubator with 5 % CO_2. All cell lines used in the study were regularly tested for mycoplasma contamination. For glucose starvation, cells were washed with PBS, then incubated with glucose-free DMEM supplemented with 10 % dialyzed FBS. Transfection was performed with Turbofect (Fermentas) or Lipofectamine 3000 (Invitrogen) according to manufacturer's protocol. To generate knockdown cells, lentiviral shRNA constructs were first transfected along with viral packaging plasmids (psPAX2 and pMD2.G) into HEK293T cells. Three days post-transfection, viral supernatant was filtered through 0.45-μm filter and infected into

targeting cells. Infected cells were then selected with 5 μg/ml puromycin.

The targeting sequences of shRNAs are as follows.

mCARM1-1; 5'-TCAGGGACATGTCTGCTTATT-3',

mCARM1-2; 5'-GCCTGAGCAAGTGGACATTAT-3',

mSKP2; 5'-GCAAGACTTCTGAACTGCTAT-3',

mTFE3-1; 5'-GTGGATTACATCCGCAAATTA-3',

mTFE3-2; 5'-TGTGGATTACATCCGCAAATT-3',

mTFEB-1; 5'-GCAGGC TGTCATGCATTATAT-3',

mTFEB-2; 5'-CCAAGAAGGATCTGGACTTAA-3',

RNA-sequencing and ChIP-sequencing analyses

The TruSeq method was used to generate RNA-seq libraries. ChIP-seq libraries were prepared using the NEXTflex ChIP-seq kit (Bioo Scientific), according to the manufacturer's instructions. RNA-seq libraries were pair-end sequenced and ChIP-seq libraries were single-end sequenced on an Illumina Hi-seq 2500 (NICEM, Seoul National University). All the RNA-seq data were mapped using Tophat package (Kim et al., 2013a) against the mouse genome (mm9). Differential analysis has been done via EdgeR package (Robinson et al., 2010). Differentially regulated genes were identified using a false discovery rate (FDR) cut-off of 1e-5 for Knockout (KO) against Knockout-Glc Starv. (KO-GS), Wild-type (WT) against Wild-type-Glc Starv. (WT-GS), WT against KO, and WT-GS against KO-GS. We did hierarchical clustering analysis using the gene expression values from all conditions and replicates for previously

selected differential genes. Specifically, we used Ward's criterion for genes with 1-(correlation coefficient) as a distance measure. Clustering heatmap was drawn using z-score that is scaled across samples for each gene. ChIP-Seq data were mapped to the mouse genome using Bowtie. The tracks were generated using uniquely aligned reads. At promoters, genes were sorted based on the expression levels, indicating that H3R17me2 as well as H3K4me3 were enriched at active promoters. We used 8,398 distal (<2.5 kbp from annotated TSSs) CBP and Med12 binding sites for enhancers, which were sorted based on H3K27ac levels. The data on H3K4me1, H3K4me3, and H3K27ac were obtained from MEFs under normal condition.

Immunofluorescence

Immunocytochemistry was performed as previously described (Kim et al., 2012). Cells grown on coverslips at a density of 7 x 10^4 cells were washed three times with PBS and then fixed with 2 % paraformaldehyde in PBS for 10 min at RT. Fixed cells were permeabilized with 0.1 % Triton X-100 in PBS (PBS-T) for 10 min at RT. Blocking was performed with 3 % bovine serum in PBS-T for 30 min. For staining, cells were incubated with antibodies for 2 hrs at RT, followed by incubation with fluorescent labeled secondary antibodies for 1 hr (Invitrogen). Cells were mounted and visualized under a confocal microscope (Zeiss, LSM700). For autophagy studies, MEF cells were transfected with GFP-LC3 and sub-cultured onto coverslips. The following day, cells were incubated with either complete media or glucose starvation media for 18 hrs. For BiFC experiment, pHA-CARM1-VC155 and pFlag-TFEB-VN173 constructs were used.

Bacterial expression and GST pull-down assay

GST-tagged constructs were transformed in Rosetta *E. coli* and purified with glutathione beads (GE Healthcare). ^{35}S-methionine-labelled TFEB deletions or CARM1 deletions were generated using TNT Quick Coupled Transcription/Translation system (Promega) according to the manufacturer's guidance. Purified proteins and *in vitro* translated proteins were diluted in binding buffer (125 mM NaCl, 20 mM Tris [pH 7.5], 10 % glycerol, 0.1 % NP-40, 0.5 mM DTT supplemented with protease inhibitors) for GST pull-down experiment. Samples were then washed four times with dilution buffer and boiled with SDS sample buffer for immunoblotting analysis.

Construction of reporter plasmids and luciferase assays

2X CLEAR (GTCACGTGACCCCAGGGTCACGTGAC) sequence were cloned into pGL2-luciferase reporter vector (Promega). MEFs were transiently transfected with luciferase reporter plasmids and luciferase activity was measured 36 hrs post-transfection and normalized by β-galactosidase expression.

Quantitative RT-PCR

Total RNAs were extracted using Trizol (Invitrogen) and reverse transcription was performed from 2.5 μg total RNAs using the M-MLV cDNA Synthesis kit (Enzynomics). The abundance of mRNA was detected by an ABI prism 7500 system or BioRad CFX384 with SYBR TOPreal qPCR 2x PreMix (Enzynomics). The quantity of mRNA was calculated using ddCt method and HPRT, GAPDH and β-actin were used as

controls. mRNA levels from mouse liver tissues were normalized by the 36B4 gene. All reactions were performed as triplicates. The following mouse primers were used in this study.

β-actin Forward (Fwd): 5’ - TAGCCATCCAGGCTGTGCTG - 3’

β-actin Reverse (Rev): 5’ - CAGGATCTTCATGAGGTAGTC - 3’

Gapdh Fwd: 5’ - CATGGCCTTCCGTGTTCCTA - 3’

Gapdh Rev: 5’ - CCTGCTTCACCACCTTCTTGA - 3’

Hprt Fwd: 5’ - GCTGGTGAAAAGGACCTCTCG - 3’

Hprt Rev: 5’ - CCACAGGACTAGAACACCTGC - 3’

36B4 Fwd: 5’- CAACCCAGCTCTGGAGAAAC - 3’

36B4 Rev: 5’- CCAACAGCATATCCCGAATC - 3’

Ulk1 Fwd: 5’- GCTCCGGTGACTTACAAAGCTG - 3’

Ulk1 Rev: 5’ - GCTGACTCCAAGCCAAAGCA - 3’

Map1lc3b Fwd: 5’ - CACTGCTCTGTCTTGTGTAGGTTG - 3’

Map1lc3b Rev: 5’ - TCGTTGTGCCTTTATTAGTGCATC - 3’

Atg12 Fwd: 5’ - TCCGTGCCATCACATACACA - 3’

Atg12 Rev: 5’ - TAAGACTGCTGTGGGGCTGA - 3’

Atg13 Fwd: 5’ - CCAGGCTCGACTTGGAGAAAA - 3’

Atg13 Rev: 5’ - AGATTTCCACACACATAGATCGC - 3’

Atg14 Fwd: 5’ - AGCGGTGATTTCGTCTATTTCG - 3’

Atg14 Rev: 5’ - GCTGTTCAATCCTCATCTTGCAT - 3’

Sirt1 Fwd: 5’ - GATACCTTGGAGCAGGTTGC - 3’

Sirt1 Rev: 5’ - CTCCACGAACAGCTTCACAA - 3’

Sqstm1 Fwd: 5’ - ATGTGGAACATGGAGGGA AGA - 3’

Sqstm1 Rev: 5’ - GGAGTTCACCTGTAGATGGGT - 3’

Vps11 Fwd: 5’ - AAAAGAGAGACGGTGGCAATC - 3’

Vps11 Rev: 5’ - AGCCCAGTAACGGGATAGTTG - 3’

Atp6v1c1 Fwd : 5’ - ACTGAGTTCTGGCTCATATCTGC - 3’

Atp6v1c1 Rev: 5’ - TGGAAGAGACGGCAAGATTATTG - 3’

Hexb Fwd: 5’ - CTGGTGTCGCTAGTGTCGC - 3’

Hexb Rev: 5’ - CAGGGCCATGATGTCTCTTGT - 3’

Neu1 Fwd: 5’ - GGACCGCTGAGCTATTGGG - 3’

Neu1 Rev: 5’ - CGGGATGCGGAAAGTGTCTA - 3’

Mcoln1 Fwd: 5’ - CTGACCCCCAATCCTGGGTAT - 3’

Mcoln1 Rev: 5’ - GGCCCGGAACTTGTCACAT - 3’

Ctns Fwd: 5’ - ATGAGGAGGAATTGGCTGCTT - 3’

Ctns Rev: 5’ - ACGTTGGTTGAACTGCCATTTT - 3’

Hspa5 Fwd: 5’ - ACTTGGGGACCACCTATTCCT - 3’

Hspa5 Rev: 5’ - ATCGCCAATCAGACGCTCC - 3’

Tfeb Fwd: 5’ - AAGGTTCGGGAGTATCTGTCTG - 3’

Tfeb Rev: 5’ - GGGTTGGAGCTGATATGTAGCA - 3’

Tfe3 Fwd: 5’ - TGCGTCAGCAGCTTATGAGG - 3’

Tfe3 Rev: 5’ - AGACACGCCAATCACAGAGAT - 3’

ChIP, two step-ChIP assays, and qRT-PCR analyses

The ChIP and sequential two step-ChIP assays were conducted as previously described (Boo et al., 2015). In brief, cells were crosslinked with 1% formaldehyde for 10 min at room temperature. After glycine quenching, the cell pellets were lysed in buffer containing 50mM Tris-HCl (pH8.1), 10mM EDTA, 1% SDS, supplemented with complete protease inhibitor cocktail (Roche), and sonicated. Chromatin extracts containing DNA fragments with an average of 250bp were then diluted tem times with dilution buffer containing 1% Triton X-100, 2mM EDTA, 150mM NaCl, 20mM Tris-HCl (pH 8.1) with complete protease inhibitor cocktail, pre-cleared with protein A/G sepharose and subjected to immunoprecipitations for overnight at 4°C. Immunocomplexes were captured by incubating 45ul of protein A/G sepharose for 2 hours at 4°C. Beads were washed with low-salt wash buffer (0.1% SDS, 1% Triton X-100, 2mM EDTA, 20mM Tris-HCl (pH 8.1), 150mM NaCl), high-salt wash buffer (0.1% SDS, 1% Triton X-100, 2mM EDTA, 20mM Tris-HCl (pH 8.1), 500mM NaCl), buffer III buffer (0.25M LiCl, 1% NP-40, 1% deoxycholate, 10mM Tris-HCl (pH 8.1), 1mM EDTA), TE buffer (10mM Tris-HCl (pH 8.0), 0.5M EDTA) and eluted in elution buffer (1% SDS, 0.1M NaHCO3). The supernatant was incubated overnight at 65°C to reverse-crosslink, digested with RNase A for 2 hours at 37°C and proteinase K for 2 hours at 55°C. ChIP and input DNA were then purified and analyzed for qRT-PCR analysis or used for constructing sequencing libraries. For the two-step ChIP assays, components were eluted from the first immunoprecipitation reaction by incubation with 10mM DTT at 37°C for 30 min and diluted 1:50 in ChIP dilution buffer followed by re-

immunoprecipitation with the second antibodies. Two-step ChIP assay was performed in essentially the same way as the first immunoprecipitations. Quantitative PCR (qPCR) was used to measure enrichment of bound DNA, and the value of enrichment was calculated by relative amount to input and ratio to IgG. All reactions were performed in triplicates.

The following primers were used in ChIP assays.

Map1lc3b Fwd: 5’ - AGCCAGTGGGATATTGGTCT - 3’

Map1lc3b Rev: 5’ - AGAGCCTGCGGTACCCTAC - 3’

Atg14 Fwd: 5’ - GAGACGCCATGATGATCTGA - 3’

Atg14 Rev: 5’ - GCCAAGGAGTGTGGGAAGTA - 3’

Atp6v1c1 Fwd: 5’ - ACTCAGTGGCAGAAGGGAGA - 3’

Atp6v1c1 Rev: 5’ - AAACACCCAGTGGAGACTGC - 3’

Hexb Fwd: 5’ - GAATTGGGACTGTGGTCGAT - 3’

Hexb Rev: 5’ - CTAGTGTCGCTGGCCCTAGT - 3’

Hspa5 Fwd: 5’ - ATTGGTGGCCGTTAAGAATG - 3’

Hspa5 Rev: 5’ - TGAAGTCGCTACTCGTTGGA - 3’

Neu1 Fwd: 5’ - AGGATGACTTCAGCCTGGTG - 3’

Neu1 Rev: 5’ - AGGATAGTATGGGCCGAACC - 3’

Mcoln1 Fwd: 5’- GGAGAGCTTCTACCGATCCT - 3’

Mcoln1 Rev: 5’ - TGCCCAGATTCTAGGAGGAA - 3’

Ctns Fwd: 5’ - CCTCTGGTAGCGTAGGT - 3’

Ctns Rev: 5’ - GCTTTTGGTGAGGTCTGTCC - 3’

Vps11 Fwd: 5’ - GGGCCGATCTTAACCTTTGT - 3’

Vps11 Rev: 5’ - AGCCCAGATGTCTTTTGTGG - 3’

Animal studies

All animal studies and procedures were approved by the Institutional Animal Care and Use Committee (IACUC) of Seoul National University. Eight- to-ten-week old male wild-type C57BL/6J mice were injected with vehicle (PEG400) or ellagic acid (10 mg/kg/day) intraperitoneally for 4 consecutive days. Mice were then fed *ad libidum* or fasted for 24 hours. Liver tissues were collected after mice were sacrificed. Sample sizes were at least n=3 to allow statistical analysis.

Statistical analysis

All experiments were performed independently at least three times. Values are expressed as mean ± s.e.m. For GFP-LC3 puncta counting, five random confocal images were chosen and the number of cells with GFP-positive dots was counted. An average of 80 cells was examined for each group and p-values were calculated using one-tailed t-test.

For animal studies, sample size for experiments were determined empirically based on previous studies to ensure appropriate statistical power. Mice in the study were randomly chosen for ellagic acid treatment and fasting. No animals were excluded from statistical analysis, and the investigators were not blinded in the studies.

Significance was analyzed using one-tailed *t*-test except for animal studies where two-tailed, unpaired *t*-test was used.

A *p*-value of less than 0.05 was considered statistically significant.

NS=Non-Significant, *p<0.05, **p<0.01, ***p<0.001.

CHAPTER IV
Conclusion

Compared to extensive studies on cytoplasmic events of autophagy, epigenetic and transcriptional regulation of autophagy occurring in the nucleus has been relatively unknown. However, accumulating evidence has unveiled the importance of epigenetic and transcriptional network that regulates autophagy (Füllgrabe et al., 2014a), opening new avenues for the development of autophagy-based clinical treatments. There is still a long way to go as little is known on the fine-tuning of autophagy through epigenetic modifications and the purpose for the regulation of histone marks during autophagy.

Here, I provide a link between energy sensing, chromatin modifications and transcriptional regulation of autophagy. My data unveil a critical link between the induction of autophagy and increase of histone H3R17 dimethylation (H3R17me2) through up-regulation of CARM1 leading to the activation of autophagy-related genes and lysosomal genes (Fig. IV-1). I report CARM1 as a previously unrecognized co-activator of TFEB, essential in exerting proper transcriptional activity. Further, I found that the histone arginine methylation directly regulates the outcome of autophagy, since ellagic acid treatment that specifically block H3R17me2 almost completely abolished CARM1-induced autophagy occurrence.

Ellagic acid is a naturally occurring polyphenol, abundant in fruits and vegetables. It was reported to have a beneficial health effect against cancer and cardiovascular diseases. But more importantly, ellagic acid has protective effect in a murine model of Crohn's disease, a disease deeply associated with autophagy defect (Rosillo et al., 2011; Xavier and Podolsky, 2007). Moreover, ellagic acid shows anti-malarial properties and when combined with chloroquine, a commonly used drug against malaria, clearly

improves disease treatment (Soh et al., 2009). It is noteworthy that chloroquine is also an autophagy inhibitor. It would be therefore interesting to study the effect of ellagic acid on autophagy-related diseases and investigate its therapeutic potential.

I found that CARM1 is regulated by SKP2-SCF E3 ubiquitin ligase-dependent degradation in the nucleus, but not in the cytoplasm, based on the exclusive nuclear localization of SKP2. Under glucose rich condition, CARM1 is degraded by SKP2-SCF E3 ubiquitin ligase in the nucleus maintaining basal level of CARM1 expression. AMPK-dependent down-regulation of SKP2 in the nucleus allows CARM1 to escape from SCF E3 ubiquitin ligase, resulting in the stabilization of CARM1 upon nutrient starvation.

Phenotypic analysis of CARM1 suggests the importance of the enzyme in autophagy. Indeed, CARM1 knock-out (KO) or enzymatic-dead knock-in(KI) mice die shortly after birth (Kim et al., 2010a; Yadav et al., 2003). This neo-lethality was presumably associated with the role of CARM1 as a transcriptional coactivator. Interestingly, this phenotype is similar to ATG5 or ATG7 KO mice, two major autophagy proteins (Komatsu et al., 2005; Kuma et al., 2004). ATG5 or ATG7 KO mice die with 24 hours after birth presumably due to nutrient and energy depletion. Independent *in vivo* studies have led to search for a possible role of CARM1 in autophagy and I found that CARM1 and its enzymatic activity is critical in proper autophagy occurrence both *in vitro* and *in vivo*.

AMPK is at the upstream of CARM1 stability. The role of AMPK in autophagy has been mainly focused on autophagy proteins in the cytoplasm at early time of starvation.

Here, I report a role of nuclear AMPK in autophagy, different to previously defined role. Indeed, in response to prolonged starvation, AMPK protein levels and activity increase in the nucleus. In our experimental setting, the transcriptional activation of autophagy and lysosomal genes occurs starting at 12 hours after glucose starvation. It is noteworthy that the time frame of nuclear AMPK accumulation is concomitant with the induction of CARM1 and subsequent transcriptional activation of autophagy genes. While an acute and rapid response of autophagy occurs primarily in the cytoplasm, prolonged starvation results in the activation of transcriptional programs and changes in the epigenetic network in the nucleus. AMPK has been known to activate autophagy through inactivation of TORC1 and phosphorylation of ULK1, all of which occur in the cytoplasm at early time of starvation. However, our results indicate that when transcription of various autophagy and lysosomal genes are up-regulated to sustain autophagy, AMPK accumulates at a later time of starvation in the nucleus and distinctly functions in coordinating the transcription of target genes involved in the outcome of autophagy. Overall, my data support the idea that when glucose starvation persists and transcription of various autophagy-related genes is needed to sustain autophagy, AMPK accumulates in the nucleus and actively controls transcription.

In conclusion, my findings provide evidence of CARM1-dependent histone arginine methylation as a critical nuclear event for epigenetic and transcriptional regulation in autophagy and shed light on a potential therapeutic targeting of the newly identified AMPK-SKP2-CARM1 signaling axis in autophagy-related diseases.

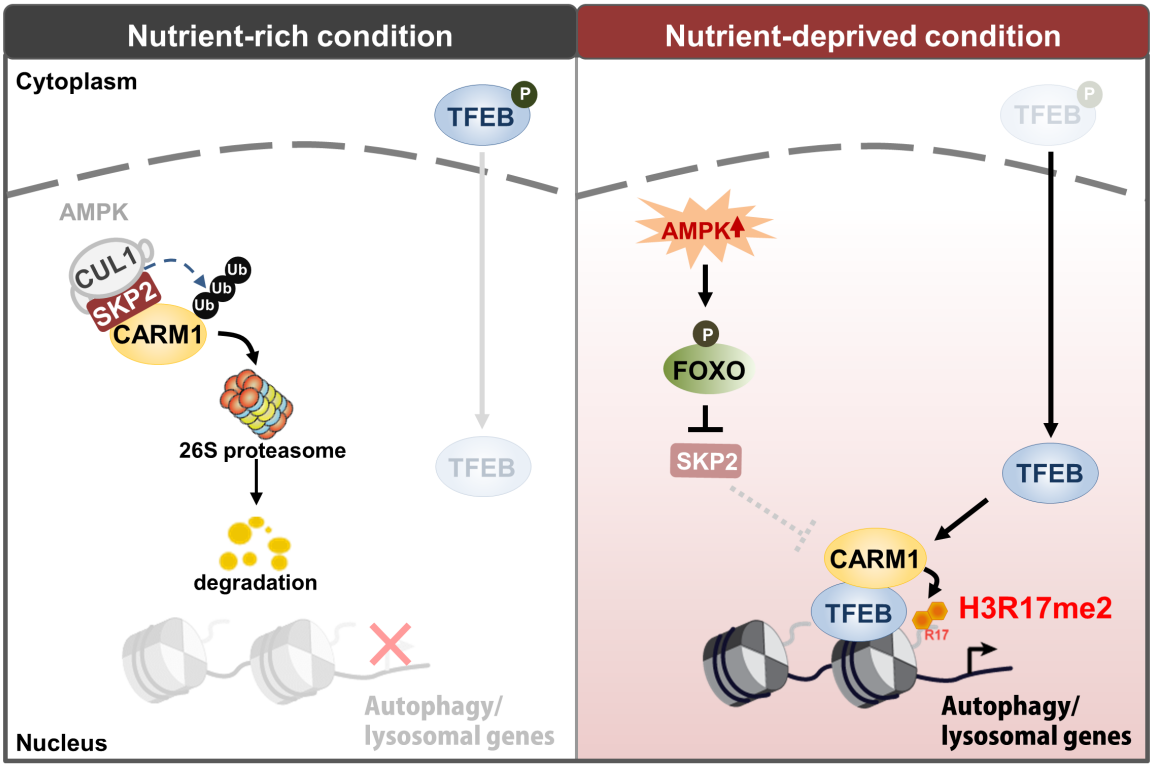

Figure IV-1. Graphical summary of the newly identified AMPK-SKP2-CARM1 signaling cascade

Proposed model depicting AMPK-SKP2-CARM1 signaling axis in the epigenetic regulation of autophagy. SKP2-SCF-E3 ligase complex degrades CARM1 under nutrient-rich condition but in nutrient-deprived condition, AMPK-dependent phosphorylation of FOXO3a downregulates SKP2 and stabilizes CARM1, which in turn functions as a co-activator of TFEB

REFERENCES

Agarwal, A., Bumm, T.G., Corbin, A.S., O'Hare, T., Loriaux, M., VanDyke, J., Willis, S.G., Deininger, J., Nakayama, K.I., and Druker, B.J. (2008). Absence of SKP2 expression attenuates BCR-ABL–induced myeloproliferative disease. Blood *112*, 1960-1970.

An, W., Kim, J., and Roeder, R.G. (2004). Ordered cooperative functions of PRMT1, p300, and CARM1 in transcriptional activation by p53. Cell *117*, 735-748.

Ballabio, A., and Gieselmann, V. (2009). Lysosomal disorders: from storage to cellular damage. Biochimica et Biophysica Acta (BBA)-Molecular Cell Research *1793*, 684-696.

Bannister, A.J., and Kouzarides, T. (2011). Regulation of chromatin by histone modifications. Cell research *21*, 381-395.

Bashir, T., Dorrello, N.V., Amador, V., Guardavaccaro, D., and Pagano, M. (2004). Control of the SCFSKP2–Cks1 ubiquitin ligase by the APC/CCdh1 ubiquitin ligase. Nature *428*, 190-193.

Bauer, U.M., Daujat, S., Nielsen, S.J., Nightingale, K., and Kouzarides, T. (2002). Methylation at arginine 17 of histone H3 is linked to gene activation. EMBO reports *3*, 39-44.

Bedford, M.T., and Clarke, S.G. (2009). Protein arginine methylation in mammals: who, what, and why. Molecular cell *33*, 1-13.

Bilodeau, M., Talarmin, H., Ilyin, G., Rescan, C., Glaise, D., Cariou, S., Loyer, P., Guguen-Guillouzo, C., and Baffet, G. (1999). SKP2 induction and phosphorylation is associated with the late G1 phase of proliferating rat hepatocytes. FEBS letters *452*, 247-253.

Bjørkøy, G., Lamark, T., Pankiv, S., Øvervatn, A., Brech, A., and Johansen, T. (2009). Monitoring autophagic degradation of p62/SQSTM1. Methods in enzymology *452*, 181-197.

Boo, K., Bhin, J., Jeon, Y., Kim, J., Shin, H.-J.R., Park, J.-E., Kim, K., Kim, C.R., Jang, H., and Kim, I.-H. (2015). Pontin functions as an essential coactivator for Oct4-dependent lincRNA expression in mouse embryonic stem cells. Nature communications *6*.

Bornstein, G., Bloom, J., Sitry-Shevah, D., Nakayama, K., Pagano, M., and Hershko, A. (2003). Role of the SCFSKP2 ubiquitin ligase in the degradation of p21Cip1 in S phase. Journal of Biological Chemistry *278*, 25752-25757.

Bruder, E., Passera, O., Harms, D., Leuschner, I., Ladanyi, M., Argani, P., Eble, J.N., Struckmann, K., Schraml, P., and Moch, H. (2004). Morphologic and molecular characterization of renal cell carcinoma in children and young adults. The American journal of surgical pathology *28*, 1117-1132.

Cardozo, T., and Pagano, M. (2004). The SCF ubiquitin ligase: insights into a molecular machine. Nature reviews Molecular cell biology *5*, 739-751.

Carrano, A.C., Eytan, E., Hershko, A., and Pagano, M. (1999). SKP2 is required for ubiquitin-mediated degradation of the CDK inhibitor p27. Nature cell biology *1*, 193-199.

Chen, S.L., Loffler, K.A., Chen, D., Stallcup, M.R., and Muscat, G.E. (2002). The Coactivator-associated Arginine Methyltransferase Is Necessary for Muscle Differentiation CARM1 COACTIVATES MYOCYTE ENHANCER FACTOR-2. Journal of Biological Chemistry *277*, 4324-4333.

Chen, Z., Zhou, Y., Song, J., and Zhang, Z. (2013). hCKSAAP_UbSite: Improved prediction of human ubiquitination sites by exploiting amino acid pattern and properties. Biochimica et Biophysica Acta (BBA)-Proteins and Proteomics *1834*, 1461-1467.

Cheng, D., Côté, J., Shaaban, S., and Bedford, M.T. (2007). The arginine methyltransferase CARM1 regulates the coupling of transcription and mRNA processing. Molecular cell *25*, 71-83.

Chevillard-Briet, M., Trouche, D., and Vandel, L. (2002). Control of CBP co-activating activity by arginine methylation. The EMBO journal *21*, 5457-5466.

Choi, A.M., Ryter, S.W., and Levine, B. (2013). Autophagy in human health and disease. New England Journal of Medicine *368*, 651-662.

Copeland, R.A., Solomon, M.E., and Richon, V.M. (2009). Protein methyltransferases as a target class for drug discovery. Nature reviews Drug discovery *8*, 724-732.

Daujat, S., Bauer, U.-M., Shah, V., Turner, B., Berger, S., and Kouzarides, T. (2002). Crosstalk between CARM1 methylation and CBP acetylation on histone H3. Current Biology *12*, 2090-2097.

David, R. (2011). Autophagy: TFEB perfects multitasking. Nature reviews Molecular cell biology *12*, 404.

Davis, M.B., Liu, X., Wang, S., Reeves, J., Khramtsov, A., Huo, D., and Olopade, O.I. (2013). Expression and sub-cellular localization of an epigenetic regulator, co-activator arginine methyltransferase 1 (CARM1), is associated with specific breast cancer subtypes and ethnicity. Molecular cancer *12*, 1.

de Narvajas, A.A.-M., Gomez, T.S., Zhang, J.-S., Mann, A.O., Taoda, Y., Gorman, J.A., Herreros-Villanueva, M., Gress, T.M., Ellenrieder, V., and Bujanda, L. (2013). Epigenetic regulation of autophagy by the methyltransferase G9a. Molecular and cellular biology *33*, 3983-3993.

Dephoure, N., Zhou, C., Villén, J., Beausoleil, S.A., Bakalarski, C.E., Elledge, S.J., and Gygi, S.P. (2008). A quantitative atlas of mitotic phosphorylation. Proceedings of the National Academy of Sciences *105*, 10762-10767.

Deter, R.L., Baudhuin, P., and De Duve, C. (1967). Participation of lysosomes in cellular autophagy induced in rat liver by glucagon. The Journal of cell biology *35*, C11-C16.

Egan, D.F., Shackelford, D.B., Mihaylova, M.M., Gelino, S., Kohnz, R.A., Mair, W., Vasquez, D.S., Joshi, A., Gwinn, D.M., and Taylor, R. (2011). Phosphorylation of ULK1 (hATG1) by AMP-activated protein kinase connects energy sensing to mitophagy. Science *331*, 456-461.

Eijkelenboom, A., and Burgering, B.M. (2013). FOXOs: signalling integrators for homeostasis maintenance. Nature reviews Molecular cell biology *14*, 83-97.

Eisenberg, T., Knauer, H., Schauer, A., Büttner, S., Ruckenstuhl, C., Carmona-Gutierrez, D., Ring, J., Schroeder, S., Magnes, C., and Antonacci, L. (2009). Induction of autophagy by spermidine promotes longevity. Nature cell biology *11*, 1305-1314.

El Messaoudi, S., Fabbrizio, E., Rodriguez, C., Chuchana, P., Fauquier, L., Cheng, D., Theillet, C., Vandel, L., Bedford, M.T., and Sardet, C. (2006). Coactivator-associated arginine methyltransferase 1 (CARM1) is a positive regulator of the Cyclin E1 gene. Proceedings of the National Academy of Sciences *103*, 13351-13356.

Füllgrabe, J., Heldring, N., Hermanson, O., and Joseph, B. (2014a). Cracking the survival code: Autophagy-related histone modifications. Autophagy *10*, 556-561.

Füllgrabe, J., Klionsky, D.J., and Joseph, B. (2014b). The return of the nucleus: transcriptional and epigenetic control of autophagy. Nature reviews Molecular cell biology *15*, 65-74.

Füllgrabe, J., Lynch-Day, M.A., Heldring, N., Li, W., Struijk, R.B., Ma, Q., Hermanson, O., Rosenfeld, M.G., Klionsky, D.J., and Joseph, B. (2013). The histone H4 lysine 16 acetyltransferase hMOF regulates the outcome of autophagy. Nature *500*, 468-471.

Feng, Q., Yi, P., Wong, J., and O'malley, B.W. (2006). Signaling within a coactivator complex: methylation of SRC-3/AIB1 is a molecular switch for complex disassembly. Molecular and cellular biology *26*, 7846-7857.

Frescas, D., and Pagano, M. (2008). Deregulated proteolysis by the F-box proteins SKP2 and β-TrCP: tipping the scales of cancer. Nature Reviews Cancer *8*, 438-449.
Fujiwara, T., Mori, Y., Chu, D.L., Koyama, Y., Miyata, S., Tanaka, H., Yachi, K., Kubo, T., Yoshikawa, H., and Tohyama, M. (2006). CARM1 regulates proliferation of PC12 cells by methylating HuD. Molecular and cellular biology *26*, 2273-2285.
Ganoth, D., Bornstein, G., Ko, T.K., Larsen, B., Tyers, M., Pagano, M., and Hershko, A. (2001). The cell-cycle regulatory protein Cks1 is required for SCFSKP2-mediated ubiquitinylation of p27. Nature cell biology *3*, 321-324.
Gao, D., Inuzuka, H., Tseng, A., Chin, R.Y., Toker, A., and Wei, W. (2009). Phosphorylation by Akt1 promotes cytoplasmic localization of SKP2 and impairs APCCdh1-mediated SKP2 destruction. Nature cell biology *11*, 397-408.
Gary, J.D., and Clarke, S. (1998). RNA and protein interactions modulated by protein arginine methylation. Progress in nucleic acid research and molecular biology *61*, 65-131.
Greer, E.L., Oskoui, P.R., Banko, M.R., Maniar, J.M., Gygi, M.P., Gygi, S.P., and Brunet, A. (2007). The energy sensor AMP-activated protein kinase directly regulates the mammalian FOXO3 transcription factor. Journal of Biological Chemistry *282*, 30107-30119.
Gstaiger, M., Jordan, R., Lim, M., Catzavelos, C., Mestan, J., Slingerland, J., and Krek, W. (2001). SKP2 is oncogenic and overexpressed in human cancers. Proceedings of the National Academy of Sciences *98*, 5043-5048.
Gwinn, D.M., Shackelford, D.B., Egan, D.F., Mihaylova, M.M., Mery, A., Vasquez, D.S., Turk, B.E., and Shaw, R.J. (2008). AMPK phosphorylation of raptor mediates a metabolic checkpoint. Molecular cell *30*, 214-226.
Hardie, D.G. (2011). AMPK and autophagy get connected. EMBO J *30*, 634-635.
Hardie, D.G., Hawley, S.A., and Scott, J.W. (2006). AMP-activated protein kinase–development of the energy sensor concept. The Journal of physiology *574*, 7-15.
Hardie, D.G., Ross, F.A., and Hawley, S.A. (2012). AMPK: a nutrient and energy sensor that maintains energy homeostasis. Nature reviews Molecular cell biology *13*, 251-262.
Harris, H., and Rubinsztein, D.C. (2012). Control of autophagy as a therapy for neurodegenerative disease. Nature Reviews Neurology *8*, 108-117.
Hawley, S.A., Davison, M., Woods, A., Davies, S.P., Beri, R.K., Carling, D., and Hardie, D.G. (1996). Characterization of the AMP-activated protein kinase kinase from rat liver and identification of threonine 172 as the major site at which it phosphorylates AMP-

activated protein kinase. Journal of Biological Chemistry *271*, 27879-27887.
Hawley, S.A., Pan, D.A., Mustard, K.J., Ross, L., Bain, J., Edelman, A.M., Frenguelli, B.G., and Hardie, D.G. (2005). Calmodulin-dependent protein kinase kinase-β is an alternative upstream kinase for AMP-activated protein kinase. Cell metabolism *2*, 9-19.
Herrero-Martín, G., Høyer-Hansen, M., García-García, C., Fumarola, C., Farkas, T., López-Rivas, A., and Jäättelä, M. (2009). TAK1 activates AMPK-dependent cytoprotective autophagy in TRAIL-treated epithelial cells. The EMBO journal *28*, 677-685.
Hershko, D.D. (2008). Oncogenic properties and prognostic implications of the ubiquitin ligase SKP2 in cancer. Cancer *112*, 1415-1424.
Hodgkinson, C.A., Moore, K.J., Nakayama, A., Steingrímsson, E., Copeland, N.G., Jenkins, N.A., and Arnheiter, H. (1993). Mutations at the mouse microphthalmia locus are associated with defects in a gene encoding a novel basic-helix-loop-helix-zipper protein. Cell *74*, 395-404.
Hong, H., Kao, C., Jeng, M.H., Eble, J.N., Koch, M.O., Gardner, T.A., Zhang, S., Li, L., Pan, C.X., Hu, Z.*, et al.* (2004). Aberrant expression of CARM1, a transcriptional coactivator of androgen receptor, in the development of prostate carcinoma and androgen-independent status. Cancer *101*, 83-89.
Hurley, R.L., Anderson, K.A., Franzone, J.M., Kemp, B.E., Means, A.R., and Witters, L.A. (2005). The Ca2+/calmodulin-dependent protein kinase kinases are AMP-activated protein kinase kinases. Journal of Biological Chemistry *280*, 29060-29066.
Imaki, H., Nakayama, K., Delehouzee, S., Handa, H., Kitagawa, M., Kamura, T., and Nakayama, K.I. (2003). Cell cycle-dependent regulation of the SKP2 promoter by GA-binding protein. Cancer research *63*, 4607-4613.
Inoki, K., Kim, J., and Guan, K.-L. (2012). AMPK and mTOR in cellular energy homeostasis and drug targets. Annual review of pharmacology and toxicology *52*, 381-400.
Inoki, K., Zhu, T., and Guan, K.-L. (2003). TSC2 mediates cellular energy response to control cell growth and survival. Cell *115*, 577-590.
Inuzuka, H., Gao, D., Finley, L.W., Yang, W., Wan, L., Fukushima, H., Chin, Y.R., Zhai, B., Shaik, S., Lau, A.W.*, et al.* (2012). Acetylation-dependent regulation of SKP2 function. Cell *150*, 179-193.
Jacques, S.L., Aquino, K.P., Gureasko, J., Boriack-Sjodin, P.A., Porter Scott, M., Copeland, R.A., and Riera, T.V. (2016). CARM1 Preferentially Methylates H3R17 over

H3R26 through a Random Kinetic Mechanism. Biochemistry *55*, 1635-1644.
Jakub, W.C., Simon, A.H., Alan, P., Angela, W., and David, C. (1998). AMP-activated protein kinase: greater AMP dependence, and preferential nuclear localization, of complexes containing the α2 isoform. Biochemical Journal *334*, 177-187.
Jin, J., Cardozo, T., Lovering, R.C., Elledge, S.J., Pagano, M., and Harper, J.W. (2004). Systematic analysis and nomenclature of mammalian F-box proteins. Genes & development *18*, 2573-2580.
Kagey, M.H., Newman, J.J., Bilodeau, S., Zhan, Y., Orlando, D.A., van Berkum, N.L., Ebmeier, C.C., Goossens, J., Rahl, P.B., and Levine, S.S. (2010). Mediator and cohesin connect gene expression and chromatin architecture. Nature *467*, 430-435.
Kauffman, E.C., Ricketts, C.J., Rais-Bahrami, S., Yang, Y., Merino, M.J., Bottaro, D.P., Srinivasan, R., and Linehan, W.M. (2014). Molecular genetics and cellular features of TFE3 and TFEB fusion kidney cancers. Nature Reviews Urology *11*, 465-475.
Kim, D., Lee, J., Cheng, D., Li, J., Carter, C., Richie, E., and Bedford, M.T. (2010a). Enzymatic activity is required for the in vivo functions of CARM1. The Journal of biological chemistry *285*, 1147-1152.
Kim, D., Pertea, G., Trapnell, C., Pimentel, H., Kelley, R., and Salzberg, S.L. (2013a). TopHat2: accurate alignment of transcriptomes in the presence of insertions, deletions and gene fusions. Genome Biol *14*, R36.
Kim, I.S., Lee, M., Park, K.C., Jeon, Y., Park, J.H., Hwang, E.J., Im Jeon, T., Ko, S., Lee, H., and Baek, S.H. (2012). Roles of Mis18α in epigenetic regulation of centromeric chromatin and CENP-A loading. Molecular cell *46*, 260-273.
Kim, J., Kim, Y.C., Fang, C., Russell, R.C., Kim, J.H., Fan, W., Liu, R., Zhong, Q., and Guan, K.-L. (2013b). Differential regulation of distinct Vps34 complexes by AMPK in nutrient stress and autophagy. Cell *152*, 290-303.
Kim, J., Kundu, M., Viollet, B., and Guan, K.-L. (2011). AMPK and mTOR regulate autophagy through direct phosphorylation of Ulk1. Nature cell biology *13*, 132-141.
Kim, J., Lee, J., Yadav, N., Wu, Q., Carter, C., Richard, S., Richie, E., and Bedford, M.T. (2004). Loss of CARM1 results in hypomethylation of thymocyte cyclic AMP-regulated phosphoprotein and deregulated early T cell development. The Journal of biological chemistry *279*, 25339-25344.
Kim, Y.R., Lee, B.K., Park, R.Y., Nguyen, N.T., Bae, J.A., Kwon, D.D., and Jung, C. (2010b). Differential CARM1 expression in prostate and colorectal cancers. BMC cancer *10*, 197.

Klionsky, D.J. (2007). Autophagy: from phenomenology to molecular understanding in less than a decade. Nature reviews Molecular cell biology *8*, 931-937.
Klionsky, D.J., Abdalla, F.C., Abeliovich, H., Abraham, R.T., Acevedo-Arozena, A., Adeli, K., Agholme, L., Agnello, M., Agostinis, P., and Aguirre-Ghiso, J.A. (2012). Guidelines for the use and interpretation of assays for monitoring autophagy. Autophagy *8*, 445-544.
Komatsu, M., Waguri, S., Ueno, T., Iwata, J., Murata, S., Tanida, I., Ezaki, J., Mizushima, N., Ohsumi, Y., and Uchiyama, Y. (2005). Impairment of starvation-induced and constitutive autophagy in Atg7-deficient mice. The Journal of cell biology *169*, 425-434.
Kondo, Y., Kanzawa, T., Sawaya, R., and Kondo, S. (2005). The role of autophagy in cancer development and response to therapy. Nature Reviews Cancer *5*, 726-734.
Kroemer, G., Mariño, G., and Levine, B. (2010). Autophagy and the integrated stress response. Molecular cell *40*, 280-293.
Kudo, N., Gillespie, J.G., Kung, L., Witters, L.A., Schulz, R., Clanachan, A.S., and Lopaschuk, G.D. (1996). Characterization of 5′ AMP-activated protein kinase activity in the heart and its role in inhibiting acetyl-CoA carboxylase during reperfusion following ischemia. Biochimica et Biophysica Acta (BBA)-Lipids and Lipid Metabolism *1301*, 67-75.
Kuhn, P., Chumanov, R., Wang, Y., Ge, Y., Burgess, R.R., and Xu, W. (2011). Automethylation of CARM1 allows coupling of transcription and mRNA splicing. Nucleic acids research *39*, 2717-2726.
Kuma, A., Hatano, M., Matsui, M., Yamamoto, A., Nakaya, H., Yoshimori, T., Ohsumi, Y., Tokuhisa, T., and Mizushima, N. (2004). The role of autophagy during the early neonatal starvation period. Nature *432*, 1032-1036.
Lam, E.W.-F., Brosens, J.J., Gomes, A.R., and Koo, C.-Y. (2013). Forkhead box proteins: tuning forks for transcriptional harmony. Nature Reviews Cancer *13*, 482-495.
Laplante, M., and Sabatini, D.M. (2013). Regulation of mTORC1 and its impact on gene expression at a glance. Journal of cell science *126*, 1713-1719.
Lee, D.Y., Teyssier, C., Strahl, B.D., and Stallcup, M.R. (2005a). Role of protein methylation in regulation of transcription. Endocrine reviews *26*, 147-170.
Lee, Y.-H., Coonrod, S.A., Kraus, W.L., Jelinek, M.A., and Stallcup, M.R. (2005b). Regulation of coactivator complex assembly and function by protein arginine methylation and demethylimination. Proceedings of the National Academy of Sciences

of the United States of America *102*, 3611-3616.
Lee, Y.-H., and Stallcup, M.R. (2009). Minireview: protein arginine methylation of nonhistone proteins in transcriptional regulation. Molecular endocrinology *23*, 425-433.
Lee, Y.H., Bedford, M.T., and Stallcup, M.R. (2011). Regulated recruitment of tumor suppressor BRCA1 to the p21 gene by coactivator methylation. Genes & development *25*, 176-188.
Levine, B., and Kroemer, G. (2008). Autophagy in the pathogenesis of disease. Cell *132*, 27-42.
Li, B., Carey, M., and Workman, J.L. (2007). The role of chromatin during transcription. Cell *128*, 707-719.
Li, H., Park, S., Kilburn, B., Jelinek, M.A., Henschen-Edman, A., Aswad, D.W., Stallcup, M.R., and Laird-Offringa, I.A. (2002). Lipopolysaccharide-induced methylation of HuR, an mRNA-stabilizing protein, by CARM1. Journal of Biological Chemistry *277*, 44623-44630.
Lin, H.-K., Chen, Z., Wang, G., Nardella, C., Lee, S.-W., Chan, C.-H., Yang, W.-L., Wang, J., Egia, A., and Nakayama, K.I. (2010). SKP2 targeting suppresses tumorigenesis by Arf-p53-independent cellular senescence. Nature *464*, 374-379.
Lin, H.K., Wang, G., Chen, Z., Teruya-Feldstein, J., Liu, Y., Chan, C.H., Yang, W.L., Erdjument-Bromage, H., Nakayama, K.I., Nimer, S.*, et al.* (2009). Phosphorylation-dependent regulation of cytosolic localization and oncogenic function of SKP2 by Akt/PKB. Nature cell biology *11*, 420-432.
Longatti, A., and Tooze, S. (2009). Vesicular trafficking and autophagosome formation. Cell Death & Differentiation *16*, 956-965.
Maiese, K., Chong, Z.Z., and Shang, Y.C. (2008). OutFOXOing disease and disability: the therapeutic potential of targeting FoxO proteins. Trends in molecular medicine *14*, 219-227.
Maiuri, M.C., Galluzzi, L., Morselli, E., Kepp, O., Malik, S.A., and Kroemer, G. (2010). Autophagy regulation by p53. Current opinion in cell biology *22*, 181-185.
Mann, M., Cortez, V., and Vadlamudi, R. (2013). PELP1 oncogenic functions involve CARM1 regulation. Carcinogenesis *34*, 1468-1475.
Martina, J.A., Chen, Y., Gucek, M., and Puertollano, R. (2012). MTORC1 functions as a transcriptional regulator of autophagy by preventing nuclear transport of TFEB. Autophagy *8*, 903-914.
Martina, J.A., Diab, H.I., Lishu, L., Jeong-A, L., Patange, S., Raben, N., and

Puertollano, R. (2014). The nutrient-responsive transcription factor TFE3 promotes autophagy, lysosomal biogenesis, and clearance of cellular debris. Science signaling *7*, ra9.
Mazure, N.M., and Pouysségur, J. (2010). Hypoxia-induced autophagy: cell death or cell survival? Current opinion in cell biology *22*, 177-180.
McGee, S.L., and Hargreaves, M. (2010). AMPK-mediated regulation of transcription in skeletal muscle. Clinical science *118*, 507-518.
Medendorp, K., Van Groningen, J., Schepens, M., Vreede, L., Thijssen, J., Schoenmakers, E., Van den Hurk, W., Geurts van Kessel, A., and Kuiper, R. (2007). Molecular mechanisms underlying the MiT translocation subgroup of renal cell carcinomas. Cytogenetic and genome research *118*, 157-165.
Mihaylova, M.M., and Shaw, R.J. (2011). The AMPK signalling pathway coordinates cell growth, autophagy and metabolism. Nature cell biology *13*, 1016-1023.
Mizushima, N. (2007). Autophagy: process and function. Genes & development *21*, 2861-2873.
Mizushima, N., and Komatsu, M. (2011). Autophagy: renovation of cells and tissues. Cell *147*, 728-741.
Mizushima, N., Levine, B., Cuervo, A.M., and Klionsky, D.J. (2008). Autophagy fights disease through cellular self-digestion. Nature *451*, 1069-1075.
Mizushima, N., and Yoshimori, T. (2007). How to interpret LC3 immunoblotting. Autophagy *3*, 542-545.
Mizushima, N., Yoshimori, T., and Levine, B. (2010). Methods in mammalian autophagy research. Cell *140*, 313-326.
Momcilovic, M., Hong, S.-P., and Carlson, M. (2006). Mammalian TAK1 activates Snf1 protein kinase in yeast and phosphorylates AMP-activated protein kinase in vitro. Journal of Biological Chemistry *281*, 25336-25343.
Naeem, H., Cheng, D., Zhao, Q., Underhill, C., Tini, M., Bedford, M.T., and Torchia, J. (2007). The activity and stability of the transcriptional coactivator p/CIP/SRC-3 are regulated by CARM1-dependent methylation. Molecular and cellular biology *27*, 120-134.
Nakayama, K., Nagahama, H., Minamishima, Y.A., Matsumoto, M., Nakamichi, I., Kitagawa, K., Shirane, M., Tsunematsu, R., Tsukiyama, T., and Ishida, N. (2000). Targeted disruption of SKP2 results in accumulation of cyclin E and p27Kip1, polyploidy and centrosome overduplication. The EMBO journal *19*, 2069-2081.

Nakayama, K.I., and Nakayama, K. (2005). Regulation of the cell cycle by SCF-type ubiquitin ligases. Seminars in cell & developmental biology *16*, 323-333.
Nixon, R.A. (2013). The role of autophagy in neurodegenerative disease. Nature medicine *19*, 983-997.
O'Brien, K.B., Alberich-Jorda, M., Yadav, N., Kocher, O., Diruscio, A., Ebralidze, A., Levantini, E., Sng, N.J., Bhasin, M., Caron, T.*, et al.* (2010). CARM1 is required for proper control of proliferation and differentiation of pulmonary epithelial cells. Development *137*, 2147-2156.
Ohkura, N., Takahashi, M., Yaguchi, H., Nagamura, Y., and Tsukada, T. (2005). Coactivator-associated arginine methyltransferase 1, CARM1, affects pre-mRNA splicing in an isoform-specific manner. Journal of Biological Chemistry *280*, 28927-28935.
Paik, W.K., Paik, D.C., and Kim, S. (2007). Historical review: the field of protein methylation. Trends in biochemical sciences *32*, 146-152.
Palmieri, M., Impey, S., Kang, H., di Ronza, A., Pelz, C., Sardiello, M., and Ballabio, A. (2011). Characterization of the CLEAR network reveals an integrated control of cellular clearance pathways. Human molecular genetics *20*, 3852-3866.
Petroski, M.D., and Deshaies, R.J. (2005). Function and regulation of cullin-RING ubiquitin ligases. Nature reviews Molecular cell biology *6*, 9-20.
Pietrocola, F., Izzo, V., Niso-Santano, M., Vacchelli, E., Galluzzi, L., Maiuri, M.C., and Kroemer, G. (2013). Regulation of autophagy by stress-responsive transcription factors. Seminars in cancer biology *23*, 310-322.
Potente, M., Urbich, C., Sasaki, K.-i., Hofmann, W.K., Heeschen, C., Aicher, A., Kollipara, R., DePinho, R.A., Zeiher, A.M., and Dimmeler, S. (2005). Involvement of Foxo transcription factors in angiogenesis and postnatal neovascularization. Journal of Clinical Investigation *115*, 2382.
Rabinowitz, J.D., and White, E. (2010). Autophagy and metabolism. Science *330*, 1344-1348.
Ramphal, R., Pappo, A., Zielenska, M., Grant, R., and Ngan, B.-Y. (2006). Pediatric Renal Cell Carcinoma. American journal of clinical pathology *126*, 349-364.
Rehli, M., Den Elzen, N., Cassady, A.I., Ostrowski, M.C., and Hume, D.A. (1999). Cloning and characterization of the murine genes for bHLH-ZIP transcription factors TFEC and TFEB reveal a common gene organization for all MiT subfamily members. Genomics *56*, 111-120.

Robinson, M.D., McCarthy, D.J., and Smyth, G.K. (2010). edgeR: a Bioconductor package for differential expression analysis of digital gene expression data. Bioinformatics *26*, 139-140.
Roczniak-Ferguson, A., Petit, C.S., Froehlich, F., Qian, S., Ky, J., Angarola, B., Walther, T.C., and Ferguson, S.M. (2012). The transcription factor TFEB links mTORC1 signaling to transcriptional control of lysosome homeostasis. Science signaling *5*, ra42.
Rodier, G., Coulombe, P., Tanguay, P.L., Boutonnet, C., and Meloche, S. (2008). Phosphorylation of SKP2 regulated by CDK2 and Cdc14B protects it from degradation by APCCdh1 in G1 phase. The EMBO journal *27*, 679-691.
Rosillo, M., Sanchez-Hidalgo, M., Cardeno, A., and De La Lastra, C.A. (2011). Protective effect of ellagic acid, a natural polyphenolic compound, in a murine model of Crohn's disease. Biochemical pharmacology *82*, 737-745.
Salih, D.A., and Brunet, A. (2008). FoxO transcription factors in the maintenance of cellular homeostasis during aging. Current opinion in cell biology *20*, 126-136.
Sardiello, M., Palmieri, M., di Ronza, A., Medina, D.L., Valenza, M., Gennarino, V.A., Di Malta, C., Donaudy, F., Embrione, V., Polishchuk, R.S.*, et al.* (2009). A gene network regulating lysosomal biogenesis and function. Science *325*, 473-477.
Sarmento, L.M., Huang, H., Limon, A., Gordon, W., Fernandes, J., Tavares, M.J., Miele, L., Cardoso, A.A., Classon, M., and Carlesso, N. (2005). Notch1 modulates timing of G1-S progression by inducing SKP2 transcription and p27Kip1 degradation. The Journal of experimental medicine *202*, 157-168.
Schulman, B.A., Carrano, A.C., Jeffrey, P.D., Bowen, Z., Kinnucan, E.R., Finnin, M.S., Elledge, S.J., Harper, J.W., Pagano, M., and Pavletich, N.P. (2000). Insights into SCF ubiquitin ligases from the structure of the Skp1–SKP2 complex. Nature *408*, 381-386.
Schurter, B.T., Koh, S.S., Chen, D., Bunick, G.J., Harp, J.M., Hanson, B.L., Henschen-Edman, A., Mackay, D.R., Stallcup, M.R., and Aswad, D.W. (2001). Methylation of histone H3 by coactivator-associated arginine methyltransferase 1. Biochemistry *40*, 5747-5756.
Selvi, B.R., Batta, K., Kishore, A.H., Mantelingu, K., Varier, R.A., Balasubramanyam, K., Pradhan, S.K., Dasgupta, D., Sriram, S., Agrawal, S.*, et al.* (2010). Identification of a novel inhibitor of coactivator-associated arginine methyltransferase 1 (CARM1)-mediated methylation of histone H3 Arg-17. The Journal of biological chemistry *285*, 7143-7152.
Settembre, C., and Ballabio, A. (2011). TFEB regulates autophagy: an integrated

coordination of cellular degradation and recycling processes. Autophagy *7*, 1379-1381.
Settembre, C., De Cegli, R., Mansueto, G., Saha, P.K., Vetrini, F., Visvikis, O., Huynh, T., Carissimo, A., Palmer, D., Klisch, T.J.*, et al.* (2013a). TFEB controls cellular lipid metabolism through a starvation-induced autoregulatory loop. Nature cell biology *15*, 647-658.
Settembre, C., Di Malta, C., Polito, V.A., Garcia Arencibia, M., Vetrini, F., Erdin, S., Erdin, S.U., Huynh, T., Medina, D., Colella, P.*, et al.* (2011). TFEB links autophagy to lysosomal biogenesis. Science *332*, 1429-1433.
Settembre, C., Fraldi, A., Jahreiss, L., Spampanato, C., Venturi, C., Medina, D., de Pablo, R., Tacchetti, C., Rubinsztein, D.C., and Ballabio, A. (2008). A block of autophagy in lysosomal storage disorders. Human molecular genetics *17*, 119-129.
Settembre, C., Fraldi, A., Medina, D.L., and Ballabio, A. (2013b). Signals from the lysosome: a control centre for cellular clearance and energy metabolism. Nature Reviews Molecular Cell Biology *14*, 283-296.
Settembre, C., Zoncu, R., Medina, D.L., Vetrini, F., Erdin, S., Erdin, S., Huynh, T., Ferron, M., Karsenty, G., and Vellard, M.C. (2012). A lysosome-to-nucleus signalling mechanism senses and regulates the lysosome via mTOR and TFEB. The EMBO journal *31*, 1095-1108.
Shackelford, D.B., and Shaw, R.J. (2009). The LKB1–AMPK pathway: metabolism and growth control in tumour suppression. Nature Reviews Cancer *9*, 563-575.
Shao, Y., Gao, Z., Marks, P.A., and Jiang, X. (2004). Apoptotic and autophagic cell death induced by histone deacetylase inhibitors. Proceedings of the National Academy of Sciences *101*, 18030-18035.
Shaw, R.J., Kosmatka, M., Bardeesy, N., Hurley, R.L., Witters, L.A., DePinho, R.A., and Cantley, L.C. (2004). The tumor suppressor LKB1 kinase directly activates AMP-activated kinase and regulates apoptosis in response to energy stress. Proceedings of the National Academy of Sciences of the United States of America *101*, 3329-3335.
Sims, R.J., Rojas, L.A., Beck, D., Bonasio, R., Schüller, R., Drury, W.J., Eick, D., and Reinberg, D. (2011). The C-terminal domain of RNA polymerase II is modified by site-specific methylation. Science *332*, 99-103.
Soh, P.N., Witkowski, B., Olagnier, D., Nicolau, M.-L., Garcia-Alvarez, M.-C., Berry, A., and Benoit-Vical, F. (2009). In vitro and in vivo properties of ellagic acid in malaria treatment. Antimicrobial agents and chemotherapy *53*, 1100-1106.
Spruck, C., Strohmaier, H., Watson, M., Smith, A.P., Ryan, A., Krek, W., and Reed, S.I.

(2001). A CDK-independent function of mammalian Cks1: targeting of SCFSKP2 to the CDK inhibitor p27Kip1. Molecular cell *7*, 639-650.
Stallcup, M.R. (2001). Role of protein methylation in chromatin remodeling and transcriptional regulation. Oncogene *20*, 3014-3020.
Steingrímsson, E., Copeland, N.G., and Jenkins, N.A. (2004). Melanocytes and the microphthalmia transcription factor network. Annu Rev Genet *38*, 365-411.
Suter, M., Riek, U., Tuerk, R., Schlattner, U., Wallimann, T., and Neumann, D. (2006). Dissecting the role of 5′-AMP for allosteric stimulation, activation, and deactivation of AMP-activated protein kinase. Journal of Biological Chemistry *281*, 32207-32216.
Sutterlüty, H., Chatelain, E., Marti, A., Wirbelauer, C., Senften, M., Müller, U., and Krek, W. (1999). p45SKP2 promotes p27Kip1 degradation and induces S phase in quiescent cells. Nature cell biology *1*, 207-214.
Suzuki, A., Okamoto, S., Lee, S., Saito, K., Shiuchi, T., and Minokoshi, Y. (2007). Leptin stimulates fatty acid oxidation and peroxisome proliferator-activated receptor α gene expression in mouse C2C12 myoblasts by changing the subcellular localization of the α2 form of AMP-activated protein kinase. Molecular and cellular biology *27*, 4317-4327.
Torres-Padilla, M.E., Parfitt, D.E., Kouzarides, T., and Zernicka-Goetz, M. (2007). Histone arginine methylation regulates pluripotency in the early mouse embryo. Nature *445*, 214-218.
Troffer-Charlier, N., Cura, V., Hassenboehler, P., Moras, D., and Cavarelli, J. (2007). Functional insights from structures of coactivator-associated arginine methyltransferase 1 domains. The EMBO journal *26*, 4391-4401.
Tsai, K.-L., Sun, Y.-J., Huang, C.-Y., Yang, J.-Y., Hung, M.-C., and Hsiao, C.-D. (2007). Crystal structure of the human FOXO3a-DBD/DNA complex suggests the effects of post-translational modification. Nucleic acids research *35*, 6984-6994.
van der Horst, A., and Burgering, B.M. (2007). Stressing the role of FoxO proteins in lifespan and disease. Nature reviews Molecular cell biology *8*, 440-450.
Visel, A., Blow, M.J., Li, Z., Zhang, T., Akiyama, J.A., Holt, A., Plajzer-Frick, I., Shoukry, M., Wright, C., and Chen, F. (2009). ChIP-seq accurately predicts tissue-specific activity of enhancers. Nature *457*, 854-858.
Wang, H., Bauzon, F., Ji, P., Xu, X., Sun, D., Locker, J., Sellers, R.S., Nakayama, K., Nakayama, K.I., and Cobrinik, D. (2010). SKP2 is required for survival of aberrantly proliferating Rb1-deficient cells and for tumorigenesis in Rb1+/-mice. Nature genetics

42, 83-88.
Wang, I.-C., Chen, Y.-J., Hughes, D., Petrovic, V., Major, M.L., Park, H.J., Tan, Y., Ackerson, T., and Costa, R.H. (2005). Forkhead box M1 regulates the transcriptional network of genes essential for mitotic progression and genes encoding the SCF (SKP2-Cks1) ubiquitin ligase. Molecular and cellular biology *25*, 10875-10894.
Wang, K., and Li, P.-F. (2010). Foxo3a regulates apoptosis by negatively targeting miR-21. Journal of Biological Chemistry *285*, 16958-16966.
Wang, L., Zhao, Z., Meyer, M.B., Saha, S., Yu, M., Guo, A., Wisinski, K.B., Huang, W., Cai, W., and Pike, J.W. (2014). CARM1 methylates chromatin remodeling factor BAF155 to enhance tumor progression and metastasis. Cancer cell *25*, 21-36.
Wang, S.C., Dowhan, D.H., Eriksson, N.A., and Muscat, G.E. (2012). CARM1/PRMT4 is necessary for the glycogen gene expression programme in skeletal muscle cells. The Biochemical journal *444*, 323-331.
Wang, Z., Wilson, W.A., Fujino, M.A., and Roach, P.J. (2001). Antagonistic controls of autophagy and glycogen accumulation by Snf1p, the yeast homolog of AMP-activated protein kinase, and the cyclin-dependent kinase Pho85p. Molecular and cellular biology *21*, 5742-5752.
Wei, W., Ayad, N.G., Wan, Y., Zhang, G.-J., Kirschner, M.W., and Kaelin, W.G. (2004). Degradation of the SCF component SKP2 in cell-cycle phase G1 by the anaphase-promoting complex. Nature *428*, 194-198.
Wolf, S. (2009). The protein arginine methyltransferase family: an update about function, new perspectives and the physiological role in humans. Cellular and molecular life sciences *66*, 2109-2121.
Wong, E., and Cuervo, A.M. (2010). Autophagy gone awry in neurodegenerative diseases. Nature neuroscience *13*, 805-811.
Woods, A., Johnstone, S.R., Dickerson, K., Leiper, F.C., Fryer, L.G., Neumann, D., Schlattner, U., Wallimann, T., Carlson, M., and Carling, D. (2003). LKB1 is the upstream kinase in the AMP-activated protein kinase cascade. Current biology *13*, 2004-2008.
Wu, Q., Bruce, A.W., Jedrusik, A., Ellis, P.D., Andrews, R.M., Langford, C.F., Glover, D.M., and Zernicka-Goetz, M. (2009). CARM1 is required in embryonic stem cells to maintain pluripotency and resist differentiation. Stem cells *27*, 2637-2645.
Wysocka, J., Allis, C., and Coonrod, S. (2005). Histone arginine methylation and its dynamic regulation. Frontiers in bioscience: a journal and virtual library *11*, 344-355.

Xavier, R., and Podolsky, D. (2007). Unravelling the pathogenesis of inflammatory bowel disease. Nature *448*, 427-434.
Xie, M., Zhang, D., Dyck, J.R., Li, Y., Zhang, H., Morishima, M., Mann, D.L., Taffet, G.E., Baldini, A., and Khoury, D.S. (2006). A pivotal role for endogenous TGF-β-activated kinase-1 in the LKB1/AMP-activated protein kinase energy-sensor pathway. Proceedings of the National Academy of Sciences *103*, 17378-17383.
Xu, W., Cho, H., Kadam, S., Banayo, E.M., Anderson, S., Yates, J.R., Emerson, B.M., and Evans, R.M. (2004). A methylation-mediator complex in hormone signaling. Genes & development *18*, 144-156.
Yadav, N., Lee, J., Kim, J., Shen, J., Hu, M.C., Aldaz, C.M., and Bedford, M.T. (2003). Specific protein methylation defects and gene expression perturbations in coactivator-associated arginine methyltransferase 1-deficient mice. Proceedings of the National Academy of Sciences of the United States of America *100*, 6464-6468.
Yamamoto, A., Tagawa, Y., Yoshimori, T., Moriyama, Y., Masaki, R., and Tashiro, Y. (1998). Bafilomycin A1 prevents maturation of autophagic vacuoles by inhibiting fusion between autophagosomes and lysosomes in rat hepatoma cell line, H-4-II-E cells. Cell structure and function *23*, 33-42.
Yang, G., Ayala, G., De Marzo, A., Tian, W., Frolov, A., Wheeler, T.M., Thompson, T.C., and Harper, J.W. (2002). Elevated SKP2 protein expression in human prostate cancer association with loss of the cyclin-dependent kinase inhibitor p27 and PTEN and with reduced recurrence-free survival. Clinical Cancer Research *8*, 3419-3426.
Yang, Y.-C., Tang, Y.-A., Shieh, J.-M., Lin, R.-K., Hsu, H.-S., and Wang, Y.-C. (2014). DNMT3B overexpression by deregulation of FOXO3a-mediated transcription repression and MDM2 overexpression in lung cancer. Journal of Thoracic Oncology *9*, 1305-1315.
Yang, Y., and Bedford, M.T. (2013). Protein arginine methyltransferases and cancer. Nature reviews Cancer *13*, 37-50.
Yang, Z., and Klionsky, D.J. (2010). Mammalian autophagy: core molecular machinery and signaling regulation. Current opinion in cell biology *22*, 124-131.
Yeh, K.-H., Kondo, T., Zheng, J., Tsvetkov, L.M., Blair, J., and Zhang, H. (2001). The F-box protein SKP2 binds to the phosphorylated threonine 380 in cyclin E and regulates ubiquitin-dependent degradation of cyclin E. Biochemical and biophysical research communications *281*, 884-890.
Yu, Z.-K., Gervais, J.L., and Zhang, H. (1998). Human CUL-1 associates with the

SKP1/SKP2 complex and regulates p21CIP1/WAF1 and cyclin D proteins. Proceedings of the National Academy of Sciences *95*, 11324-11329.
Yue, W.W., Hassler, M., Roe, S.M., Thompson-Vale, V., and Pearl, L.H. (2007). Insights into histone code syntax from structural and biochemical studies of CARM1 methyltransferase. The EMBO journal *26*, 4402-4412.
Zhang, H., Kobayashi, R., Galaktionov, K., and Beach, D. (1995). pl9 skp1 and p45 SKP2 are essential elements of the cyclin A-CDK2 S phase kinase. Cell *82*, 915-925.
Zhang, L., and Wang, C. (2006). F-box protein SKP2: a novel transcriptional target of E2F. Oncogene *25*, 2615-2627.
Zhao, G.-Q., Zhao, Q., Zhou, X., Mattei, M., and De Crombrugghe, B. (1993). TFEC, a basic helix-loop-helix protein, forms heterodimers with TFE3 and inhibits TFE3-dependent transcription activation. Molecular and cellular biology *13*, 4505.
Zheng, N., Schulman, B.A., Song, L., Miller, J.J., Jeffrey, P.D., Wang, P., Chu, C., Koepp, D.M., Elledge, S.J., and Pagano, M. (2002). Structure of the Cul1–Rbx1–Skp1–F boxSKP2 SCF ubiquitin ligase complex. Nature *416*, 703-709.
Zhou, G., Myers, R., Li, Y., Chen, Y., Shen, X., Fenyk-Melody, J., Wu, M., Ventre, J., Doebber, T., and Fujii, N. (2001). Role of AMP-activated protein kinase in mechanism of metformin action. Journal of clinical investigation *108*, 1167.

국문 초록 / ABSTRACT IN KOREAN

오토파지 (자식작용)는 종간에 잘 보존된 세포 생존 기작으로 영양분 고갈에 대해 세포의 생존 및 항상성 유지를 위한 필수적인 생리 기전이다. 특히 세포가 영양분 결핍 상황에 노출 되었을 경우 오토파지를 통해 세포 내 불필요한 구성 요소 및 소기관을 분해하여 필요한 에너지원으로 생산해냄으로써 체내의 다양한 스트레스를 극복하는 기능을 수행한다.

오토파지에 대한 연구는 최근까지도 대부분 세포질에 국한되어 있었다. 이는 오토파지가 세포질에서 일어나는 현상으로 알려져 있고, 스트레스 상황하에서 신속하게 작동해야 하는 기전이기 때문으로 이전까지의 연구는 대부분 스트레스 신호에 의해 세포질에 존재하던 오토파지 단백질들이 어떻게 변형되고 단백질들 간의 결합이 어떻게 달라지는지에 초점이 맞추어져 있었다. 즉, 최근까지도 오토파지에 대한 후성 유전학 및 전사 조절에 대한 연구는 거의 진행되지 않았다.

본 연구에서는 coactivator-associated arginine methyltransferase 1 (CARM1) 이라는 아르기닌 메틸화 효소가 핵 내에서 오토파지 작용에 핵심적으로 기능하는 단백질임을 증명하였다. 오토파지 또한 핵에서 유전자가 발현됨으로써 일어나는 현상이기 때문에 오토파지 조절에 있어 핵 내에서의 유전자 발현 조절이 중요할 것으로 예상하였고 특히 히스톤 단백질의 후성 유전학적인 변형이 필수적일 것으로 기대하였다. 따라서 다양한 영양분 결핍 상황에 대해서 변하는 히스톤 단백질의 변형을 스크리닝한 결과 히스톤 H3의 아르기닌 17번에 메틸화가 유도됨을 확인하였고 메틸화를 유도하는 CARM1 효소의 단백질 양 또한 증가되는 것을 관찰하였다.

CARM1 단백질 복합체 정제를 통해 정상 상황에서는 SKP2-SCF E3 유비퀴틴화 효소에 의해 CARM1 단백질이 분해되지만 영양분 결핍 상황에서는 SKP2의 전사 감소가 유도되어 CARM1 단백질의 분해가 저해되고 결과적으로 CARM1의 양이 증가하는 것을 확인하였다. 특히 세포에 당 결핍 상황이 지속될 경우 AMP-activated protein kinase (AMPK) 인산화 효소가 활성화 되면서 FOXO3라는 전사 인자를 인산화 시키고 인산화 된 FOXO3는 SKP2의 전사 과정을 저해함으로써 CARM1 단백질이 안정화 된다는 것을 규명하였다.

안정화 된 CARM1 단백질은 Transcription factor EB (TFEB) 이라는 전사 인자와 결합하여 히스톤 H3 아르기닌 17번의 메틸화를 유도하면서 다양한 오토파지 및 라이소좀 유전자들의 발현을 조절하는 것을 확인하였다.

이번 연구를 통해 스트레스 상황에서 핵 내의 CARM1 단백질에 의한 히스톤 아르기닌 메틸화 조절이 일어나고 이것이 오토파지 활성에 핵심적이라는 사실을 증명하여 오토파지에서의 후성 유전학적 조절 메터니즘을 새롭게 구축하였다. 또한 AMPK-SKP2-CARM1으로 이어지는 중요한 신호 전달 축을 새롭게 규명하여 오토파지의 조절 기작에 대해 새로운 모델을 제시하였다.

주요어:

CARM1, 오토파지 (자식작용), 히스톤 아르지닌 메틸화, 후성 유전학적 조절, 전사 조절, TFEB, AMPK, SKP2.

학번: 2009-20340